Universidade do Minho
Escola de Engenharia

Carlos José Fortunas Teixeira

CFD-based tool to support CNT synthesis via CVD

janeiro de 2019

CFD-based tool to support CNT synthesis via CVD
Carlos José Fortunas Teixeira

UMinho | 2019

Universidade do Minho
Escola de Engenharia

Carlos José Fortunas Teixeira

CFD-based tool to support CNT synthesis via CVD

Tese de Doutoramento
Programa Doutoral em
Líderes para as Indústrias Tecnológicas

Trabalho efetuado sob a orientação de
Professor Doutor Luís Alexandre Rocha
Professor Doutor Alexandre Ferreira da Silva

janeiro de 2019

ACKNOWLEDGEMENTS

It would not have been possible to write this thesis without the help and kindness support of the people around me, to only some of whom it is possible to give particular mention.

Undoubtedly, above all, I would like to thank my Parents, Sisters and family for their unequivocal support at all times. My mere expression of thanks likewise does not suffice.

This thesis would have not been possible without the help, support, friendship and patience of my supervisors Prof. Luis Rocha and Prof. Alexandre da Silva, not to mention their unsurpassed knowledge and professionalism. Their advices and guidance at few points of my work have been considered invaluable in both an academic and a personal level. Additionally, I would like to acknowledge the NECSTLab group for the opportunity to work with them during my stay at the Massachusetts Institute of Technology.

I would like to acknowledge the financial support of the *Fundação para a Ciência e Tecnologia* for the granted fund and also the academic support from the MIT Portugal doctoral program. I also would like to mention the financial, academic and technical support of both the University of Minho, Guimarães and the Massachusetts Institute of Technology, Cambridge MA and their staff. The libraries, laboratories and other facilities have been indispensable. I also would like to mention the people, who helped me in my stay at the MIT, for their friendship, kindness and support.

Next, I would like to thank my colleagues and friends in the various groups I had the joy of meet and work with. Starting with the ones from my academic year in the doctoral program, followed with the people from the NECSTLab group, from which I emphasize Hayden Cornwell and Richard Li, and my Portuguese Boston family. To all of them, I thank for their company, help, friendship and support.

I would also like to dedicate a single paragraph to my girlfriend, Cátia, for her company, friendship, help, unconditional support and, most importantly, patience.

Finally, I would like to give acknowledgement to all my friends, which have followed my work, supported and encouraged me with their unlimited friendship and company, some of whom have already been mentioned.

The author, Carlos José Fortunas Teixeira, was supported by a national Portuguese scholarship from FCT - scholarship reference: SFRH / BD / 52350 / 2013.

This work was supported by the FCT - Fundação para a Ciência e a Tecnologia - with the reference project UID/EEA/04436/2013, by FEDER funds through the COMPETE 2020 - Programa Operacional Competitividade e Internacionalização (POCI) - with the reference project POCI-01-0145-FEDER-006941; and by the project "IAMAT – Introduction of advanced materials technologies into new product development for the mobility industries", with reference MITP-TB/PFM/0005/2013, under the MIT-Portugal program exclusively financed by FCT.

RESUMO

Ao longo dos últimos anos, tem havido bastante interesse na aplicação de Nanotubos de Carbono (CNTs) devido às suas propriedades únicas, principalmente a nível mecânico e elétrico. Contudo, os processos de síntese, como a Deposição Química a Vapor (CVD), são bastante imprevisíveis e inconsistentes, levando a uma metodologia de tentativa-erro quando se pretende extrapolar resultados. Como alternativa, nesta tese é proposta e desenvolvida uma ferramenta, baseada em métodos computacionais de dinâmica de fluidos (CFD), de suporte à compreensão do processo e à transição entre diferentes *setups* de CVD.

O desenvolvimento desta ferramenta começa com uma análise de sensibilidade, baseada em métodos CFD, a modelos computacionais de quatro setups CVD reais para a síntese de CNTs. Nesta análise foi pretendido avaliar que parâmetros de processo mais influenciam as condições de síntese.

Tal informação permite ajustar os parâmetros de processo de forma a obter as condições de síntese desejadas e, consequentemente, desenvolver a ferramenta de suporte à transição entre diferentes *setups* de CVD. Definindo esta transição como o processo de replicar as condições de síntese medidas num dado (primeiro) *setup*, num outro (segundo) *setup*, a metodologia proposta é baseada num problema de otimização, onde é pretendido reduzir o erro percentual entre as condições de síntese de ambos os *setups*. Os resultados mostraram um erro percentual abaixo dos 2% para a maior parte dos casos testados e nunca superior a 7% para os restantes casos, o que valida a metodologia proposta do ponto de vista do modelo computacional.

A ferramenta de transição foi ainda melhorada com a integração dos efeitos da temperatura do forno, parâmetro do processo CVD ainda não considerado, nas condições de síntese. Estes efeitos foram avaliados através de uma análise de sensibilidade. Uma vez validada a hipótese, a ferramenta de transição foi alterada considerando a temperatura do forno e foi testada para vários casos. Os resultados obtidos mostraram uma redução média de 63% do erro percentual anterior.

Para explorar e entender as capacidades dos métodos CFD, foi criado um caso de estudo, onde reações químicas foram incluídas num modelo para resolver problemas existentes na síntese de CNTs quando é usado um novo catalisador. Através do estudo das

reações químicas e interações existentes entre os vários componentes, é possível analisar outras dependências existentes no processo de síntese, permitindo ultrapassar as limitações encontradas no *setup* experimental.

Por último, a inclusão das reações químicas no modelo foi proposta como forma de estudar a transição entre setups de CVD, onde o processo de síntese de CNTs é feito com diferentes hidrocarbonetos. A integração destas capacidades possibilitaria a análise de condições de síntese, resultantes da interação química dos diversos gases. Adicionalmente, é espectável a validação experimental da metodologia de transição desenvolvida. Tal validação, quer seja feita em dois *setups* existentes no mesmo grupo de investigação ou entre diferentes grupos, potenciaria a metodologia como uma ferramenta robusta na transferência de conhecimento e resultados, como ainda em técnicas de *scale up* da síntese de nanotubos de carbono.

O desenvolvimento deste trabalho de investigação resultou numa melhor compreensão acerca da dinâmica de fluidos in das interações entre gases que ocorrem durante a fase de crescimento da síntese de CNTs por CVD. Esta compreensão foi usada para o desenvolvimento duma metodologia de transição, baseada em mimica de condições, para suporte à transferência de conhecimento entre diferentes *setups* de CVD. Foi ainda analisada a integração de reações químicas nos modelos CFD, que potenciariam a metodologia proposta para abordar a transição entre setups CVD que usem diferentes gases. No entanto, este trabalho computacional deve ser validado, uma vez que ainda existem questões cientificas a abordar. Por exemplo, que reações químicas ocorrem, quando usados diferentes gases? Ou, que condições de síntese devem ser replicadas entre estes *setups*? Estas e outras questões devem ser abordadas em trabalho futuro.

ABSTRACT

Over the last years, there has been a high interest in Carbon Nanotubes' (CNTs) applications due to their unique properties, mainly at mechanical and electrical levels. However, current synthesis processes, such as Chemical Vapor Deposition (CVD), are highly unpredictable and inconsistent, which leads to an exhaustive trial-and-error methodology when extrapolating results. Alternatively, a Computational Fluid Dynamics (CFD) based tool to support the transition process between two distinct CVD setups is here proposed and developed.

For the correct development of such tool, a CFD-based sensitivity analysis was first performed to the models of four distinct and real CVD processes to synthesize CNTs. Such analysis intended to give a better understanding of the whole process by evaluating which process parameters affect the most the synthesis conditions. Such understanding of the process' fluid dynamics would enable the targeting of specific synthesis conditions by adjusting the process parameters.

With such insights of the process' fluid dynamics, the model to support the transition between two different CVD setups was designed. Defining this transition as the act of mimicking the synthesis conditions obtained in one tube in the other, the proposed methodology was based in an optimization problem, intended to minimize the percentual error between the conditions measured in both setups. Results have shown a total percentual error less than 2% for most of the tested cases and never higher than 7% for the remaining ones, which validates the proposed methodology.

The transition model was then improved with the integration of the furnace temperature effects on the synthesis conditions. These effects were evaluated by a sensitivity analysis. Once the proposed hypothesis was validated, the transition model was altered considering the furnace temperature. The obtained results showed an average reduction of 63% of the previously achieved percentual error.

Further capabilities of the CVD setups modelling via CFD tools were assessed by a case study, where chemical reactions kinetics were included in the model in order to solve a few uniformity issues in the CNT synthesis process, when addressing the usage of a different catalyst. Including the interactions between the compounds, the chemical reactions kinetics enable the analysis of further dependencies existent in the CVD process,

which gave some insights to be considered for overcoming the encountered issues in the experimental work.

Finally, the inclusion of the chemical reactions kinetics in the transition model was proposed as a way for it to tackle transition between CVD setups, whose CNT synthesis is based in different hydrocarbons. The inclusion of such capabilities would enable the analysis of other synthesis conditions, resulted from the interaction between the different compounds. Moreover, experimental validation of the designed transition methodology is envisioned. Such validation, either within the same research group or between different groups, would potentiate the methodology as a robust tool to support knowledge transfer as well as scale-up techniques in the carbon nanotubes synthesis.

The development of this research work resulted in a better understanding of the fluid dynamics and compounds interactions occurring during the growth phase of the CNT synthesis by CVD. Such understanding was used to develop a conditions mimicking based transition methodology to support knowledge transfer between different CVD setups. It was also analyzed the integration of chemical reactions in the CFD model, which would potentiate the proposed methodology to tackle the transition between CVD setups using different compounds. Nonetheless, this computational work should be validated, as there are still research questions to be addressed. For instance, what chemical reactions occur when using different compounds? Or, what would be a suitable synthesis condition to be mimicked between these setups? These and other issues should be tackled in future research work.

TABLE OF CONTENTS

LIST OF FIGURES

LIST OF TABLES

LIST OF SYMBOLS

Symbol	Description	SI Units
$a_1 \sim a_7$	Gases' Interval Coefficients	-
A	Pre-exponential factor	s^{-1}
C	Carbon	-
C_p	Gases' Specific Heat Capacity at Constant Pressure	$J.kg^{-1}.K^{-1}$
C_2H_2	Acetylene	-
C_2H_4	Ethylene	-
ctr	Height of tube center ($Dist\ B = 0$)	m
CO	Carbon monoxide	-
CO_2	Carbon dioxide	-
E	Total energy of an analyzed system	J
E_a	Activation energy	J
E_{in}	Energy entering the system	J
E_{out}	Energy leaving the system	J
$Error_{C2H4}$	Percentual error of a certain $Position$ in the second tube domain, in relation to the desired ethylene concentration	%
$Error_{Position}$	Percentual error of a certain $Position$ in the second tube domain, in relation to the desired synthesis conditions	%
$Error_{Temp}$	Percentual error of a certain $Position$ in the second tube domain, in relation to the desired mixture's temperature	%
$Error_{Variable}$	Percentual error of a certain $Variable$ for a certain $Position$ in the second tube domain	%
$Error_{Veloc}$	Percentual error of a certain $Position$ in the second tube domain, in relation to the desired mixture's velocity	%
D_P^V	Percentual dependency of variable V on parameter P	-
D_{PS}^V	Percentual dependency of variable V on parameter P in setup S	-
$Desired_{Value}$	Desired value for any given synthesis condition	-
$Dist\ A$	Distance between tube entrance and substrate	m
$Dist\ B$	Distance between tube center and substrate	m
f	External forces	N
f_i^{end}	Vector with values of function f for indexes $\geq i$	-

He	Helium	-
H	Hydrogen (atom)	-
H_2	Hydrogen (molecule)	-
H_2O	Water	-
k	Reaction's constant rate	$mol.l^{-1}.s^{-1}$
$kr_{Section\ A_i}$	Set of values of the kinetic rate across the weave's center	$kg.mol.m^{-3}.s^{-1}$
kr_i	Kinetic rate of a given line	
KR_s	Overall kinetic rate across the weave for each simulation	
L	Substrate's width	m
m	Mass	kg
mv	Momentum	$kg.m.s^{-1}$
n	Unit vector	-
Na	Sodium	-
$NaOH$	Sodium hydroxide	-
PE_i	Percentual Error between consecutive pair of iterations $i-1$ and i	%
$Position_{Value}$	Value of a given synthesis condition for a certain $Position$ in the second tube domain	-
r	Tube radius	m
R	Universal Gas Constant	$J.K^{-1}.mol^{-1}$
R_s	Specific Gas Constant	$J.K^{-1}.mol^{-1}$
R_P^V	Overall percentual ranking of variable V on parameter P	%
sbs	Height at which a 10 mm square substrate is when positioned at the bottom of the tube	m
S	Surface of the control volume	-
t	Time	s
T	Temperature	K
v	Velocity	$m.s^{-1}$
$V_{parameter}^{level}$	Value of variable V for a given $parameter-level$ combination	-
$V_{s_P}^{\ L}$	Value of variable V, obtained in a simulation containing the $P-L$ combination	-
Var_i	A variable's average for iterations i	-
X_P^V	Set containing all values of variable V calculated for parameter P	-
ρ	Density	$kg.m^{-3}$

$\boldsymbol{\Omega}$	Volume of the control volume	-
Δ_P^V	Variation caused by parameter P in variable V	-

LIST OF TERMS

CAD	Computer-Aided Design
CFD	Computational Fluid Dynamics
CNTs	Carbon Nanotubes
CV	Control Volume
CVD	Chemical Vapor Deposition
FDM	Finite Differences Method
FEM	Finite Elements Method
FVM	Finite Volumes Method
MWCNT	Multi-Walled Carbon Nanotube
SWCNT	Single-Walled Carbon Nanotube

Chapter 1

INTRODUCTION

1.1. Carbon Nanotubes

A Carbon Nanotube (CNT) is a cylinder-shaped structure with a diameter in the nanometer range but with a length in micrometer range. A CNT is composed by one or more concentric cylinders, made up of a hexagonal lattice of carbon atoms [1–5]. Thus, a CNT can be Single- (SWCNT) or Multi-walled (MWCNT), depending on the number of concentric tubes it has (see Figure 1.1a). Moreover, the orientation of these walls with respect to the hexagonal lattice - the CNTs' chiral vector - affects the CNTs properties. For instance, depending on this orientation, the CNT can have metallic or semiconducting properties (see Figure 1.1b) [2,4].

After Iijima's analysis in 1991 [8], research around CNTs and nanotechnology expanded tremendously, especially on the investigation of their properties and how to take advantage of them in technological applications [1–3,5]. At molecular level, the carbon bonds in the hexagon lattice grant CNTs superb strength in the axial direction. Compared to steel, CNTs have a Young's modulus and a tensile strength over 8 and 50 times greater, respectively [1–3,5]. Simultaneously, having a low density (6 times lower than that of

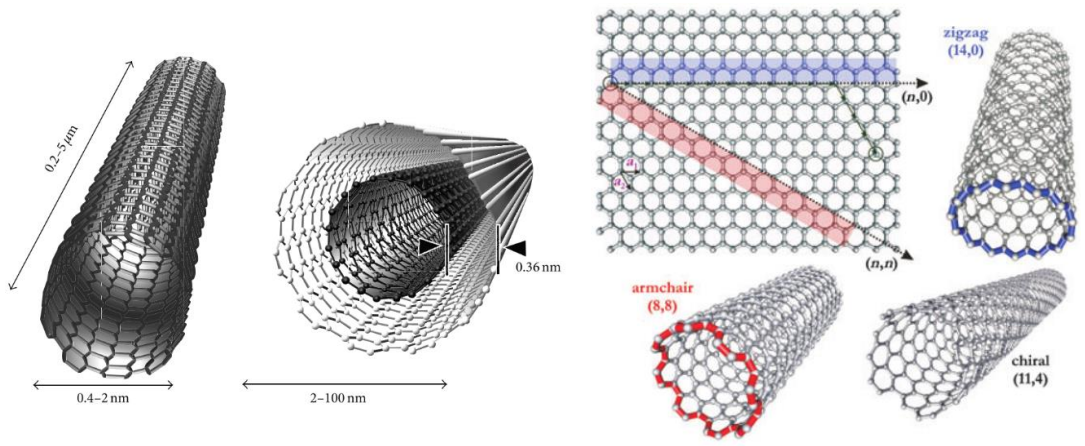

(a) **(b)**

Figure 1.1: (a) Single and Multi-walled CNTs; (b) CNTs configuration based on its geometric arrangement. (Reprinted from [6] and [7], respectively. Licensed under a Creative Commons Attribution License).

steel), CNTs have a tensile strength over 300 times greater than steel, which pertains their potential as structural materials. From an electrical point of view, depending on its chiral vector, CNTs can be either metallic or semiconductor. Thus, they can be used as transistors or current-carrying wires in nanoscale circuits [1,2]. In both these applications, CNTs outperform currently used materials such as copper and silicon. For instance, they can sustain current densities 1000 times greater than silicon [1,2].

The usage of CNTs in technological applications, especially in electronics, is further enhanced by outstanding thermal properties. CNTs are stable at temperatures higher (up to 3 times) than that of metal wires used in microchips [1,2]. They also display better thermal conductivity than diamond and copper. Such thermal properties enable CNTs to be used in much denser, i.e. faster, circuits than the present edge of microtechnology.

The CNTs' unique mechanical, electrical and thermal properties have encouraged research envisioning their technological application in innumerous fields, such as media, entertainment, health, communication, transport and environment [1,2,4,5]. However, current CNT synthesis using CVD techniques is not fully understood and it is poorly controlled and not easy on a large scale [1,2].

1.1.1. Carbon Nanotubes' Applications

The aforementioned CNTs' outstanding properties enable them to be used as structural or active elements. When used as a structural element, CNTs can be added to other materials, usually polymers, in order to enhance their mechanical properties [4,9].

For example, authors have increased a polymer's Young's Module by embedding CNTs [10]. On the other hand, CNTs can be used as an active component, i.e. in ways where other properties, such as conductivity and piezo-resistivity, are more interesting [4,11]. For instance, CNT-based films characterized in [11] are reported to have improved electrical properties, which pertains CNT usage in nano- and micro-scaled devices. Such devices are the ones which can most benefit with CNT integration, in the sense that both CNTs' electrical and mechanical characteristics would improve them.

For better understanding of this subsection, it is essential to distinguish some terms. A transducer is a device that converts a signal in one form of energy to another form of energy. For instance, a sensor is used to detect a parameter in one form of energy and report it in another, often an electrical signal. On the contrary, an actuator accepts energy and produces movement (action) [12]. Thus, transducers include, but are not limited to, both sensors and actuators, i.e. some transducers, for example, only convert signals, without detecting parameters nor producing movement.

CNT-based Sensors

The transducers with detection capabilities - sensors - continue to make significant impact in everyday life with applications in several areas, such as automotive, biomedical, food and security [4,13]. Regardless of the targeted application, there has been a strong demand for producing highly selective, sensitive, responsive and cost effective sensors. Moreover, the advent of nanotechnology have led researchers to foster the creation of miniaturized sensors, leading to reduced weight, power consumption and cost. The discovery of CNTs and their distinct properties has triggered interest among researchers to develop CNT-based sensors. These have the potential of revolutionizing the sensor industry, being considered a next generation of sensors technology [4].

According to the literature, CNTs have been used, as the sensing element, in pressure, flow, thermal, gas, optical, mass, position, stress, strain, chemical and biological sensors. Such variety of sensing elements is possible with distinct CNTs' properties, achieved by changing the conditions of the CNTs' synthesis, i.e. growth; and, in some cases, performing some post-synthesis processes (as functionalization). In order to sense a certain parameter, CNTs can either: (i) be used per se, i.e. without any post-processing [4,14–17]; (ii) be combined with other material, creating a nanocomposite [4,18–26]; or (iii) serve as a read-out component, which electrically transmits the reaction of a specific

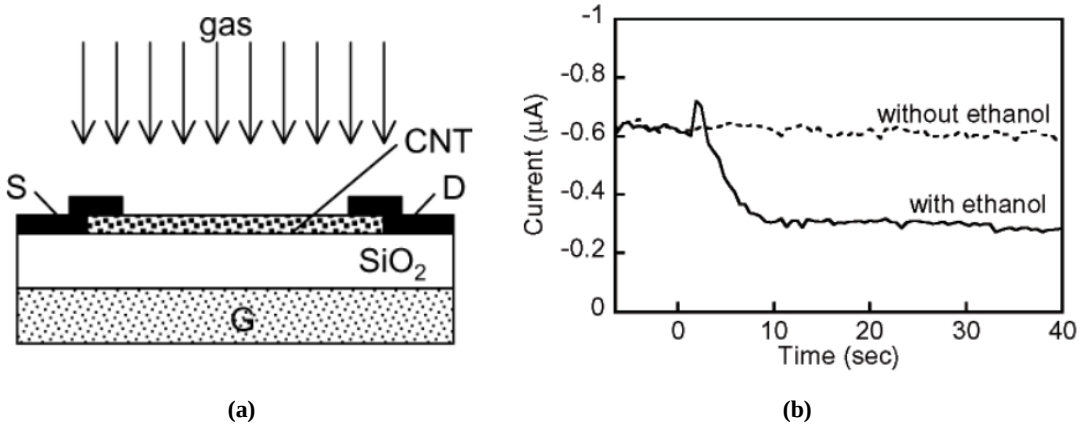

Figure 1.2: (a) Someya's sensor's cross-section and (b) its current response. (Adapted with permission from [17], Copyright 2003 American Chemical Society).

element, with whom the CNTs were previously coated, to a certain condition in the environment, normally another element [27,28].

In the first case, i.e. when CNTs are used independently, it is easier to construct functional sensors, as no post-processing is required. For instance, by densely compacting CNTs between two metal electrodes, Ghosh et al. [14] have constructed a flow sensor, where the CNTs produce an electrical voltage response directly related with the fluid flow. Also taking advantage of CNTs' electrical responses, Someya et al. [17] reported current spike occurring when a CNT-based transistor is in contact with alcoholic vapors, such as ethanol (Figure 1.2).

The integration of CNTs with other material, forming a nanocomposite, has been used not only to alter the sensorial element's properties, but also to simplify its usage in certain scenarios [9]. The inclusion of such materials in CNTs is performed by covalent or non-covalent bonding techniques, e.g. adsorption, attachment, embedment, electro-polymerization, encapsulation, etc. [13]. By filtering and drying a mixture of CNTs and a liquid compound, Dharap et al. [18] developed a CNT film sensor capable of sensing strain in multiple locations and in different directions, and reacting via voltage changes. Inspired by typical configurations of capacitive pressure sensors, authors in [25] have constructed and characterized a flexible pressure sensor based in CNTs embedded in a flexible polymeric substrate, and achieved a linear response over a large pressure range (see Figure 1.3). Envisioning ammonia detection, Chopra et al. [23] have coated a circular copper disk with CNTs, whose resonant frequency shifts in relation to the sensed ammonia. Moreover, the system is considered *"suitable for apps that prohibit physical connections or require non-destructive testing"* [4].

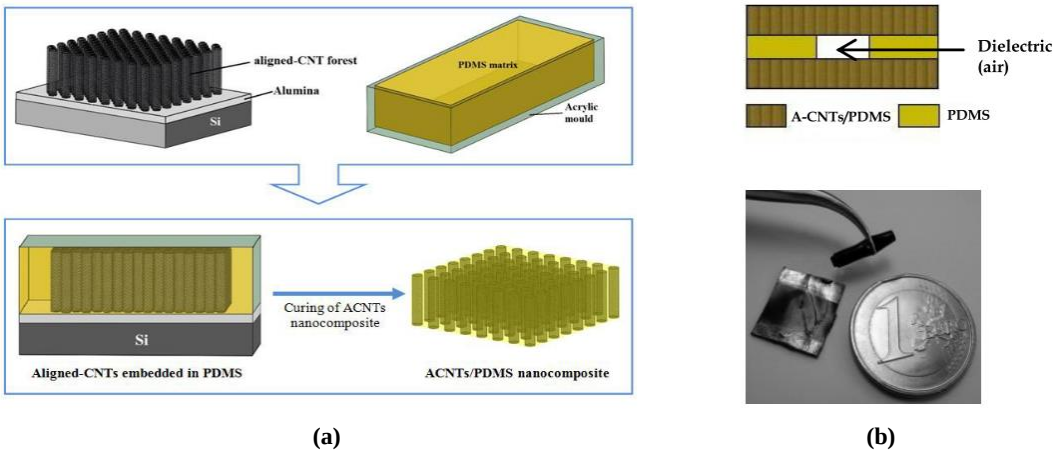

Figure 1.3: (a) CNTs embedding process used to construct a flexible pressure sensor; (b) image of the constructed sensor. (Adapted from [25], Copyright 2012, with permission from Elsevier).

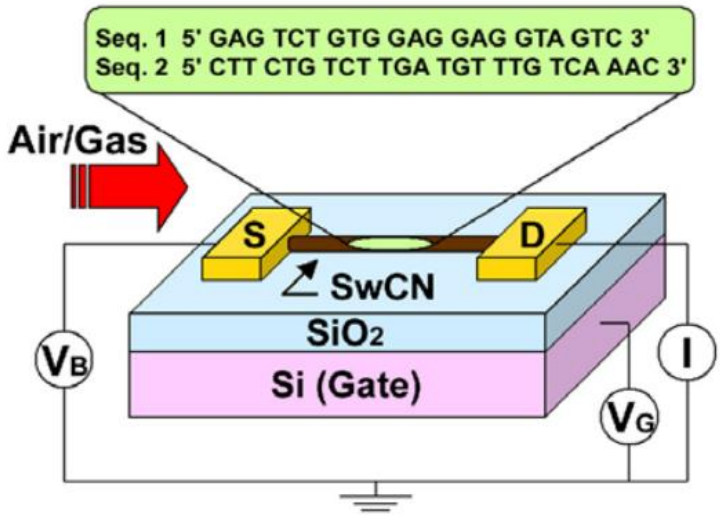

Figure 1.4: Staii's sensor's schematic. (Adapted with permission from [28], Copyright 2005 American Chemical Society).

Coating CNTs with other element results in altered sensing capabilities and CNTs' properties, such as their solubility and biocompatibility [13]. This methodology has become highly promising due to CNTs' unique properties, specially their high surface-to-volume ratio and fast electron-transfer kinetics. The environment conditions, to whom the CNTs react can be altered by properly selecting the element to coat the nanotubes. For instance, following such methodology, Snow et al. [27] have constructed a chemical vapor sensor, where the CNTs' capacitance is highly sensitive to a wide range of vapors. Similarly, Staii et al. [28] have proposed the usage of CNTs coated with single-stranded DNA to detect a wide variety of gases (see Figure 1.4).

In order to analyze the CNTs' potential to filter, capture and detect low levels of biological markers of disease, authors in [29] developed a microfluidic device to

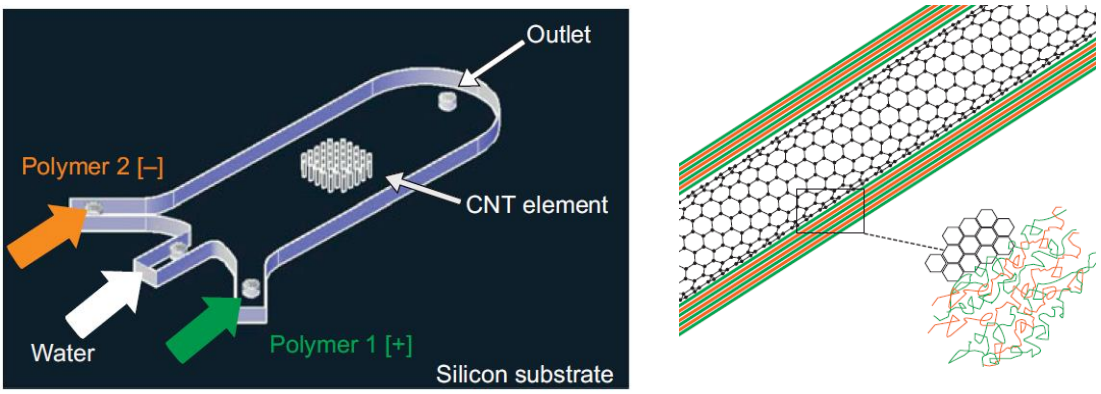

Figure 1.5: (a) Microfluidic device constructed by Yost et al. to coat CNTs; (b) Graphical representation of a coated CNT. (Adapted from [29], licensed under a Creative Commons Attribution 4.0 License).

controllably functionalize individual CNTs throughout the CNT array (see Figure 1.5). Using this device, Yost et al. have coated CNTs, which were successfully used to capture prostate-specific antigen. Moreover, due to the device's high controllability, the resulting CNTs have the potential to isolate nano-sized bioparticles, such as viruses or DNA.

CNT-based Actuators

Similar to sensors, transducers with actuation capabilities, i.e. actuators, are also receiving high interest for applications, such as robotics, optical displays, micro-switches and medical prosthetic devices, especially the polymeric based ones, due to their large displacement and rapid response for a reasonably applied voltage [30,31]. Moreover, CNTs' unique physiochemical properties have triggered their potential usage in electrochemical actuation systems, where they have shown comparable or superior performances than other alternatives in various types of macro, micro and nanoscopic applications [30,31].

One way of achieving actuation based in CNTs is through the deflection of a macroscopic sheet made of billions of CNTs, which occurs when a voltage is applied [30–32]. The deflection reverses when the voltage potential is reversed. Moreover, it has been shown that, if a square wave is applied, oscillations up to at least 15 Hz are observable [32]. These sheets are formed by filtering, rinsing and drying a polymer-CNT mixture, resulting in randomly entangled structures of several hundred CNTs. CNT-based actuation can be achieved in cantilevers with one [30] or various sheets [31] (see Figure 1.6). In both these approaches, displacements of several millimeters have been reported, which, although appearing small, is considered large in comparison with other transducers excited with similar voltages [31].

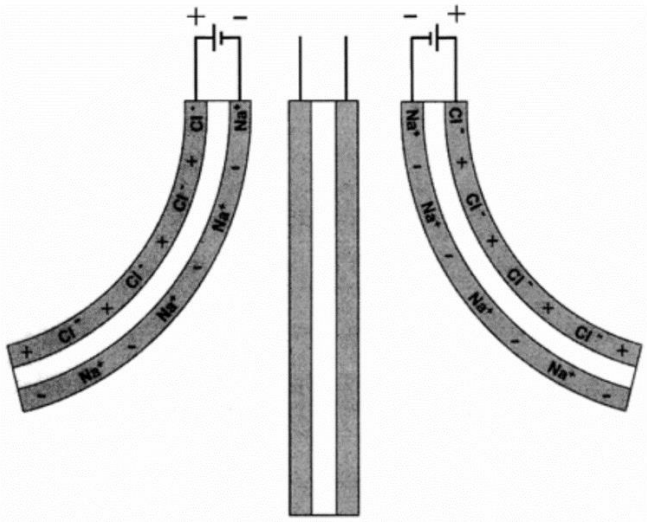

Figure 1.6: Cantilever with two sheets of CNTs (grey) and one layer of adhesive (white). Depending on the applied voltage, it can bend to the left or the right. (From [32], reprinted with permission from AAAS).

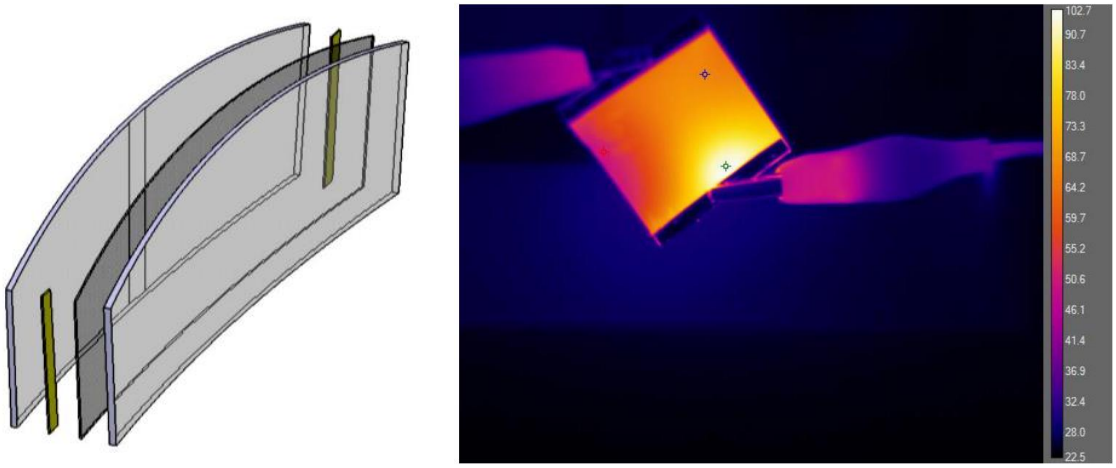

(a) **(b)**

Figure 1.7: (a) Schematic diagram of the transparent CNT layer sandwiched between two glass layers; (b) Infrared thermal image obtained with a thermal camera (temperature in Celsius). (Reprinted from [34], licensed under a Creative Commons Attribution 4.0 License).

Taking advantage of the CNTs' optical, thermal and electrical properties, authors have constructed a transparent conductive film which heats up when a voltage is applied [33,34]. Such transparent heater was considered ideal to construct defrosting or deicing windshields. In this work, transparent CNT layers were spin coated, one by one, and sandwiched between two glass layers. A voltage was then applied using two electrodes and a thermal camera was used to capture the film temperature (see Figure 1.7). Authors have constructed and tested films with various number of layers, which affects the film thermal properties, and achieved temperatures in the order of 100 ^{o}C. Further characterization tests, such as stability, repeatability and transmittance, were performed to these film heaters and authors have identified their potential application in car/aircraft windshields, deicers of

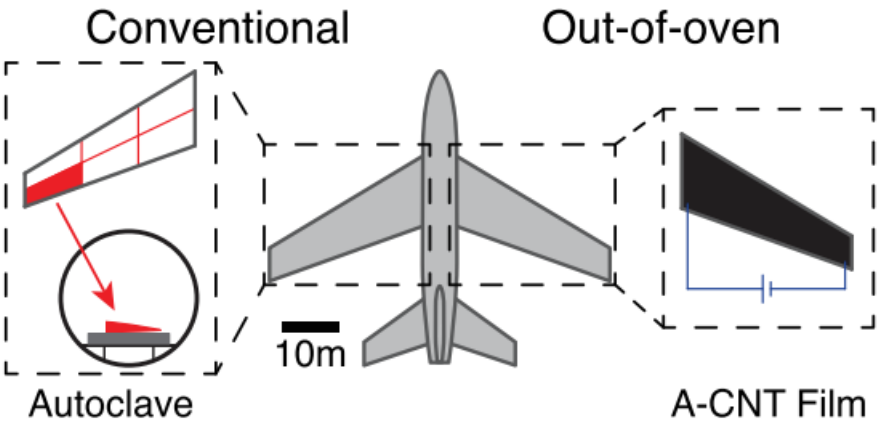

Figure 1.8: Comparison between the conventional autoclave and the Out-of-Oven techniques. (Adapted with permission from [35], Copyright 2015 American Chemical Society).

aircraft wings or wind turbine blades [33,34].

Also exploiting CNTs thermal properties, Jeonyoon et al. have developed a methodology to cure polymeric composites more efficiently [35–39]. In their work, a resistive heating film of CNTs is placed in the outer surface of the polymeric composite, and is heated by application of a controlled voltage. Such methodology enables the composite to be cured in a more efficient way than the conventional autoclave procedure. Moreover, since it does not require the composite to be placed inside the autoclave for curing, this *"Out-of-Oven"* technique (as the authors call it) allows a higher volume to be cured simultaneously, resulting in a reduction of the curing energy, which has great advantage in the aeronautics industry (see Figure 1.8).

It is undoubtable that CNT-related areas of research have suffered a phenomenal growth in the last decades [4]. The exceptional properties, which have allowed CNTs to be used in transducers and other devices, have also pertained their potential to increase the devices' characteristics, such as sensitivity and dynamic range. These specifications are of most importance for the technological world, as fields of micro- and nano-electronics are gaining popularity year after year.

Thus, it is expected that, in the near future, CNT-based transducers will trigger investigation of their usage in many applications, such as biomedical, automotive, food, monitoring, agriculture, manufacturing, etc. However, there are hurdles and obstacles in the CNTs synthesis which must be successfully tackled in order to fulfill the CNTs' potential in sensorial and actuation applications [4].

1.1.2. Carbon Nanotube Synthesis

As aforementioned, the CNTs unique properties have triggered research interest in their application in various fields, ranging from sensors and actuators to enhanced polymeric composites. Nonetheless, the potential of these applications relies in the production of CNTs.

Among the methods for CNT synthesis, such as Arc-discharge [40], Laser-ablation [41], and Low-pressure Flames [42], Chemical Vapor Deposition (CVD) is the most widely used, mainly due to its low setup cost, simplicity and high production yield [1,2,5,43,44]. The CVD process is based on the chemical reaction that occurs inside a chamber and depends on the combination of different compounds and conditions, such as pressure and temperature.

Figure 1.9 depicts a graphical representation of the CVD process to synthesize CNTs. For this specific case, the process takes a hydrocarbon gas, which serves as a precursor, and decomposes it in order for the Carbon atoms to precipitate on top of the substrate, and thus synthetize the CNTs. The decomposition of the precursors is performed inside a tube furnace at high temperatures (400-1200 ^{o}C) so that the hydrocarbon gas undergoes pyrolysis [1,5,44]. As a local pyrolysis is targeted, in order to ensure that the CNTs grow on top of a surface, a catalyst coats the substrate surface, pin-pointing the gas decomposition.

Besides the hydrocarbon, other compounds are present in the process, namely a reducer and an inert gas. The reducer, usually hydrogen, is crucial to reduce the iron oxide formed on the catalyst thin film, and to perform the dewetting of catalyst to enable the carbon atom adsorption. On the other hand, the inert gas, generally helium or argon, is

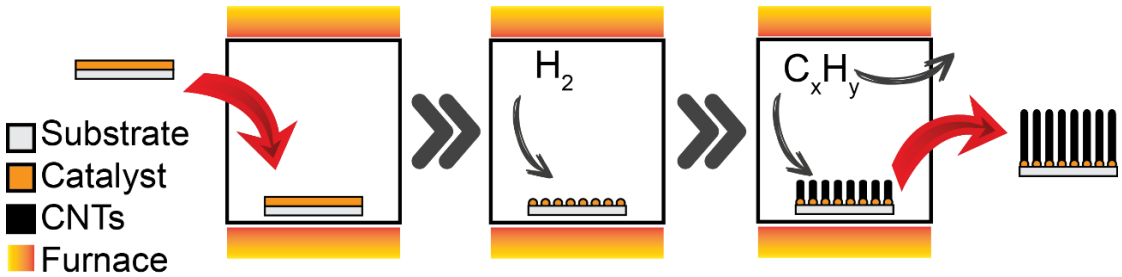

Figure 1.9: Graphical representation of the CVD process to synthesize CNTs. After a sample, consisting of a substrate and catalyst, is placed in a chamber, a reducer gas, hydrogen, is used to reduce the catalyst into smaller particles, upon which, the carbon, resulted from the decomposition of a hydrocarbon, is deposited.

mainly used to ensure total pressure control and heat transfer during the whole process.

This section only presents a brief description of the CVD synthesis process. Further analysis of this technique, as well as a comparison between the three processes, are presented in more detail in chapter 2.

1.2. Problem Statement and Hypothesis

Although CNTs' unique properties have triggered interest in their application in innumerous fields [1,2,4,5,45], current CNT synthesis is highly influenced by a wide range of parameters, such as temperature, pressure and concentrations of the used compounds [46,47]. Consequently, it is difficult to predict and to tune the final result, the CNTs' properties.Moreover, controlling how each parameter influences the result will, most likely, lead to an extensive trial-and-error tuning process rather than a systematic approach [46–49]. Oliver, C et al. [48] have performed a statistical analysis on the CNT growth process and verified the process' variability and how time demanding the tunning process is. Such results' inconsistency hinders the understanding and the extrapolation of research findings and, as a consequence, limits knowledge transfer between different setups and CNT's application in different fields.

In order to tackle such bottleneck, the hypothesis of developing a reliable computational model to support the transition between different CVD setups to synthesize CNTs is here proposed and analyzed. By enabling a better fundamental understanding of the synthesis process, such model would permit a systematic approach, when transitioning between setups rather than following a time-consuming trial-and-error methodology. Moreover, it could also be used to implement scale-up principles and to synthesize CNTs in a more efficient way to achieve optimal performance for targeted applications [46–49].

1.3. Motivation

As aforementioned, it is envisioned the development of a computational model of the CVD process as a way to tackle its inconsistencies, which limit the extrapolation of research findings. Overcoming such issue would enable the design and the implementation of robust methodologies to scale up the CNT synthesis, leading to higher production yields. Moreover, if such computational model is used to develop methodologies to transition

between different setups, research findings and knowledge could be more easily transferred, which would strengthen and improve the process's worldwide research goals.

Being such a complex work, it comprises various technological areas. In order to design the envisioned model, it is required an understanding of concepts related with the CNT synthesis, the CVD process, computational modelling and analysis, within others. It is this described importance of the research work, as well as this broad scope of technological areas comprised by it, that motivates the author to perform such work.

1.4. Research Questions and Objectives

Envisioning the development of a computational tool to support the transition between different CVD setups, there are some research questions, which represent the project's main plan. The proper investigation of this research plan should answer the proposed questions:

- Which conditions affect the CNTs' synthesis in the CVD process?
- How are these synthesis conditions affected by the process parameters?
- How can CVD process setups be different?
- How should the transition between setups be defined?
- Which synthesis conditions are considered critical?
- How can these synthesis conditions be changed?
- Are there any other parameters relevant to the setups' transition?

In order to tackle these research questions, and thus develop the envisioned computational tool, several intermediate objectives should be fulfilled:

- Proper understanding of the CVD process to synthesize CNTs, focusing of the process parameters effects on the synthesis conditions;
- Robust methodology for the transition between setups, depending on the various process parameters;
- Analysis of further potentials of the CFD tools.

1.5. Methodology

Figure 1.10 depicts a graphical representation of the various steps followed

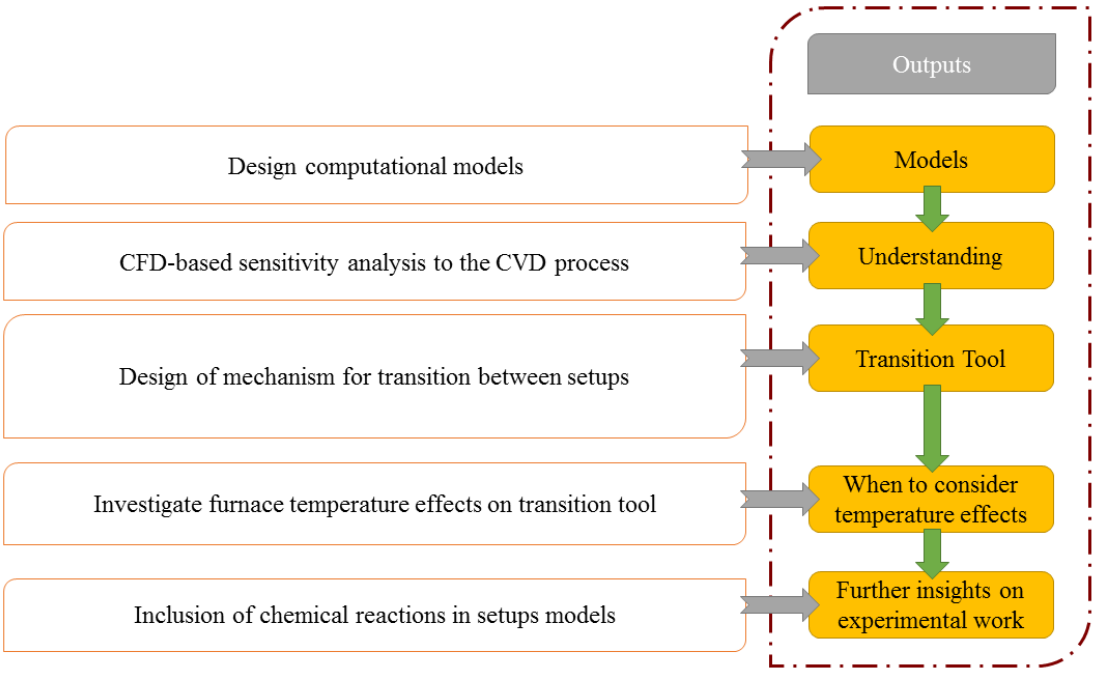

Figure 1.10: Graphical schematic of the followed methodology throughout this work.

throughout this work alongside with the respective outputs of each step.

Firstly, prior to any analysis or transition model development, the computational models of the various CVD setups must be performed. These computational models are used in every one of the upcoming steps. Thus, their correct design and the definition of the simulations are crucial.

Envisioning the development of such reliable transition model, a better understanding of the synthesis process should be firstly accessed. Thus, a Computational Fluid Dynamics (CFD) based sensitivity analysis is here applied to the Chemical Vapor Deposition (CVD) synthesis process of CNTs to understand the fluid dynamics, which occur inside the tube reactor. The presented sensitivity analysis addresses the effects of each process parameter in the inner tube synthesis conditions. By identifying and understanding these effects through numerical tools, it becomes then possible to target and achieve specific synthesis conditions by adjusting the process parameters.

Such CFD analysis was then used to support the transition between two distinct setups by mimicking the conditions obtained in one setup in the other. The proposed methodology is based in an optimization problem, where the metric to minimize is the error between the conditions at a certain point and the desired ones.

The transition methodology was then improved by also considering the tube's

temperature as a process parameter, whose variation would affect the addressed synthesis conditions by influencing the heat transferred to the mixture. These effects were validated by a sensitivity analysis and results have shown that the improved transition methodology would have more impact, in relation to the non-improved one, when the substrate in the second setup already has an envisioned site to be positioned.

Finally, chemical reactions kinetics were included in the CFD modelling of CVD setups in order to support experimental work, which envisioned to solve certain uniformity issues of the CNT synthesis process, when addressing the usage of a new catalyst. By also consider the compounds interactions during the reduction phase of the CVD process, a sensitivity analysis, addressing the dependencies that some process parameters have in the catalyst particles formation, was performed. Such analysis gave some insights on the next steps that should be followed in the experimental work in order to overcome the encountered issues.

Additionally, results obtained when including chemical reactions kinetics in the CFD modelling have triggered the hypothesis that further study on their integration could enable the design and development of a transition methodology focused in CVD setups, whose CNT synthesis is based in different hydrocarbons.

1.6. Thesis Overview and Structure

Considering the previously defined methodology, this thesis is structured as follow.

The current chapter depicts an introduction to the proposed research. It briefly describes CNTs, the most used synthesis process (CVD) and some of their potential applications. Next, the research hypothesis proposed in this thesis is stated, as well as what research questions should be answered and which objectives should be met in order to achieve the envisioned goal. Lastly, it presents the methodology followed in this thesis as well as its final contributions.

As aforementioned, the main goal is to develop a CFD-based methodology to support the transition between different CVD setups to synthesize CNTs. Thus, in chapter 2, an overview of the existent state of the art is presented. Such overview includes a comparison between different methods to synthesize CNTs; various process parameters used in the literature to synthesize CNTs via the CVD process; and an overview of several

applications of CFD techniques, not only regarding the CVD process, but also in other technological fields.

Next, in chapter 3, a description of the designed CFD models is presented. It starts by depicting the addressed setups, followed by each simulated compound's properties and the procedure to select simulation conditions such as the mesh size and the number of iterations to perform in each simulation.

In chapter 4, in order to evaluate the synthesis conditions dependency on the process parameters, a sensitivity analysis was performed, which resulted in a better understanding on the CVD process and on which process parameter most affects the synthesis conditions inside the tube during the growth phase.

Such understanding was then used to design a methodology to support the transition between different setups (detailed in chapter 5). As previously described, the transition was addressed as an optimization problem that envisioned to minimize the percentual error when comparing the defined synthesis conditions measured in both tubes. Due to its effects on the compounds' flow throughout the tube, the furnace temperature was posteriorly included in the transition methodology as a way to improve the obtained results.

Then, in chapter 6, a case study addressing the capabilities of CFD modelling was proposed. It envisioned the addition of chemical reactions kinetics to the CFD models to tackle growth uniformity issues encountered when studying CNT synthesis based in a sodium-based catalyst. Validating that these issues are due to a poor catalyst particles formation, a CFD model, addressing the compounds interactions during this phase, was designed and analyzed. Such case study gave some insights that chemical reactions kinetics could be added to the previously proposed transition methodology in order to address the transition between CVD setups, whose synthesis is based in different hydrocarbons.

Finally, chapter 7 sums up the conclusions and contributions of the performed work and proposes some guidelines to be followed as future work.

1.7. Contributions

The research work developed throughout this thesis is supported by the Leaders for Technical Industries (LTI) PhD program, within the Engineering Design and Advanced Manufacturing (EDAM) focus area of the MIT Portugal Program. The LTI PhD program

focus on product and process innovation, as well as decision-making, taking into account economics, management and social aspects.

This perspective is evident in the developed research work. The work regards the understanding and the consistency improvement of a widely used process to synthesize CNTs. As previously referred, the CNTs' unique properties have triggered high interest in their application in several industrial sectors, such as automotive, aeronautics and electronics. Since their synthesis processes are still unpredictable and unreliable, such industrial applications are highly limited. Moreover, although there is a lot of researchers tackling the CNTs synthesis and applications, these also find limitations while learning from each other. Such knowledge transfer is also hindered by the synthesis processes' inconsistency and unpredictability.

Focused in applying a CFD-based approach to foster a better understanding of the synthesis process, this thesis proposes a more methodic transition process between different setups for synthesizing CNTs. Such understanding of the synthesis process has the potential to be used to transfer knowledge between researchers, which can lead to a faster application of the CNTs' potential in the envisioned industrial sectors.

1.8. Publications

The development of this research work resulted in the writing and submission of a few scientific papers, listed below.

- C Teixeira, A. Ferreira da Silva, L. A. Rocha, "Computational Fluid Dynamics Sensitivity Analysis of Carbon Nanotubes Synthesis", International Nano Letters (2018) [waiting for peer-revision; submitted in 25-10-2018];
- C Teixeira, A. Ferreira da Silva, L. A. Rocha, "A Computational Fluid Dynamics based tool to support Carbon Nanotubes synthesis by Chemical Vapor Deposition", Materials Research Express (2019) [waiting for peer-revision; submitted in 02-01-2019];
- C Teixeira, A. Ferreira da Silva, L. A. Rocha, "Review on Carbon Nanotubes synthesis by Chemical Vapor Deposition", Journal of Engineering Physics and Thermophysics (2018) [waiting for peer-revision; submitted in 08-10-

2018];

- C Teixeira, A. Ferreira da Silva, L. A. Rocha, "A Computational Fluid Dynamics based Sensitivity Analysis of the Chemical Vapor Analysis process to synthesize Carbon Nanotubes", Journal of Thermal Science and Engineering Applications (2018) [waiting for peer-revision; submitted in 09-10-2018];
- C Teixeira, A. Ferreira da Silva, L. A. Rocha, "Carbon Nanotubes Synthesis: Targeting Optimal Growing Conditions via Computational Fluid Dynamics tools", Poster presented at 5th Nano Today Conference, 6-10 December 2017, Hawaii USA.

References

[1] M. Kumar, Y. Ando, Chemical Vapor Deposition of Carbon Nanotubes: A Review on Growth Mechanism and Mass Production, J. Nanosci. Nanotechnol. 10 (2010) 3739–3758. doi:10.1166/jnn.2010.2939.

[2] A. Matyushov, Growth of Carbon Nanotubes via Chemical Vapor Deposition, Citeseer, 2008. http://www.sciencedirect.com/science/article/pii/S0925963500004465.

[3] K. Balasubramanian, M. Burghard, Chemically functionalized carbon nanotubes, Small. 1 (2005) 180–92. doi:10.1002/smll.200400118.

[4] N. Sinha, J. Ma, J.T.W. Yeow, Carbon Nanotube-Based Sensors, J. Nanosci. Nanotechnol. 6 (2006) 573–590. doi:10.1166/jnn.2006.121.

[5] S.A. Moshkalyov, A.L.D. Moreau, H.R. Guttiérrez, M.A. Cotta, J.W. Swart, Carbon nanotubes growth by chemical vapor deposition using thin film nickel catalyst, Mater. Sci. Eng. B. 112 (2004) 147–153. doi:10.1016/j.mseb.2004.05.038.

[6] J.M. Tan, P. Arulselvan, S. Fakurazi, H. Ithnin, M.Z. Hussein, A Review on Characterizations and Biocompatibility of Functionalized Carbon Nanotubes in Drug Delivery Design, J. Nanomater. 2014 (2014). doi:http://dx.doi.org/10.1155/2014/917024.

[7] Y.M. Manawi, M.A. Atieh, A Review of Carbon Nanomaterials' Synthesis via the Chemical Vapor Deposition (CVD) Method, Materials (Basel). 5 (11AD) 1996–1944. doi:10.3390/ma11050822.

[8] S. Iijima, Helical microtubules of graphitic carbon, Nature. 354 (1991). doi:10.1038/354056a0.

[9] C. Li, E.T. Thostenson, T. Chou, Sensors and Actuators based on Carbon Nanotubes and their composites: A Review, Compos. Sci. Technol. 68 (2008) 1227–1249.

[10] A.T. Sepúlveda, A.J. Pontes, J.C. Viana, R.G. de Villoria, F. Fachin, B.L. Wardle, L. a Rocha, Flexible sensor for blood pressure measurement., Conf. Proc. IEEE Eng. Med. Biol. Soc. 2011 (2011) 512–5. doi:10.1109/IEMBS.2011.6090092.

[11] Q. Cao, J.A. Rogers, Ultrathin Films of Single-Walled Carbon Nanotubes for Electronics and Sensors: A Review of Fundamental and Applied Aspects, Adv. Mater. 21 (2009) 29–53. doi:10.1002/adma.200801995.

[12] A. Agarwal, J. Lang, Foundations of analog and digital electronic circuits, Morgan Kaufmann Publishers, 2005.

[13] K. Balasubramanian, M. Burghard, Biosensors based on carbon nanotubes, Anal. Bioanal.

Chem. 385 (2006) 452–68. doi:10.1007/s00216-006-0314-8.

[14] S. Ghosh, Carbon Nanotube Flow Sensors, Science (80-.). 299 (2003) 1042–1044. doi:10.1126/science.1079080.

[15] J. Kong, N.R. Franklin, C. Zhou, Nanotube Molecular Wires as Chemical Sensors, 287 (2000) 622–625.

[16] Y.-T. Jang, S.-I. Moon, J.-H. Ahn, Y.-H. Lee, B.-K. Ju, A simple approach in fabricating chemical sensor using laterally grown multi-walled carbon nanotubes, Sensors Actuators B Chem. 99 (2004) 118–122. doi:10.1016/j.snb.2003.11.004.

[17] T. Someya, J. Small, P. Kim, C. Nuckolls, J.T. Yardley, Alcohol vapor sensors based on single-walled carbon nanotube field effect transistors, Nano Lett. 3 (2003) 877–881. doi:10.1021/nl034061h.

[18] P. Dharap, Z. Li, S. Nagarajaiah, E. V Barrera, Nanotube film based on single-wall carbon nanotubes for strain sensing, Nanotechnology. 15 (2004) 379–382. doi:10.1088/0957-4484/15/3/026.

[19] S. Sotiropoulou, N.A. Chaniotakis, Carbon nanotube array-based biosensor, Anal. Bioanal. Chem. 375 (2003) 103–5. doi:10.1007/s00216-002-1617-z.

[20] K.G. Ong, K. Zeng, C.A. Grimes, A wireless, passive carbon nanotube-based gas sensor, IEEE Sens. J. 2 (2002) 82–88. doi:10.1109/JSEN.2002.1000247.

[21] K.S. V Santhanam, R. Sangoi, L. Fuller, A chemical sensor for chloromethanes using a nanocomposite of multiwalled carbon nanotubes with poly(3-methylthiophene), Sensors Actuators B Chem. 106 (2005) 766–771. doi:10.1016/j.snb.2004.09.034.

[22] R.K. Roy, M.P. Chowdhury, A.K. Pal, Room temperature sensor based on carbon nanotubes and nanofibres for methane detection, Vacuum. 77 (2005) 223–229. doi:10.1016/j.vacuum.2004.08.023.

[23] S. Chopra, A. Pham, J. Gaillard, A. Parker, A.M. Rao, Carbon-nanotube-based resonant-circuit sensor for ammonia, Appl. Phys. Lett. 80 (2002) 4632–4634. doi:10.1063/1.1486481.

[24] M. Zhang, W. Gorski, Electrochemical sensing based on redox mediation at carbon nanotubes, Anal. Chem. 77 (2005) 3960–3965. doi:10.1021/ac050059u.

[25] A.T. Sepúlveda, R.G. De Villoria, J.C. Viana, A.J. Pontes, B.L. Wardle, L.A. Rocha, Flexible Pressure Sensors: Modeling and Experimental Characterization, Procedia Eng. 47 (2012) 1177–1180. doi:10.1016/j.proeng.2012.09.361.

[26] Carmen K.M. Fung, Maggie Q.H. Zhang, Zaili Dong, Wen J. Li, Fabrication of CNT-based MEMS piezoresistive pressure sensors using DEP nanoassembly, in: 5th IEEE Conf. Nanotechnology, 2005., IEEE, 2005: pp. 353–356. doi:10.1109/NANO.2005.1500728.

[27] E.S. Snow, F.K. Perkins, E.J. Houser, S.C. Badescu, T.L. Reinecke, Chemical detection with a single-walled carbon nanotube capacitor, Science (80-.). 307 (2005) 1942–1945. doi:10.1126/science.1109128.

[28] C. Staii, M. Chen, A. Gelperin, A.T. Johnson, DNA-Decorated Carbon Nanotubes for Chemical Sensing, (2005) 4–9.

[29] A.L. Yost, S. Shahsavari, G.M. Bradwell, R. Polak, F. Fachin, R.E. Cohen, G.H. McKinley, M. Toner, M.F. Rubner, B.L. Wardle, Layer-by-layer functionalized nanotube arrays: A versatile microfluidic platform for biodetection, Microsystems Nanoeng. 1 (2015) 15037. doi:10.1038/micronano.2015.37.

[30] B.J. Landi, R.P. Raffaelle, M.J. Heben, J.L. Alleman, W. VanDerveer, T. Gennett, Single Wall Carbon Nanotube - Nafion Composite Actuators, Nano Lett. 2 (2002) 1329–1332. doi:10.1021/nl025800h.

[31] J. Fraysse, A.I. Minett, O. Jaschinski, G.S. Duesberg, S. Roth, Carbon nanotubes acting like actuators, Carbon N. Y. 40 (2002) 1735–1739. doi:10.1016/S0008-6223(02)00041-6.

[32] R.H. Baughman, Carbon Nanotube Actuators, Science (80-.). 284 (1999) 1340–1344. doi:10.1126/science.284.5418.1340.

[33] S.K. Loganathan, V. Rollin, D. Kim, Rapid Heat Generation using Carbon Nanotubes, in: 58th AIAA/ASCE/AHS/ASC Struct. Struct. Dyn. Mater. Conf., 2017. doi:10.2514/6.2017-1366.

[34] S.K. Loganathan, Windshield Defrost and Deice using Carbon Nanotubes Composite, Embry-Riddle Aeronautical University, 2016.

[35] J. Lee, I.Y. Stein, S.S. Kessler, B.L. Wardle, Aligned carbon nanotube film enables thermally induced state transformations in layered polymeric materials, ACS Appl. Mater. Interfaces. 7 (2015) 8900–8905. doi:10.1021/acsami.5b01544.

[36] J. Lee, X. Ni, F. Daso, X. Xiao, D. King, J.S. Gómez, T.B. Varela, S.S. Kessler, B.L. Wardle, Advanced carbon fiber composite out-of-autoclave laminate manufacture via nanostructured out-of-oven conductive curing, Compos. Sci. Technol. (2018) 1–10. doi:10.1016/j.compscitech.2018.02.031.

[37] J. Lee, I.Y. Stein, E.F. Antunes, S.S. Kessler, B.L. Wardle, Out-of-Oven Curing of Polymeric Composites Via Resistive Microheaters Comprised of Aligned Carbon Nanotube Networks, in: 20th Int. Conf. Compos. Mater., 2015.

[38] J. Lee, F. Daso, S.S. Kessler, B.L. Wardle, Carbon Fiber Prepreg Composite Laminates Cured Via Conductive Curing Using Nanoengineered Nanocomposite Heaters, in: 21st Int. Conf. Compos. Mater., Xi'an, 2017.

[39] J. Lee, In Situ Curing of Polymeric Composites via Resistive Heaters Comprised of Aligned Carbon Nanotube, Massachusetts Institute of Technology, 2014.

[40] G. Gamaly, T.W. Ebbesen, Mechanism of carbon nanotube formatio in the arc discharge, Am. Phys. Soc. 52 (1995) 2083–2089.

[41] A. Morales, C. Lieber, A laser ablation method for the synthesis of crystalline semiconductor nanowires, Science. 279 (1998) 208–11. http://www.ncbi.nlm.nih.gov/pubmed/9422689.

[42] M.J. Height, J.B. Howard, J.W. Tester, J.B. Vander Sande, Flame synthesis of single-walled carbon nanotubes, Carbon N. Y. 42 (2004) 2295–2307. doi:10.1016/j.carbon.2004.05.010.

[43] I. Hinkov, S. Farhat, C.P. Lungu, A. Gicquel, F. Silva, A. Mesbahi, O. Brinza, C. Porosnicu, A. Anghel, Microwave Plasma Enhanced Chemical Vapor Deposition of Carbon Nanotubes, J. Surf. Eng. Mater. Adv. Technol. 4 (2014) 196–209. doi:10.4236/jsemat.2014.44023.

[44] K.A. Shah, B.A. Tali, Synthesis of carbon nanotubes by catalytic chemical vapour deposition: A review on carbon sources, catalysts and substrates, Mater. Sci. Semicond. Process. 41 (2016) 67–82. doi:10.1016/j.mssp.2015.08.013.

[45] J.W. Yan, K.M. Liew, L.H. He, Analysis of single-walled carbon nanotubes using the moving Kriging interpolation, Comput. Methods Appl. Mech. Eng. 232 (2012) 56–67. doi:10.1016/j.cma.2012.03.025.

[46] H. Endo, K. Kuwana, K. Saito, D. Qian, R. Andrews, E.A. Grulke, CFD prediction of carbon nanotube production rate in a CVD reactor, Chem. Phys. Lett. 387 (2004) 307–311. doi:10.1016/j.cplett.2004.01.124.

[47] A.G. Sánchez, L.D. Lvova, V.L. Garza, R.R. Doval, M. de L.M. Sánchez, Computational fluid dynamics in the carbon nanotubes synthesis by chemical vapor deposition, Mater. Res. Soc. Symp. Proc. Vol. 1446 (2012) 25–31. doi:10.1557/opl.2012.1607.

[48] C.R. Oliver, E.S. Polsen, E.R. Meshot, S. Tawfick, S.J. Park, M. Bedewy, A.J. Hart, Statistical analysis of variation in laboratory growth of carbon nanotube forests and recommendations for improved consistency., ACS Nano. 7 (2013) 3565–80. doi:10.1021/nn400507y.

[49] R. White, D. King, Combined Experimental and Simulation (CFD) Analysis on Performance of a Horizontal Tube Reactor Used To Produce Carbon Nanotubes, 7th Int.Conf.on CFD Miner. Process Ind. (2009) 1–5.

Chapter 2

STATE OF THE ART

The main goal of this research work is to design a tool, based in Computational Fluid Dynamics (CFD), to support the transition process between different setups to synthesize Carbon Nanotubes (CNTs). This transition process is currently performed by following a trial-and-error methodology, which, due to the synthesis processes' inconsistency, is a time consuming task [1–4]. Alternatively, a more systematic approach is envisioned.

In this chapter a comprehensive literature review is performed. Firstly, three processes to synthesize CNTs are presented: (i) Arc-discharge; (ii) Laser-ablation; and (iii) Chemical Vapor Deposition (CVD). Although the latter is the most widely used, a comparison between these processes is also presented, giving a better understanding of their operation principle as well as their advantages and disadvantages.

Secondly, a more in-depth study of the CVD process is presented. Here, the critical components in each different phase of the process are described. Moreover, a review of various works found in the literature is performed, depicting several possible compounds combinations which resulted in CNT growth. This analysis demonstrates the CVD process' wide range of possibilities.

Lastly, a description of the working principle of CFD tools is presented, followed by a review on several works, where the CFD capabilities were applied. This review starts by enumerating applications in a broader perspective, narrowing then to CNT synthesis. Performing this review, gives a better understanding on how to take advantage of the CFD capabilities as well as which issues could be encountered.

2.1. CNT Synthesis Processes

Since their discovery in 1991 [5], Carbon Nanotubes (CNTs) have been gaining research interest on the study of their extraordinary properties and applications in various technological fields [6–9]. The three main techniques to synthesize CNTs are: (i) Arc-discharge; (ii) Laser-ablation; and (iii) Chemical Vapor Deposition [10,11]. In this section, these methods are briefly described, depicting their capabilities, and posteriorly compared by analyzing their advantages and disadvantages.

2.1.1. Arc-discharge

In 1991, fine threads of pure carbon were reported by Sumio Iijima when using the arc-discharge technique [5]. Later, in 1993, CNTs were synthesized using a metal catalyst in this method [12,13]. Thus arc-discharge is the oldest method to synthesize CNTs [14]. A typical setup of the arc-discharge technique to synthesize CNTs is illustrated in Figure 2.1.

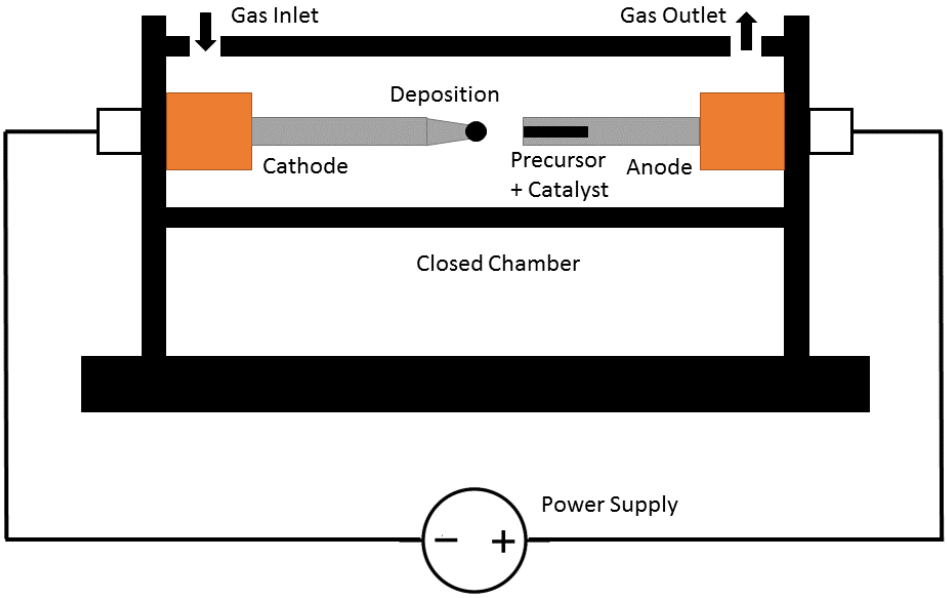

Figure 2.1: Schematic of a typical setup to synthesize CNTs via the Arc-discharge technique.

This method uses a DC-current supply to generate an electrical arc discharge between two electrodes to rapidly produce the high temperature (> 3000 ºC) required to evaporate carbon atoms from a graphite-based precursor, which are then deposited, forming CNTs [10,14–17]. The electrodes are initially kept independently in a vacuum chamber. An inert gas, usually helium or argon, is flown through the chamber to increase the carbon deposition rate. Once the chamber pressure is stabilized, the arc can be generated. Thus, the power supply (20 V and 100 A) is turned on, and the positive electrode (anode) is gradually brought closer to the negative one to strike the electric arc. The arc rapidly increases the temperature at the end of the anode, forming a carbon-based plasma, which is then deposited onto the negative electrode (cathode). In order to boost the deposition, besides graphite, the anode is also packed with a catalyst, such as iron, cobalt or nickel, whose atoms are also evaporated into the plasma. The electrodes are kept about one millimeter apart to keep the CNT deposition in the cathode constant until the desired length is reached. The power supply is then turned off and the setup is left for cooling.

Although the electrical arc is a suitable technique to rapidly generate the required temperature to evaporate the carbon atoms into a plasma, its control plays an important role when synthesizing CNTs by the arc-discharge process [14,15]. Moreover, the resulting yield and purity of the CNTs also depend on the inert gas atmosphere pressure. If proper precaution is not taken, the carbon-based plasma would be unstable and carbon soot materials are formed in the chamber walls.

2.1.2. Laser-ablation

The laser-ablation technique was first used to synthesize CNTs by Thess et al. in 1996 [18]. Similar to the arc-discharge process, laser-ablation relies in the vaporization of carbon atoms, which are then deposited into a substrate [14]. A graphical representation of a typical setup of the laser-ablation method is depicted in Figure 2.2.

The laser-ablation method uses a laser to rapidly heat up (> 3000 ºC) and vaporize a graphite-based precursor, placed inside a quartz tube, filed with an inert gas [10,19–21]. Moreover, similar to the arc-discharge method, the precursor is doped with a metallic catalyst, such as iron, nickel or cobalt, which eases the carbon atoms deposition. The inert gas, usually argon or helium, serves as an atmosphere, through which the carbon-metal plasma is carried out until the deposition site, where it cools down and condense into CNTs

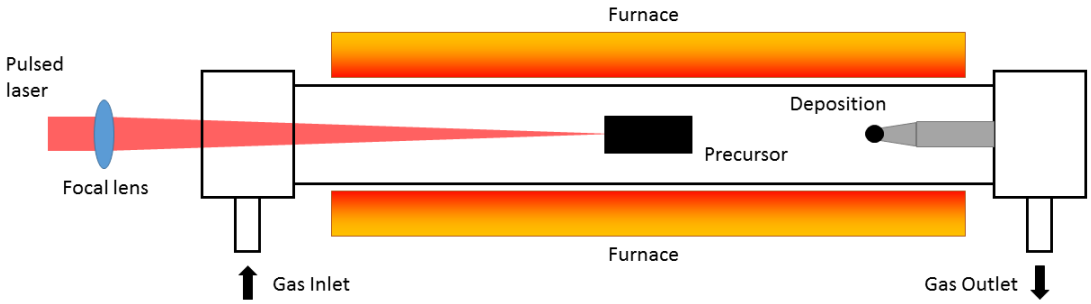

Figure 2.2: Schematic of a typical setup to synthesize CNTs via the Laser-ablation technique.

[21]. This process goes on by changing the laser's focus point across the precursor's surface.

When compared to the arc-discharge technique, the laser-ablation produces purer CNTs due to the evaporation stability [22]. However, it also has control issues related with the evaporation process. For instance, the laser is a critical parameter to tune and control. Not only can the laser configuration (continuous, single or double pulsed) be changed but also its wavelength [21,22]. Moreover, similar to what occurs in the arc-discharge method, the plasma-atmosphere interaction also plays a role in the CNTs yield. Thus, proper attention should be taken when tunning the inert gas pressure and flow [14].

2.1.3. Chemical Vapor Deposition

On the contrary to the arc-discharge and laser ablation techniques, which use localized high temperatures to decompose a solid precursor, the Chemical Vapor Deposition (CVD) is essentially a thermal dehydrogenation reaction of a hydrocarbon gas [11,14]. CNT synthesis by the CVD method was first achieved by Yacaman et al. in 1993 [23]. Figure 2.3 graphically depicts a typical CVD setup to synthesize CNTs.

As aforementioned, this technique is based in the temperature-driven breakdown of a hydrocarbon gas, such as ethylene and acetylene, into hydrogen and carbon atoms

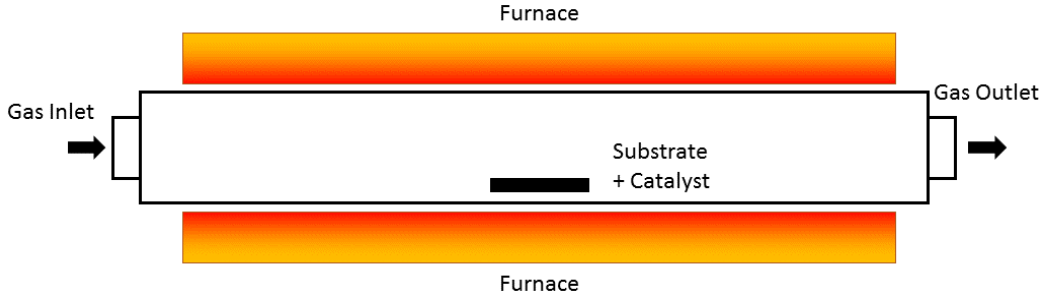

Figure 2.3: Schematic of a typical setup to synthesize CNTs via the Chemical Vapor Deposition technique.

[6,10,11]. This dehydrogenation reaction occurs inside a quartz tube, heated by a furnace (400-1200 ºC), through which the hydrocarbon is flown. Once decomposed, the carbon atoms are deposited in a substrate, previously coated with a metallic catalyst, such as iron, nickel and cobalt. Similarly to the other methods to synthesize CNTs, this catalyst eases the carbon atoms deposition into CNTs [14]. In order to control the pressure inside the tube without affecting the compounds reactions, an inert gas, such as argon and helium, is also flown through the tube, creating an inert atmosphere. Moreover, this gas is also used to clean the tube prior to the synthesis process.

When compared to the arc-discharge and laser ablation processes, the type of precursor is in gaseous form, instead of solid, which considerably reduces the required temperature to isolate the carbon atoms (400-1200 ºC instead of > 3000 ºC) [11,14]. In addition, it does not require as complex equipment, facilitating the CVD usability. Furthermore, the major process parameter to control is the gases flows. Not only the hydrocarbon, which affects the generated carbon atoms, but also the inert gas, which affects the pressure inside the tube.

2.1.4. Comparison

Previously, three different techniques to synthesize CNTs were presented and briefly described: (i) arc-discharge; (ii) laser-ablation; and (iii) chemical vapor deposition (CVD). On recap, they have some similarities. For instance, all three rely on a thermal breakdown of a carbon-based precursor in order to individualize the carbon atoms. Moreover, a metallic catalyst, such as iron, nickel or cobalt, is used to reduce the breakdown temperature and thus boost this process. In addition, an inert gas, such as argon or helium, is used to control the process pressure as well as to create an inert atmosphere for the breakdown reaction to occur.

As for these techniques' differences, these are related with the physical mechanisms used to achieve the thermal breakdown. Using a carbon-based precursor in a solid state, such as graphite, in both the arc-discharge and laser ablation methods a higher temperature is necessary to achieve the carbon atoms evaporation (>3000 ºC), when compared to the CVD, which uses temperatures in the 400-1200 ºC range. Another difference between the techniques is where the catalyst is positioned. In the CVD technique, it is usually positioned in the deposition site, targeting a localized dehydrogenation of the hydrocarbon gas. On the

other two processes, the precursor is doped with catalyst particles, being both of them heated up into a plasma plume, which travels through the inert atmosphere until the deposition site.

The similarities and differences between the three different techniques, previously presented and described, induce some dependencies of the result, i.e. the synthesized CNTs, on a few process parameters [10,11,14]. Table 2.1 presents these dependencies as well as each synthesis process advantages and disadvantages.

Due to its complexity, Laser-ablation is the CNT production technique with most variables to control. Besides the aforementioned laser's wavelength and power, the atmosphere should be controlled. It can be altered by the inert gas flow and pressure, as well as by the furnace temperature. On the other hand, arc-discharge is the process with less dependencies on individual variables. Although also having an inert atmosphere, which affects the plasma-plume behavior, and having an arc discharge to control instead of a laser,

Table 2.1: Comparison between the Arc-discharge, the Laser-ablation and the CVD techniques to synthesize CNTs (adapted from [10,11,14]).

Technique	Arc-discharge	Laser-ablation	CVD
Variables to control	• Arc current • Inert gas • Pressure	• Amount of catalyst • Laser (power and wavelength) • Temperature • Pressure • Inert gas	• Hydrocarbon gas • Flow • Temperature • Catalyst
Yield	Low	Low	High
Operating Temp.	> 3000 ºC	> 3000 ºC	400-1200 ºC
Purity	Low	Medium	Medium to High
Cost	High	High	Low
Advantages	• Controlled atmosphere not required (open-air synthesis has been achieved [57]) • Not as expensive as Laser-ablation	• Higher quality and yield than Arc-discharge	• More controlled synthesis • Ideal for scale-up • High production yield [6]
Disadvantages	• Produced CNTs are tangled (limited applications) • Rely on carbon atoms evaporation (>3000 ºC)	• Produced CNTs are tangled (limited applications) • Rely on carbon atoms evaporation (>3000 ºC)	• May have graphite layers in the CNTs caps, not ideal for certain applications [10]

it does not use an external furnace, thus reducing the number of variables to control. As for the CVD technique, its simplicity makes the materials selection the only control variables. Furthermore, operating at lower synthesis temperature increases the process stability and, thus, its controllability. Due to these physical differences, the CVD process has a lower setup cost than the others [10,11,14].

As for the produced CNTs, in the arc-discharge and the laser-ablation techniques the CNTs' purity is compromised by their high operation temperature, which leads to the formation of unwanted carbon soot materials [14]. Moreover, the produced CNTs are tangled and may have structural defects, hindering their applications. This instability, resulted from the processes' complexity, reduces the CNTs production rate.

Besides being the synthesis process with the highest production yield, the Chemical Vapor Deposition is the technique with the most controlled synthesis, mainly due to its targeted hydrocarbon decomposition and deposition. Moreover, it requires lower temperatures than the Arc-discharge and Laser-ablation (400-1200 ^{o}C compared to >3000 ^{o}C) and achieves untangled growth, which eases the CNTs application [6,7,9,24]. This advantages pertain the process' scalability [11,14].

2.2. CNTs Synthesis by Chemical Vapor Deposition

As aforementioned, CVD is the most popular process to synthesize CNTs, due to its simplicity, low-cost and high controllability of the synthesis [6,10]. This technique is based on the thermal decomposition of a hydrocarbon gas - precursor - and posterior precipitation and deposition of the resulting carbon atoms in a catalyst sample, placed inside a quartz tube. Besides the precursor, the CVD process usually involves a reducer and an inert gas as well. While the former is used to reduce the catalyst into small particles, where the carbon atoms will be deposited, the inert gas is mainly used to ensure pressure control and heat transfer during the whole process. This section, describes in more detail the CVD process to synthesize CNTs, starting with a brief overview of all its different phases, followed by an overview of the process parameters found in the literature, namely the used compounds and the furnace temperature.

2.2.1. The CVD Process Phases

As previously stated, the two main phases of the CVD process to synthesize CNTs

are the reduction and the synthesis phases. However, there are a total of common five distinct phases in the whole process (see Figure 2.4): (1) cleaning; (2) reduction; (3) synthesis; (4) delamination; and (5) cooling.

During the cleaning phase, both the tube is cleaned by flowing the inert gas through it. The goal is to reset the tube inner conditions in terms of gas composition, being mainly composed of the inert gas.

The second phase - reduction - is important by two reasons. Firstly, it is in this phase that the furnace is heated until the desired temperature (400 - 1200 ^{o}C), necessary for the CNT synthesis. Secondly, it is in this phase that the catalyst film is decomposed into nanoparticles. Example images taken before and after such phenomenon are presented in Figure 2.5. Such nanoparticles define the density and vertical alignment of the CNTs. Basically, sets where the carbon atoms are going to aggregate during the growth phase.

As suggested by its name, it is in the synthesis phase (number 3) when the CNTs' growth occurs, which is a result of the local decomposition of the hydrocarbon gas pyrolysis

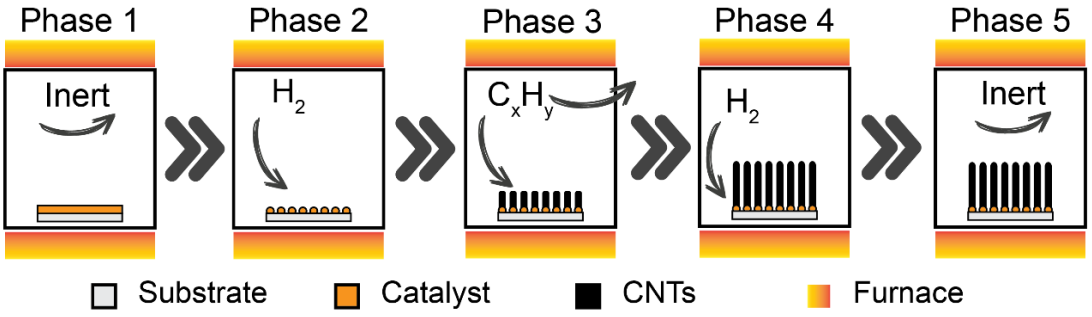

Figure 2.4: Graphical representation of all five phases the CVD process to synthesize CNTs: (1) cleaning; (2) reduction; (3) synthesis; (4) delamination; and (5) cooling.

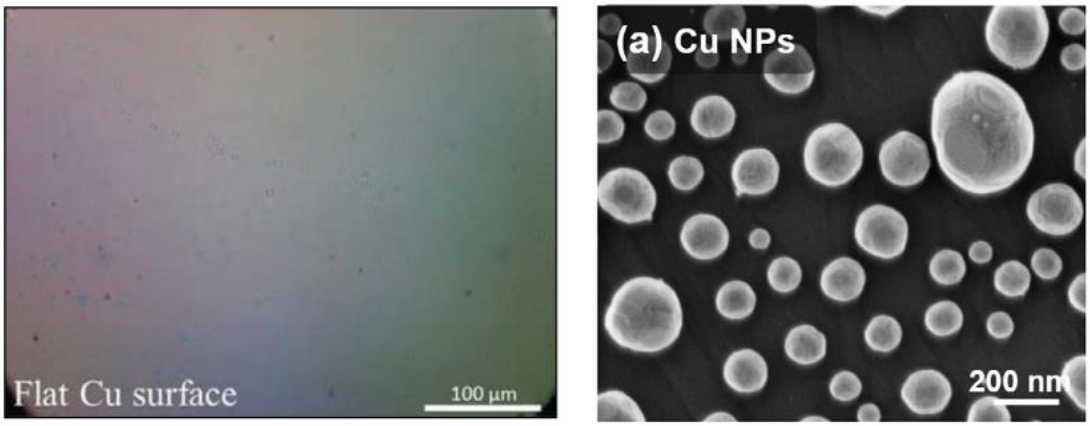

(a) **(b)**

Figure 2.5: Images of a copper catalyst (a) before and (b) after its reduction from film into nanoparticles. (Adapted from [58,59], licensed under a Creative Commons Attribution 3.0 License).

and the aggregation of its carbon atoms onto the catalyst nanoparticles. Moreover, it is possible to add a carrier gas to support the CNT growth. This process is highly dependent on the temperature throughout the tube, the gas flows, pressure, and the substrate position inside the tube, among others.

The fourth phase - delamination - is an optional one. Its main goal is to delaminate the CNTs from the catalyst base. This is achieved with a dewetting phase, where the high temperatures and the presence of H_2 increases the catalyst particles mobility, which aids the CNTs' releasing.

Lastly, the cooling phase is used to prepare the tube for its opening and the CNTs removal. In this phase, only the inert gas is passing through the tube to enhance the heat transfer. It also removes other gases from the tube to ensure the user's safety when opening the tube.

As suggested by this five-phase procedure, the CNT synthesis by CVD involves many process parameters, which have influence in the final result. Being a process, which relies in the thermal decomposition of compounds, it highly depends on the temperature and the compounds as well as catalyst selection. The following section depict a brief overview of these parameters.

2.2.2. The CVD Process Parameters

Table 2.2 compiles the process parameters used in several studies from the literature to synthesize CNTs. The depicted parameters are: (i) the hydrocarbon precursor; (ii) the carrier gas; (iii) the reducer; (iv) the inert gas; (v) the catalyst; and (vi) the process temperature.

The hydrocarbon’s molecular structure affects the morphology of the produced CNTs. Various types of hydrocarbons have been successfully used to synthesize CNTs [6,11,14], and the most commonly used are acetylene (C_2H_2) [25], methane (CH_4) [26], xylene (C_8H_{10}) [27], ethanol (C_2H_5OH) [28], benzene (C_6H_6) [29], ethylene (C_2H_4) [30] and carbon monoxide (CO) [31]. Thus, properly selecting the used precursor can increase the CNT growth rate [11]. For instance, linear hydrocarbons, such as methane, ethylene and acetylene, thermally decompose into atomic carbon atoms (pyrolysis), leading to straight CNTs. On the other hand, cyclic hydrocarbons like benzene and xylene produce relatively tangled CNTs.

Table 2.2: Compilation of various compounds, catalysts and temperatures used in the literature to synthesize CNTs via the CVD process.

Ref.	Precursors	Carrier	Reducer	Inert	Catalyst	Temp. [ºC]
[25]	Acetylene Ethylene	Nitrogen	Hydrogen	-	Iron	650-800
[26]	Methane	-	-	Argon	Cobalt Nickel Iron	1000
[27]	Acetylene Xylene	Ferrocene	Hydrogen	Argon	-	550-800
[60]	Acetylene	Nitrogen	Hydrogen	-	Iron	700
[28]	Methane Ethane Ethanol	-	Hydrogen	Argon	Iron Cobalt Molybdenum	700-800
[29]	Benzene	-	Hydrogen	Argon	Ferrocene Cobaltocene Nickelocene	900
[30]	Methane Ethane Ethylene	-	Hydrogen	-	Cobalt Nickel Iron	500-700
[35]	Cyclohexanol Xylene	Nitrogen	-	-	Ferrocene	750
[61]	Xylene	Ferrocene	Hydrogen	Argon	Nickel	700-850
[32]	Xylene	Ferrocene	-	-	-	800
[62]	Butane	-	Hydrogen	Helium	Iron	500-700
[36]	Ethanol	-	-	Argon	Iron	800
[63]	Benzene	-	Hydrogen	Argon	Iron	1060
[23]	Acetylene	Nitrogen	Hydrogen	-	Iron	700
[31]	Carbon Monoxide	-	-	Argon	Molybdenum Nickel Cobalt	1200
[38]	Carbon monoxide Ethylene	-	Hydrogen	Argon	Iron Molybdenum	800
[64]	Methane	-	Hydrogen	-	Iron Cobalt Nickel	1070
[65]	Benzene	Thiophene	Hydrogen	-	Ferrocene	1200
[33]	Fullerene	Ethanol	-	Argon	Iron Cobalt	850
[66]	Methane Alcohol Ethylene Cyclohexane	-	Hydrogen	-	Nickel Iron Cobalt Molybdenum	400
[34]	Methanol	Ethanol	-	Argon	Iron Cobalt	550-800
[67]	Ethylene	-	Hydrogen	Argon	Aluminum	750
[68]	Acetylene	Nitrogen	Hydrogen	-	Nickel	900
[69]	Xylene	-	Hydrogen	Argon	Ferrocene	780-860
[37]	Acetone	Thiophene	-	Argon	Ferrocene	1170

Besides the hydrocarbon-based precursor, a carrier gas, such as nitrogen (N_2) and ferrocene ($C_{10}H_{10}Fe$), can also be injected into the tube during the synthesis phase. Such inclusion can be done as a way to inject catalyst particles into the tube, as an alternative to priory placing it in the tube. Authors in [27,32] mixed the hydrocarbon precursor with

ferrocene, which would thermally decompose, leading the iron particles to interact directly with the precursor, synthesizing CNTs. On the other hand, the carrier gas can be included in the synthesis phase to help the precursor decomposition and carbon's aggregation to the catalyst particles. For instance, ethanol can be used to ease the hydrocarbon decomposition [33,34].

As aforementioned, the reducer is used to reduce the catalyst into smaller particles, which would serve as base to synthesize CNTs. The dominant selection for the reducer is hydrogen (H_2). The only exceptions are when: (i) the catalyst is inserted inside the tube as a powder [26,31,35]; (ii) the hydrocarbon precursor is also used as the reducer [36]; or (iii) all compounds are injected simultaneous, being the CNTs collected in a structure placed inside the tube [37].

As a way to control the pressure and the compounds flow inside the tube, as well as to maintain the heat transfer, an inert gas can be used in the CVD process. Argon (Ar) and helium (He) are the most commonly used ones (see Table 2.2). In the cases where there is no inert gas involved in the process, the conditions inside the tube are controlled using the reducer and/or the carrier gas, usually hydrogen (H_2) and nitrogen (N_2), respectively.

Alongside with the hydrocarbon precursor, the catalyst is also considered one of the process parameters, whose selection most influences the CNT synthesis [6,11,14]. Properly selection of the used catalyst can improve the CNTs yield and quality. As previously stated, catalyst particles serve as nucleation sites for the CNT growth. Various options were found in the literature, and the most common are metallic catalysts, such as iron (Fe) [25], nickel (Ni) [26], cobalt (Co) [30] and molybdenum (Mo) [38].

Finally, CNT synthesis by CVD has been achieved in various temperatures (see Table 2.2). Being based in the thermal decomposition of compounds, the CVD process only requires temperatures within a certain range (400-1200 ^{o}C) to be used. The fact that certain CNT growth can be achieved at smaller temperatures than others only depends on the compounds and catalyst used.

2.3. CFD Fundamentals

Computational Fluid Dynamics (CFD) is a branch of the fluid mechanics field, developed in the late 1920s, which uses mathematical modeling and numerical algorithms

to analyze problems involving fluid flows and heat transfer [39–43]. Advances in numerical description of all types of fluid flows have matured CFD into a powerful numerical tool in many industries, considered as *"the traditional method for experimentation and analytical modelling to solve fluid flow problems"* [39]. These problems are described by partial differential equations, which cannot be analytically solved. Alternatively, CFD simulations use discretization methods to approximate those differential equations into a system of algebraic equations, which can then be computationally solved via numerical algorithms [42]. Such usage of CFD methods has been triggered by the associated low costs and reduced time consumption, when compared to trial-and-error experimentation processes. However, these advantages rely on solving the equations accurately. Since the numerical algorithms used in CFD simulations are an iterative process, if enough iterations are not performed, the exact solution is not produced [42].

2.3.1. Phases of a CFD simulation

In order to tackle such fluid flow problems, typical CFD simulations consist of three main phases: (1) the pre-processing; (2) the solver; and (3) the post-processing. Each one deals with crucial components of the CFD methodology.

The first phase - the pre-processing - consists in the introduction and description of all relevant data for the problem solving [42]. Such data is formulated as:

- Definition of the computational domain, i.e. geometry, to be modelled;
- Discretization of the computational domain into a mesh;
- Definition of the fluid properties, such as density, viscosity, modal mass, etc;
- Definition of the variables to be analyzed;
- Definition of domain's boundary conditions.

The solver is the phase responsible for the numerical algorithms implementation. Since it is in this phase that the final solution is computed, the solver is the main phase of a CFD simulation [40]. During this phase, the following steps are executed:

- Integration of the fluid related differential equations;
- Approximation of the differential equations into a system of algebraic equations;
- Iteratively solve the algebraic equations until a convergence criterion is meet.

After the numerical algorithms are performed, the computed solution can be analyzed in the post-processing phase. Most CFD simulations are equipped with data visualization tools to support this phase. Typical visualization tools are plots, flow streamlines and surfaces graphics.

2.3.2. Components of a CFD simulation

As previously described, each one of the three phases (pre-processing, solver, and post-processing) has its own steps, which, when combined, comprise the components of a CFD simulation. These will be briefly described in this section. Since the pre-processing phase is the one mostly defined by the user, an example of a CFD simulation setup was thought and a figure depicting each of its components is presented.

Geometry

Usually described by a Computer-Aided Design (CAD) model, the geometry is a 3D representation of the physical system to be analyzed in the CFD simulation. Figure 2.6 depicts the CAD model, used in the CFD simulation example. The used shape was a cylindrical tube, with 10 mm radius and 10 cm length.

Mesh

Discretizing the simulation domain into a mesh consists in dividing it in smaller volumes (also referred as cells or elements). This set of elements physically describe the geometry points into which the differential equations will be later discretized [40,42]. A

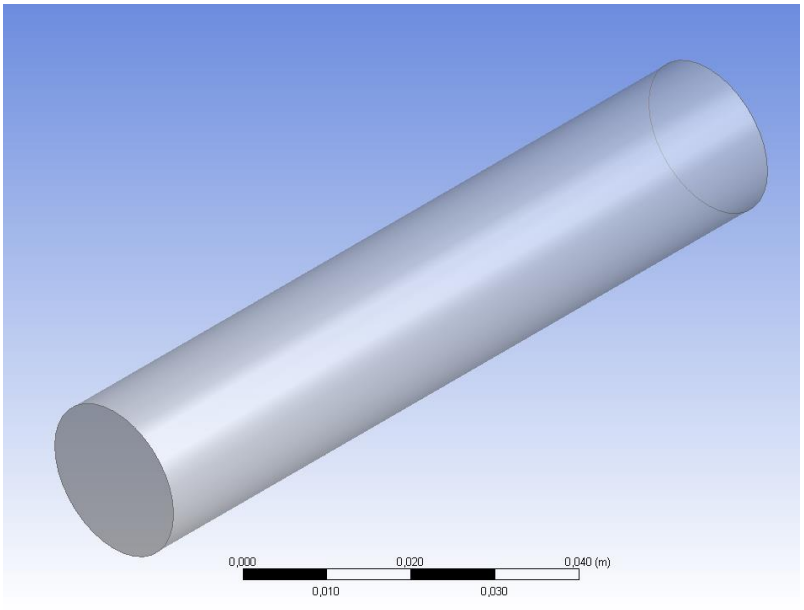

Figure 2.6: Model of the cylindrical shape to be used in the CFD simulation example.

finer mesh, containing more elements, leads to a solution where more points are being computed per iteration. This not only increases the solution resolution but also the computational demands and the simulation time, since more points are being computed. Figure 2.7 depicts two possible meshes for the CFD simulation example. As shown, a finer mesh results into more elements.

Boundary conditions

These conditions complement the model geometry by representing a set of constraints to be taken into account in the CFD simulation. They can express any constant flow, pressure, temperature, initial conditions, etc. These boundary conditions are later used by the solver as parameters for the equations to be solved.

For the CFD example, it was thought a simulation where gases would flow through the designed cylindrical tube. Thus, its ends were set as the inlet and outlet, whereas the lateral surface was set as a fixed-wall. These conditions are shown in Figure 2.8. The inlet defines which gases enter the tube, at what temperature and velocity. The temperature of the wall can also be defined.

Mathematical model

As aforementioned, CFD tools are used to solve fluid flows problems expressed by a set of differential equations. This mathematical model is the starting point of the numerical method used by the CFD solver. The behavior of a fluid is determined by a set of conservation laws, which describe the variation of a given property, such as mass,

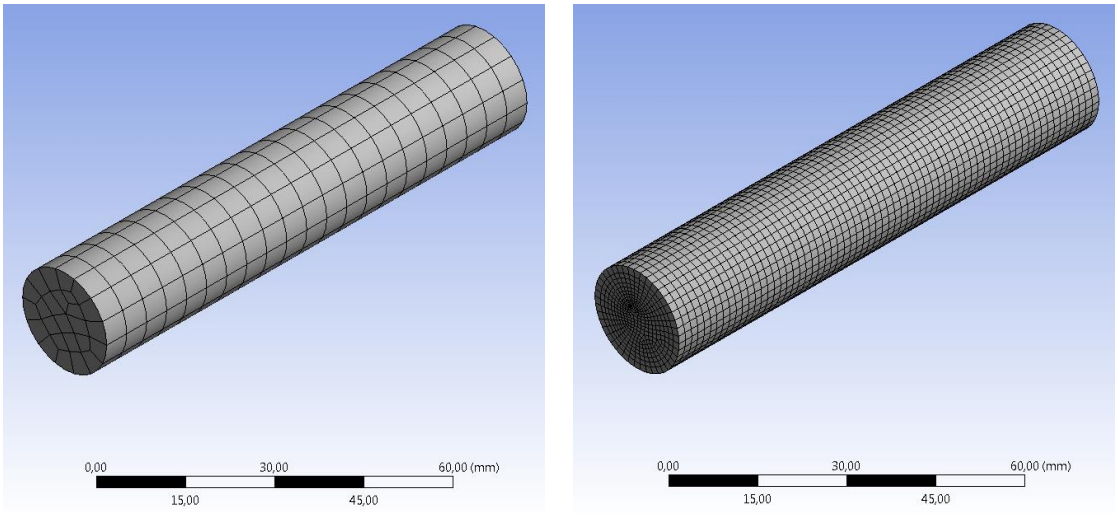

(a) **(b)**

Figure 2.7: A (a) coarse and (b) finer mesh of the cylindrical shape to be used in the CFD simulation example.

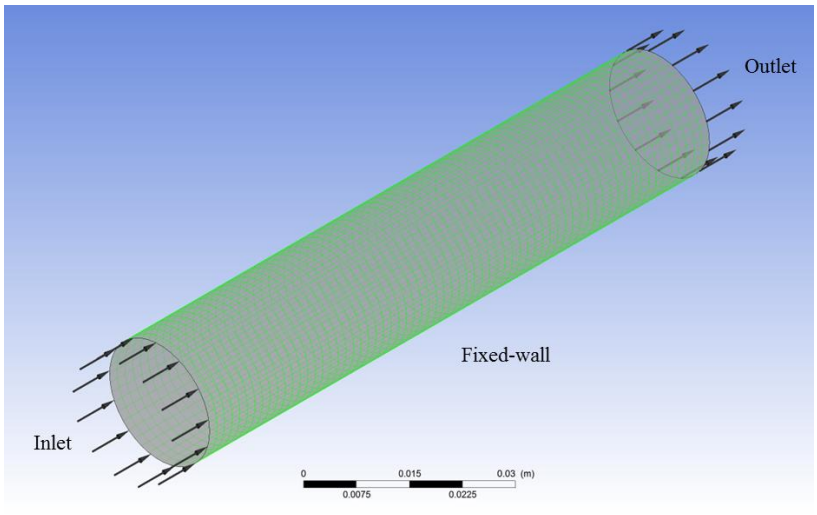

Figure 2.8: The specified boundary conditions for the CFD simulation example: an inlet, an outlet and a fixed-wall.

momentum or energy, for a given quantity of matter [40,42]. In this quantity of matter, the law of conservation of mass states that the variation of mass (m) with time (t) is zero (see Eq. 2.1). As for momentum (mv), which can only be changed by external forces (f), the conservation law is expressed by Eq. 2.2, where v stands for velocity. Eq. 2.3 expresses the law of conservation of energy (E), which depends on the total energy entering or leaving the addressed quantity of matter (E_{in} and E_{out}, respectively).

$$\frac{dm}{dt} = 0 \qquad \textbf{Eq. 2.1}$$

$$\frac{d(mv)}{dt} = \sum f \qquad \textbf{Eq. 2.2}$$

$$\frac{d(E)}{dt} = \sum E_{in} - \sum E_{out} \qquad \textbf{Eq. 2.3}$$

In fluids, however, since following a specific parcel of matter is difficult, it is more convenient to apply these laws to a spatial region, referred as the control volume (CV) [42]. In this region, the law of conservation of mass of a fluid with density ρ can be written as in Eq. 2.4, where the first parcel denotes variation of mass within the volume itself (Ω) and the second parcel represents changes of mass due to fluid entering or leaving the region, through its surface S, with a given velocity v. The unit vector n only denotes if the fluid is entering or leaving the control volume.

$$\frac{\partial}{\partial t}\int_{\Omega} \rho \, d\Omega + \int_{S} \rho v \cdot n \, dS = 0 \qquad \textbf{Eq. 2.4}$$

As for the law of conservation of momentum, it can be expressed by Eq. 2.5, where the external forces f can be surface forces (pressure, stresses or surface tensions) or body forces (gravity or centrifugal forces) [42]. The first parcel of the equation is the time rate change of the momentum in the volume itself (Ω), whereas the second parcel represents variations of momentum due to fluid entering or leaving the volume, through its surface S, with a given velocity v.

$$\frac{\partial}{\partial t}\int_{\Omega} \rho v \, d\Omega + \int_{S} \rho v v \cdot n \, dS = \sum f \qquad \textbf{Eq. 2.5}$$

The law of conservation of energy is expressed by Eq. 2.6. As before, the first parcel represents the time rate change of energy (e) in the volume (Ω) and the second one denotes variations of energy due to fluid flows through its surface S.

$$\frac{\partial}{\partial t}\int_{\Omega} e\rho \, d\Omega + \int_{S} e\rho v \cdot n \, dS = \sum E_{in} - \sum E_{out} \qquad \textbf{Eq. 2.6}$$

These laws of conservation are combined into a mathematical model of differential equations, which describe the behavior of any fluid in a given system. They are used by the CFD tool to tackle any fluid related problem and to produce a solution to it.

Discretization method

In order to solve the mathematical model, the differential equations must be approximated into a system of algebraic equations, which can then be computationally solved. This approximation is performed using a suitable discretization method [42]. The mostly used approaches are the Finite Differences, Finite Volume and Finite Elements Methods.

The Finite Differences Method (FDM) is the easiest method to use for simple geometries. Using the conservation equations in differential form as its starting point, FDM uses polynomial fitting algorithms to approximate the differential equations for each node of the mesh. This results in one algebraic equation per node, at which the value of a certain variable is unknown. The variable values are then calculated using those algebraic equations and not taking into account the values in neighbor nodes. Its disadvantages are

the usage restriction in less complex geometries, and it does not ensure the conservation laws, requiring more attention [42].

The Finite Volumes Method (FVM) uses the integral form of the conservation equations as its starting point. Using the domain's mesh, it divides the geometry into a finite number of contiguous CVs. The conservation equations are applied to each CV and interpolation is used to generate a value of a certain variable at its center. This results in an algebraic equation for each CV center, which depends on the neighbor CVs. Since the geometry mesh only defines the CVs limits, and not the nodes for discretization, FVM can be used in any type of mesh, regardless of its complexity.

Similar to FVM, the Finite Elements Method (FEM) breaks the domain into a set of discrete volumes, which are generally triangular or quadrilateral based. The differential equations are approximated by a linear function, constructed from the variable's values at the corners of each element, ensuring the solution continuity. Since it uses triangular or quadrilateral based discretization, FEM is suitable to any arbitrary geometry, regardless of its complexity, and are relatively easy to analyze mathematically. However, its application is compromised if the geometry mesh is not well structured [42].

Solver method

The discretization process results in a system of algebraic equation, whose solution describe how fluids behave throughout the analyzed geometry. There are two types of methods to compute this solution: direct and indirect methods [40].

Direct methods, such as the Gaussian Elimination, use algebraic operations to simplify and solve the equations system. Their efficiency decreases with the system size, since more operations are required. In order to achieve a reliable solution to the fluid problem, a denser mesh, with more elements, is required, which increases the equation system size and, consequently, decreases the efficiency of the direct methods. For such reason, typical CFD tools rarely use direct methods to solve the algebraic system [40,42].

Instead of mathematically solving the algebraic equation system, indirect methods, also referred as iterative methods, tackle the problem by guessing a solution for the system. The algebraic equations are then used to evaluate this solution by its residual error. This residual error is then used to support the guessing process of a new solution. This process is repeated iteratively until a convergence criterion is met [42].

Convergence criterion

As aforementioned, typical CFD tools use iterative methods to solve the system of algebraic equations. These methods are constantly guessing a solution to the system and use the residual errors to improve the generated solution. Since they are not mathematically solving the system, this iterative procedure can be continuously performed [40,42]. Thus a previously specified convergence criterion is used to stop it. Usually it is defined as a maximum residual error when evaluating the current solution. Moreover, typical CFD tools also allow the specification of a maximum number of iterations to perform, after which the iterative method stops, regardless of whether the convergence criterion was met.

2.4. Usage of CFD Tools

CFD has proven to be a powerful low-cost and faster tool to numerically solve fluid flow problems in many industries [39–43]. Thus, there are several companies which have invested in the development and distribution of CFD codes [44]. These commercial codes have been widely used in various fields, such as aerospace, automotive, healthcare, construction, etc [45]. Amongst others, the most commonly used FEM/FVM codes are ANSYS FLUENT, ANSYS CFX, ANSYS FLOTRAN, ADINA, STAR-CD, COMSOL, FLOW3D, FIDAP and CFD-ACE. The choice on one commercial code over the others depend on their computational capabilities and specifications, the used discretization method and, perhaps most importantly, price. These software are licensed commercially or educationally, permanently or yearly and their licenses can range up to a few tens of thousands of US Dollars [44–46].

In the literature, CFD tools have been used to model and understand various systems, such as the avascular tumor growth [47], the respiratory system [48], interactions between fluids and moving objects [49]. Regarding CNTs, the usage of such numerical tools has been reported to assist their production [4], interpreting the synthesis process [1] and predict its performance [3]. This section presents a few works where CFD tools have been used, not only applied to CNT synthesis but also in other fields.

2.4.1. CFD Tools Applications

The CFD capabilities have been used to analyze and understand systems in a wide range of technological fields. From medical applications to more technical ones, CFD tools

can be used to analyze fluid-fluid and fluid-solid interactions in any system.

For example, Collis et al. have validated the usage of CFD tools to analyze drug- and nutrient-limited tumor growth [47]. With the intention to obtain a better understanding of a drug treatment efficacy, the cancer was studied as a multiscale system and the correct discretization of its microstructure and microvasculature was accessed.

Also in the medical field, authors used CFD tools to analyze flow-tissue interactions present in the respiratory system [48]. More specifically, they focused in the lung deformation due to airflow. Combining different types of airways and lung parenchyma, they constructed a robust model, which was posteriorly validated by clinical measurements. Figure 2.9 depicts their results when measuring the oxygen partial pressure in various sections of a healthy and diseased lungs. On the latter, the unhealthy section was the bottom one, which was not oxygenated.

In a more technical-themed application, Yang et al. have developed a CFD-based model to study interactions between a fluid and a rotating structure [49]. The understanding of these interactions is considered critical to the design and evaluation of hydro-turbines, jet-engines and heart pumps. In fact, the model was applied to a hydro-turbine under a prescribed angular velocity, which was used to numerically validate the model's accuracy. Figure 2.10 shows the effects of the fluid in the rotating system. Due to the fluid impact, the system starts spinning in a clockwise motion, which also has an effect in the fluid behavior.

In his paper, Blocken performed a review on the CFD application in urban physics [50]. Referring to the heat and mass transfer in urban environments and its interactions, urban physics are usually modelled by CFD tools. In his review, the author lists various

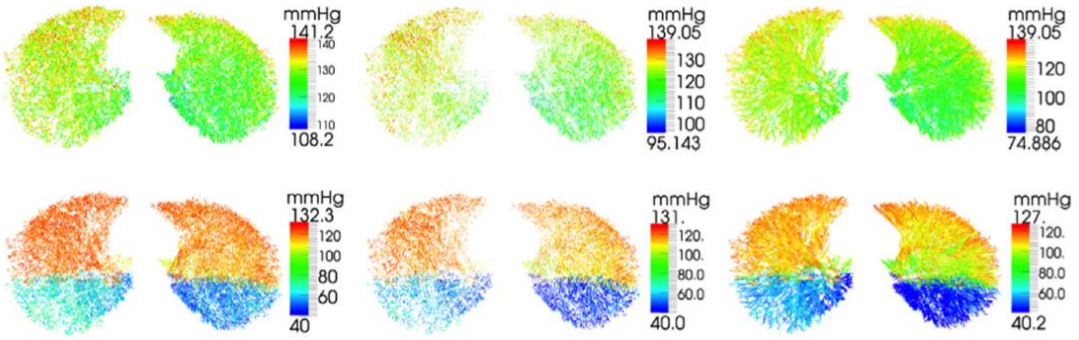

Figure 2.9: Results obtained by Roth et al. when measuring the oxygen partial pressure in the respiratory zone (left), blood capillaries (middle), and pulmonary veins (right) of the healthy (top) and diseased (bottom). (Reprinted from [48], Copyright (2017), with permission from Elsevier).

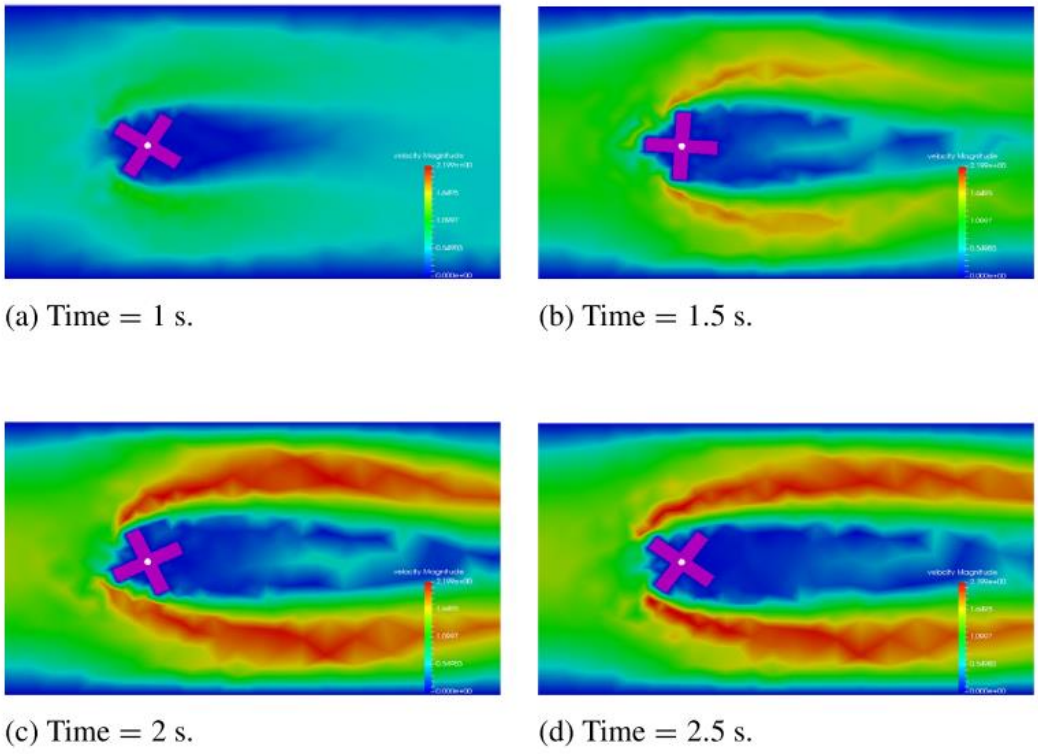

Figure 2.10: Simulation of the effects of a fluid in a rotating system performed by Yang et al. It is presented the evolution of magnitude of velocity with time. (Reprinted from [49], Copyright (2016), with permission from Elsevier).

examples where CFD has been applied to this field, pertaining its capabilities and potential: urbanization, climate change, energy, health, security, etc.

In [51], Xiang et al. also addressed the CFD capabilities, more specifically, in the evaluation of intracranial aneurysms. After proposing that both high and low wall shear stress drive the aneurysm growth, authors delineated different wall shear stress parameter to be analyzed via CFD tools. Although being promising, the application of CFD in aneurysm still requires further research regarding the comparison between the CFD results and their clinical utility.

CFD tools were also used to simulate a Light Emitting Diode (LED) luminaire as a way to complement its characterization [52]. Due to existing regulations regarding the illumination field of view in the automotive industry, the thermal resistance of a LED is a critical parameter when designing an efficient cooling package. Thus, authors have combine characterization with CFD simulation to more accurately analyze the LED luminaires, when attached on a heatsink (see Figure 2.11).

All these studies pertain the CFD capabilities and potential on analyzing and

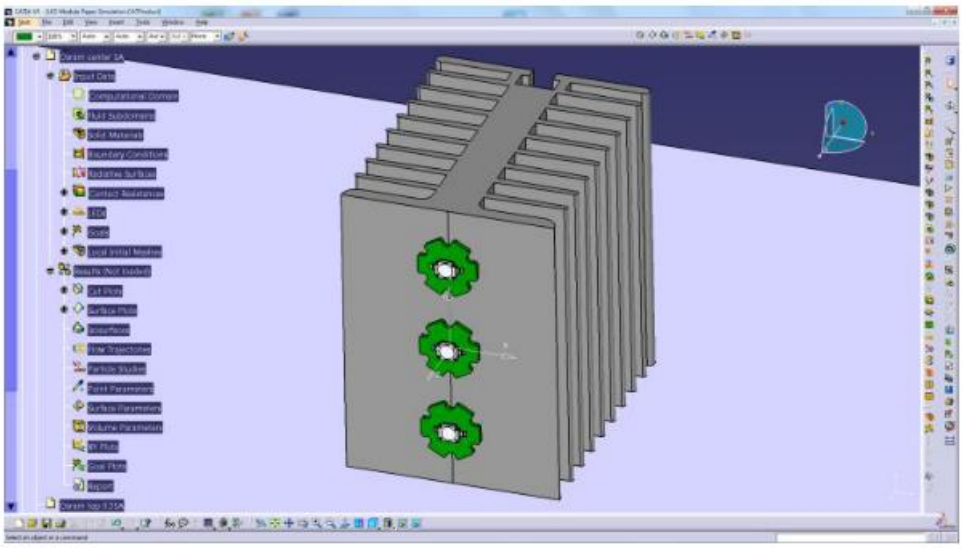

Figure 2.11: Simulation setup used to characterize LEDs when attached to a heatsink. (Reprinted from [52], Copyright (2015), with permission from ASME).

understanding systems from a wide range of fields. Moreover, since it combines heat transfer and gas flows, the CVD process seems a great example where CFD can be applied.

2.4.2. CFD Applied to CNT Synthesis

For the specific case of CNTs, various authors have used CFD analysis to understand their synthesis via the CVD process. As aforementioned, combining heat transfers and gas flows, this process is a great example, which can take advantage of the CFD capabilities.

For instance, Endo et al. have successfully used CFD tools to mathematically predict the production rate of CNTs in a xylene-based CVD method [1]. In their setup, the tube had two distinct furnaces: one preheater, at 240 ºC; and the main furnace, at 700 ºC. The former only serves to preheat the compounds before they reach the main reaction site,

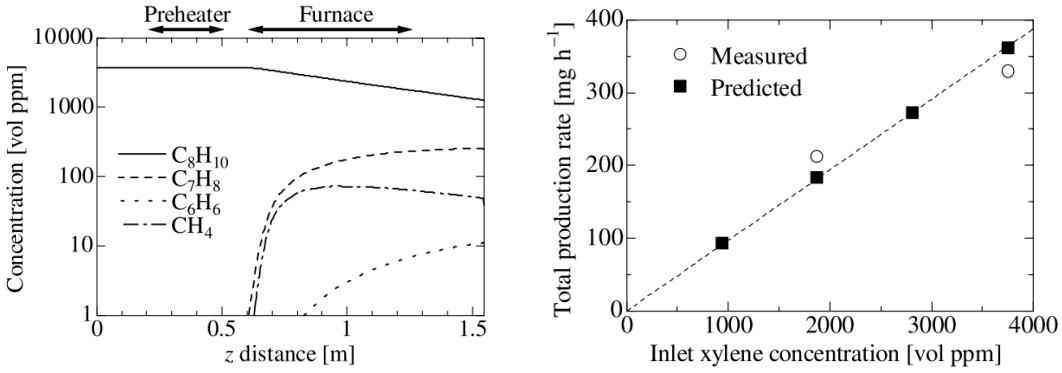

(a) **(b)**

Figure 2.12: (a) Compounds concentrations throughout the tube, measured by simulation; (b) comparison between the CNTs production rate predicted by the CFD model and experimentally measured. (Reprinted from [1], Copyright (2004), with permission from Elsevier).

which eases the hydrocarbon breakdown. Their model considered various gas reactions and the production rate was accessed by measuring the compounds concentrations throughout the tube. The model was then validated by comparing the obtained results with experimental data. The achieved results are achieved in Figure 2.12.

Envisioning the implementation of scale-up techniques, authors in [4] have constructed a 3D model of a CVD setup to synthesize CNTs. The model was then analyzed via CFD tools as a way to understand the gases streamlines and the temperature profile throughout the tube. Such understanding of the various interactions inside the tube gave the authors insights on how to explain several experimental observations, hence being considered crucial to implement the desired scale-up techniques.

Similarly, Sanchez et al. constructed a CFD model of an experimental benzene-based CVD setup and, which was then analyzed to observe the influences the gas flows on the CNTs growth [3]. The model was simulated for various gas flows and authors have accessed their effects on the temperature (see example in Figure 2.13), velocity, turbulence and concentrations profiles throughout the tube. Such analysis was then experimentally validated, which pertain its usage to optimize the process parameters and achieve better control of the CNT deposition patterns.

Addressing the prediction of the CNTs diameter, authors have combined mathematical equations and CFD simulations to construct a model to predict the formation of catalyst particles in an xylene-ferrocene based CVD synthesis [53,54]. The mathematical equations, used to simulate the formation of catalyst particles from ferrocene, were combined with the CFD model of the authors' CVD setup in order to address the dependencies of this phenomenon on other process parameters, such as the reaction

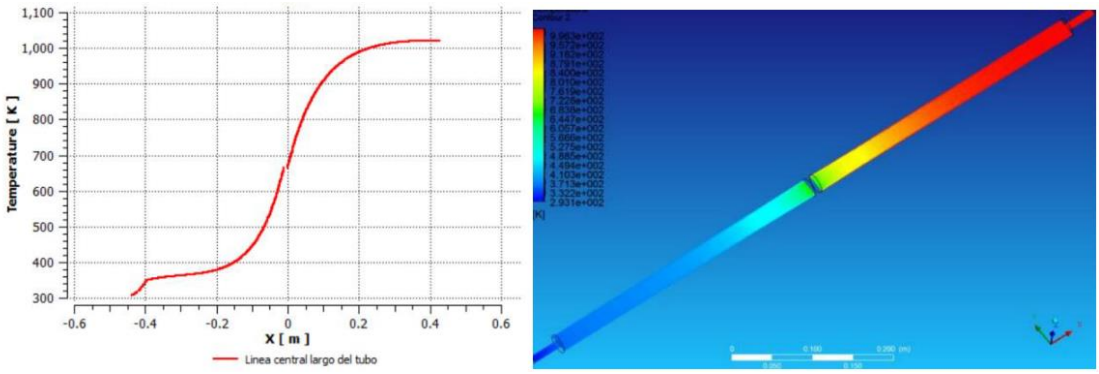

Figure 2.13: Distribution of temperature throughout the tube, measured by simulation. (Reprinted from [3], Copyright (2012), with permission by Cambridge University Press).

temperature throughout the tube.

Also addressing catalyst particles formation, Hinkov et al. have used CFD to analyze the various interactions and reactions between compounds in a plasma reactor CVD process based in the methane decomposition in a Nickel catalyst [24]. Here, authors used plasma activation as a route to ease particles formation to synthesize Multi-Walled CNTs (MWCNTs). The Plasma Enhanced CVD process was modelled via CFD techniques to analyze the particles formation dependencies in the process parameters. Such dependencies were also confirmed by experimental results, which validate the proposed model.

The effects of gas flows in MWCNTs synthesis were analyzed by CFD tools in [55]. Here, an acetylene-nitrogen synthesis in a nickel catalyst CVD process was modelled to address the gas flows impact on the CNT synthesis on two substrate positions inside the tube. Results enable authors to select which position would lead to more constant CNT growth, which was validated by experimental work.

2.5. Thesis Framework

As aforementioned, this research work envisions to develop a CFD-based tool to support the transition between different CVD setups to synthesize CNTs. Due to the process' influence by various parameters, it is difficult to predict the final result, leading to an extensive trial-and-error process when tuning the CNT synthesis [1–4]. For instance, a statistical analysis of the CVD process verified its variability and how time demanding the tunning process is [2]. This results inconsistency hinders the understanding and the extrapolation of research findings.

In order to understand the CVD process, the performance of a CFD-based sensitivity analysis was thought (see section 1.5). As referred in the previous section, several authors have used CFD tools to better understand the CNT synthesis process by CVD, either focusing on the gases streamlines inside the tube [4] or on the CNT growth itself [1,3,55]. For instance, White et al. used CFD to analyze the gases streamlines and temperature profile, without changing the process parameters [4]. Also without varying the process parameters, Li et al. analyzed the profiles of several conditions, such as temperature, velocity and pressure, throughout the tube for a single set of gas flows [55].

However, performing a study on the CVD process without changing process

parameters only allows the analysis of a specific case, resulting in a very narrow understanding of the whole process. Alternatively, Sanchez et al. varied the gas flows and analyzed their effects in the temperature, velocity and concentration profiles [3]. Endo et al. focused on measuring the compounds concentrations throughout the tube for various gases flows [1]. Nonetheless, these studies were performed for a small set of cases (3 and 4, respectively). Moreover, in these sets of cases, only one gas flow was altered (Sanchez et al. varied the inert gas, whereas Endo et al. changed the hydrocarbon gas flow).

In the performed sensitivity analysis (see chapter 4), every gas flow was tested for various possible values, resulting in a wider set of scenarios. Measuring the conditions inside the tube, such as temperature, velocity and concentrations, for each case allows the analysis of how these conditions are affected by the gas flows.

Regarding the development of a transition methodology, when envisioning to achieve CNT synthesis in a given setup, this is usually performed by a trial-and-error tuning where the process parameters are constantly being changed while attempting CNT synthesis [1–4]. On the other hand, if CNTs are already being grown in a given setup, physical measurements can be collected from both setups in order to mimic and tune the synthesis conditions inside the tube [56]. However, this methodology cannot be followed for every synthesis condition, as some measurements require the tube to be opened, which alter the conditions.

Alternatively, in this thesis (see chapter 5), performing these measurements via CFD tools allows an easier comparison between conditions in different setups, as each set of measurements can be performed without physically performing the CVD process, resulting in a faster tuning process. Moreover, since these measurements are made computationally, comparison algorithms can be followed for various synthesis scenarios in order to automatize the selection of process parameters which result in the same synthesis conditions between different setups.

2.6. Final Considerations

In this chapter, a comprehensive literature review regarding the various aspects of this research main goal was presented. Such review enabled the understanding of the research main keywords as well as of the existent works in the scientific world.

A comparison between three different techniques to synthesize CNTs was performed. Taking into account their advantages and disadvantages, it was possible to understand why the CVD process is the most widely used one. Thus, a more in-depth study of its operation principle was performed by analyzing the critical components of its phases. Moreover, this in-depth study was complemented by a review of various works using different CVD configurations to synthesize CNTs. This analysis resulted in a better understanding of the process principle of operation and the importance of each one of its phases.

Regarding the usage of CFD tools, their fundamentals were presented, by describing each one of its components and phases. This understanding of concepts enabled the performance of a literature review considering various CFD-based works. This review started by enumerating applications in various fields, narrowing them to CNT synthesis. By analyzing the existent works, enabled the development of a perspective on the CFD capabilities and how to take advantage of them.

References

[1] H. Endo, K. Kuwana, K. Saito, D. Qian, R. Andrews, E.A. Grulke, CFD prediction of carbon nanotube production rate in a CVD reactor, Chem. Phys. Lett. 387 (2004) 307–311. doi:10.1016/j.cplett.2004.01.124.

[2] C.R. Oliver, E.S. Polsen, E.R. Meshot, S. Tawfick, S.J. Park, M. Bedewy, A.J. Hart, Statistical analysis of variation in laboratory growth of carbon nanotube forests and recommendations for improved consistency., ACS Nano. 7 (2013) 3565–80. doi:10.1021/nn400507y.

[3] A.G. Sánchez, L.D. Lvova, V.L. Garza, R.R. Doval, M. de L.M. Sánchez, Computational fluid dynamics in the carbon nanotubes synthesis by chemical vapor deposition, Mater. Res. Soc. Symp. Proc. Vol. 1446 (2012) 25–31. doi:10.1557/opl.2012.1607.

[4] R. White, D. King, Combined Experimental and Simulation (CFD) Analysis on Performance of a Horizontal Tube Reactor Used To Produce Carbon Nanotubes, 7th Int.Conf.on CFD Miner. Process Ind. (2009) 1–5.

[5] S. Iijima, Helical microtubules of graphitic carbon, Nature. 354 (1991). doi:10.1038/354056a0.

[6] M. Kumar, Y. Ando, Chemical Vapor Deposition of Carbon Nanotubes: A Review on Growth Mechanism and Mass Production, J. Nanosci. Nanotechnol. 10 (2010) 3739–3758. doi:10.1166/jnn.2010.2939.

[7] A. Matyushov, Growth of Carbon Nanotubes via Chemical Vapor Deposition, Citeseer, 2008. http://www.sciencedirect.com/science/article/pii/S0925963500004465.

[8] K. Balasubramanian, M. Burghard, Chemically functionalized carbon nanotubes, Small. 1 (2005) 180–92. doi:10.1002/smll.200400118.

[9] S.A. Moshkalyov, A.L.D. Moreau, H.R. Guttiérrez, M.A. Cotta, J.W. Swart, Carbon nanotubes growth by chemical vapor deposition using thin film nickel catalyst, Mater. Sci. Eng. B. 112 (2004) 147–153. doi:10.1016/j.mseb.2004.05.038.

[10] N. Sinha, J. Ma, J.T.W. Yeow, Carbon Nanotube-Based Sensors, J. Nanosci. Nanotechnol.

6 (2006) 573–590. doi:10.1166/jnn.2006.121.

[11] K.A. Shah, B.A. Tali, Synthesis of carbon nanotubes by catalytic chemical vapour deposition: A review on carbon sources, catalysts and substrates, Mater. Sci. Semicond. Process. 41 (2016) 67–82. doi:10.1016/j.mssp.2015.08.013.

[12] S. Iijima, T. Ichihashi, Single-shell carbon nanotubes of 1-nm diameter, Nature. 363 (1993) 603–605. doi:10.1038/363603a0.

[13] D.S. Bethune, C.H. Kiang, M.S. de Vries, G. Gorman, R. Savoy, J. Vazquez, R. Beyers, Cobalt-catalysed growth of carbon nanotubes with single-atomic-layer walls, Nature. 363 (1993) 605–607. doi:10.1038/363605a0.

[14] N.M. Mubarak, E.C. Abdullah, N.S. Jayakumar, J.N. Sahu, An overview on methods for the production of carbon nanotubes, J. Ind. Eng. Chem. 20 (2014) 1186–1197. doi:10.1016/j.jiec.2013.09.001.

[15] N. Arora, N.N. Sharma, Arc discharge synthesis of carbon nanotubes: Comprehensive review, Diam. Relat. Mater. 50 (2014) 135–150. doi:10.1016/j.diamond.2014.10.001.

[16] N. Arora, N.N. Sharma, Sustained arc temperature: Better marker for phase transformation of carbon black to multiwalled carbon nanotubes in arc discharge method, Mater. Res. Express. 3 (2016). doi:10.1088/2053-1591/3/10/105030.

[17] K.H. Maria, T. Mieno, Synthesis of single-walled carbon nanotubes by low-frequency bipolar pulsed arc discharge method, Vacuum. 113 (2015) 11–18. doi:10.1016/j.vacuum.2014.11.025.

[18] A. Thess, R. Lee, P. Nikolaev, H. Dai, P. Petit, J. Robert, C. Xu, Y.H. Lee, S.G. Kim, A.G. Rinzler, D.T. Colbert, G.E. Scuseria, D. Tomanek, J.E. Fischer, R.E. Smalley, Crystalline Ropes of Metallic Carbon Nanotubes, Science (80-.). 273 (1996) 483–487. doi:10.1126/science.273.5274.483.

[19] A. Morales, C. Lieber, A laser ablation method for the synthesis of crystalline semiconductor nanowires, Science. 279 (1998) 208–11. http://www.ncbi.nlm.nih.gov/pubmed/9422689.

[20] J. Chen, X. Gui, Z. Lin, Z. Tang, M.M. Lee, A. Wokaun, T. Lippert, Pulsed ultra-violet laser interactions with ultra-low-density porous carbon nanotube sponges, Carbon N. Y. 93 (2015) 604–610. doi:10.1016/j.carbon.2015.05.089.

[21] J. Chrzanowska, J. Hoffman, A. Małolepszy, M. Mazurkiewicz, T.A. Kowalewski, Z. Szymanski, L. Stobinski, Synthesis of carbon nanotubes by the laser ablation method: Effect of laser wavelength, Phys. Status Solidi. 252 (2015) 1860–1867. doi:10.1002/pssb.201451614.

[22] C.D. Scott, S. Arepalli, P. Nikolaev, R.E. Smalley, Growth mechanisms for single-wall carbon nanotubes in a laser-ablation process, Appl. Phys. A Mater. Sci. Process. 72 (2001) 573–580. doi:10.1007/s003390100761.

[23] M. José-Yacamán, M. Mikiyoshida, L. Rendón, J.G. Santiesteban, M. Jos, M. Miki-Yoshida, L. Rendón, J.G. Santiesteban, Catalytic growth of carbon microtubules with fullerene structure growth of carbon microtubules with fullerene structure, Appl. Phys. Lett. 62 (1993) 202–204. doi:10.1063/1.109315.

[24] I. Hinkov, S. Farhat, C.P. Lungu, A. Gicquel, F. Silva, A. Mesbahi, O. Brinza, C. Porosnicu, A. Anghel, Microwave Plasma Enhanced Chemical Vapor Deposition of Carbon Nanotubes, J. Surf. Eng. Mater. Adv. Technol. 4 (2014) 196–209. doi:10.4236/jsemat.2014.44023.

[25] K. Hernadi, A. Fonseca, J.B. Nagy, D. Bernaerts, A.A. Lucas, Fe-catalyzed carbon nanotube formation, Carbon N. Y. 34 (1996) 1249–1257. doi:10.1016/0008-6223(96)00074-7.

[26] J. Kong, A.M. Cassell, H. Dai, Chemical vapor deposition of methane for single-walled carbon nanotubes, Chem. Phys. Lett. 292 (1998) 567–574. doi:10.1016/S0009-2614(98)00745-3.

[27] D. He, H. Li, W. Li, P. Haghi-Ashtiani, P. Lejay, J. Bai, Growth of carbon nanotubes in six orthogonal directions on spherical alumina microparticles, Carbon N. Y. 49 (2011) 2273–

2286. doi:10.1016/j.carbon.2011.01.060.

[28] T. Tomie, S. Inoue, M. Kohno, Y. Matsumura, Prospective growth region for chemical vapor deposition synthesis of carbon nanotube on C-H-O ternary diagram, Diam. Relat. Mater. 19 (2010) 1401–1404. doi:10.1016/j.diamond.2010.08.005.

[29] R. Sen, A. Govindaraj, C.N.R. Rao, Carbon nanotubes by the metallocene route, Chem. Phys. Lett. 267 (1997) 276–280. doi:10.1016/S0009-2614(97)00080-8.

[30] U. Narkiewicz, M. Podsiadły, R. Jędrzejewski, I. Pełech, Catalytic decomposition of hydrocarbons on cobalt, nickel and iron catalysts to obtain carbon nanomaterials, Appl. Catal. A Gen. 384 (2010) 27–35. doi:10.1016/j.apcata.2010.05.050.

[31] H. Dai, A.G. Rinzler, P. Nikolaev, A. Thess, D.T. Colbert, R.E. Smalley, Single-wall nanotubes produced by metal-catalyzed disproportionation of carbon monoxide, Chem. Phys. Lett. 260 (1996) 471–475. doi:10.1016/0009-2614(96)00862-7.

[32] B.Q. Wei, R. Vajtai, Y. Jung, J. Ward, R. Zhang, G. Ramanath, P. Ajayan, Organized assembly of carbon nanotubes, Nature. 416 (2002) 495–496. doi:10.1038/416495a.

[33] S. Maruyama, Y. Miyauchi, T. Edamura, Y. Igarashi, S. Chiashi, Y. Murakami, Synthesis of single-walled carbon nanotubes with narrow diameter-distribution from fullerene, Chem. Phys. Lett. 375 (2003) 553–559. doi:10.1016/S0009-2614(03)00907-2.

[34] S. Maruyama, R. Kojima, Y. Miyauchi, S. Chiashi, M. Kohno, Low-temperature synthesis of high-purity single-walled carbon nanotubes from alcohol, Chem. Phys. Lett. 360 (2002) 229–234. doi:10.1016/S0009-2614(02)00838-2.

[35] Y. Shirazi, M.A. Tofighy, T. Mohammadi, A. Pak, Effects of different carbon precursors on synthesis of multiwall carbon nanotubes: Purification and Functionalization, Appl. Surf. Sci. 257 (2011) 7359–7367. doi:10.1016/j.apsusc.2011.03.146.

[36] Z. Yong, L. Fang, Z. Zhi-hua, Synthesis of heterostructured helical carbon nanotubes by iron-catalyzed ethanol decomposition, Micron. 42 (2011) 547–552. doi:10.1016/j.micron.2011.01.007.

[37] J.M. Feng, R. Wang, Y.L. Li, X.H. Zhong, L. Cui, Q.J. Guo, F. Hou, One-step fabrication of high quality double-walled carbon nanotube thin films by a chemical vapor deposition process, Carbon N. Y. 48 (2010) 3817–3824. doi:10.1016/j.carbon.2010.06.046.

[38] J.H. Hafner, M.J. Bronikowski, B.R. Azamian, P. Nikolaev, A.G. Rinzler, D.T. Colbert, K.A. Smith, R.E. Smalley, Catalytic growth of single-wall carbon nanotubes from metal particles, Chem. Phys. Lett. 296 (1998) 195–202. doi:10.1016/S0009-2614(98)01024-0.

[39] T. Norton, D.-W. Sun, Computational fluid dynamics (CFD) - an effective and efficient design and analysis tool for the food industry: A review, Trends Food Sci. Technol. 17 (2006) 600–620. doi:10.1016/j.tifs.2006.05.004.

[40] H.K. Versteeg, W. Malalasekera, An Introduction to Computational Fluid Dynamics - The Finite Volume Method, 2nd ed., Pearson Education, 2007.

[41] J. Tu, G. Yeoh, C. Liu, Computational fluid dynamics: A practical approach, 3rd ed., Elsevier B.V., Oxford, UK, 2018.

[42] J. Ferziger, M. Peric, Computational methods for fluid dynamics, 3rd ed., Springer, 2002.

[43] R.A. Pieritz, R. Mendes, R.F.A.F. da Silva, C.R. Maliska, CFD studio: An educational software package for CFD analysis and design, Comput. Appl. Eng. Educ. 12 (2004) 20–30. doi:10.1002/cae.10055.

[44] P. Kopyt, W. Gwarek, A Comparison of Commercial CFD Software Capable of Coupling to External Electromagnetic Software for Modeling of Microwave Heating Process, in: Proc. 6th Semin. Comput. Model. Microw. Power Eng., Citeseer, Austin, Texas USA, 2004: pp. 33–39.

[45] W. Jeong, J. Seong, Comparison of effects on technical variances of computational fluid dynamics (CFD) software based on finite element and finite volume methods, Int. J. Mech. Sci. 78 (2014) 19–26. doi:10.1016/j.ijmecsci.2013.10.017.

[46] T. Glatzel, C. Litterst, C. Cupelli, T. Lindemann, C. Moosmann, R. Niekrawietz, W. Streule, R. Zengerle, P. Koltay, Computational fluid dynamics (CFD) software tools for microfluidic applications – A case study, Comput. Fluids. 37 (2008) 218–235. doi:10.1016/j.compfluid.2007.07.014.

[47] J. Collis, M.E. Hubbard, R.D. O'Dea, Computational modelling of multiscale, multiphase fluid mixtures with application to tumour growth, Comput. Methods Appl. Mech. Eng. 309 (2016) 554–578. doi:10.1016/j.cma.2016.06.015.

[48] C.J. Roth, L. Yoshihara, M. Ismail, W.A. Wall, Computational modelling of the respiratory system: Discussion of coupled modelling approaches and two recent extensions, Comput. Methods Appl. Mech. Eng. 314 (2016) 473–493. doi:10.1016/j.cma.2016.08.010.

[49] K. Yang, P. Sun, L. Wang, J. Xu, L. Zhang, Modeling and simulations for fluid and rotating structure interactions, Comput. Methods Appl. Mech. Eng. 311 (2016) 788–814. doi:10.1016/j.cma.2016.09.020.

[50] B. Blocken, Computational Fluid Dynamics for Urban Physics: Importance, scales, possibilities, limitations and ten tips and tricks towards accurate and reliable simulations, Build. Environ. 91 (2015) 219–245. doi:10.1016/j.buildenv.2015.02.015.

[51] J. Xiang, V.M. Tutino, K. V. Snyder, H. Meng, CFD: Computational fluid dynamics or confounding factor dissemination? the role of hemodynamics in intracranial aneurysm rupture risk assessment, Am. J. Neuroradiol. 35 (2014) 1849–1857. doi:10.3174/ajnr.A3710.

[52] B. Marovic, J. Petroski, M. Clark, Analyzing temperature changes in powered LEDs by combining thermal and radiometric characterization with computational fluid dynamics, in: ASME 2015 Int. Tech. Conf. Exhib. Packag. Integr. Electron. Photonic Microsystems, San Francisco, USA, 2015: pp. 1–8.

[53] K. Kuwana, K. Saito, Modeling CVD synthesis of carbon nanotubes: Nanoparticle formation from ferrocene, Carbon N. Y. 43 (2005) 2088–2095. doi:10.1016/j.carbon.2005.03.016.

[54] K. Kuwana, H. Endo, K. Saito, D. Qian, R. Andrews, E.A. Grulke, Catalyst deactivation in CVD synthesis of carbon nanotubes, Carbon N. Y. 43 (2005) 253–260. doi:10.1016/j.carbon.2004.09.008.

[55] M. Li, Z. Xu, Z. Li, Y. Chen, J. Guo, H. Huo, H. Zhou, H. Huangfu, Z. Cao, H. Wang, An experimental and CFD study on gas flow field distribution in the growth process of multi-walled carbon nanotube arrays by thermal chemical vapor deposition, Cryst. Res. Technol. 51 (2016) 702–707. doi:10.1002/crat.201600104.

[56] S.S. Wicks, Mechanical Enhancement of Woven Composites with Radially Aligned Carbon Nanotubes (CNTs): Investigation of Mode I Fracture Toughness, Massachusetts Institute of Technology, 2010.

[57] A. Joseph Berkmans, M. Jagannatham, D. Rohit Reddy, P. Haridoss, Synthesis of thin bundled single walled carbon nanotubes and nanohorn hybrids by arc discharge technique in open air atmosphere, Diam. Relat. Mater. 55 (2015) 12–15. doi:10.1016/j.diamond.2015.02.004.

[58] Y.P. Hsieh, Y.W. Wang, C.C. Ting, H.C. Wang, K.Y. Chen, C.C. Yang, Effect of catalyst morphology on the quality of CVD grown graphene, J. Nanomater. 2013 (2013). doi:10.1155/2013/393724.

[59] M. Marchena, Z. Song, W. Senaratne, C. Li, X. Liu, D. Baker, J.C. Ferrer, P. Mazumder, K. Soni, R. Lee, V. Pruneri, Direct growth of 2D and 3D graphene nano-structures over large glass substrates by tuning a sacrificial Cu-template layer, 2D Mater. 4 (2017) 025088. doi:10.1088/2053-1583/aa69b5.

[60] W. Li, S. Xie, L. Qian, B. Chang, B. Zou, Large-scale synthesis of aligned carbon nanotubes, Science (80-.). 274 (1996) 0–2. doi:10.1038/358220a0.

[61] G. Atthipalli, R. Epur, P.N. Kumta, M. Yang, J.K. Lee, J.L. Gray, Nickel catalyst-assisted

vertical growth of dense carbon nanotube forests on bulk copper, J. Phys. Chem. C. 115 (2011) 3534–3538. doi:10.1021/jp108624n.

[62] S. Santangelo, G. Messina, G. Faggio, M. Lanza, A. Pistone, C. Milone, Calibration of reaction parameters for the improvement of thermal stability and crystalline quality of multi-walled carbon nanotubes, J. Mater. Sci. 45 (2010) 783–792. doi:10.1007/s10853-009-4001-y.

[63] M. Endo, K. Takeuchi, K. Kobori, K. Takahashi, H.W. Kroto, A. Sarkar, Pyrolytic Carbon Nanotubes from Vapor-Grown Carbon Fibers, Carbon N. Y. 33 (1995) 873–881.

[64] E. Flahaut, a Govindaraj, A. Peigney, C. Laurent, A. Rousset, C.N.R. Rao, Synthesis of single-walled carbon nanotubes using binary (Fe, Co, Ni) alloy nanoparticles prepared in situ by the reduction of oxide solid solutions, Chem. Phys. Lett. 300 (1999) 236–242. doi:10.1016/S0009-2614(98)01304-9.

[65] H.M. Cheng, F. Li, X. Sun, S.D.M. Brown, M.A. Pimenta, A. Marucci, G. Dresselhaus, M.S. Dresselhaus, Bulk morphology and diameter distribution of single-walled carbon nanotubes synthesized by catalytic decomposition of hydrocarbons, Chem. Phys. Lett. 289 (1998) 602–610. doi:10.1016/S0009-2614(98)00479-5.

[66] A. Grüneis, M.H. Rümmeli, C. Kramberger, D. Grimm, T. Gemming, A. Barreiro, P. Ayala, T. Pichler, H. Kuzmany, C. Schamann, R. Pfeiffer, J. Schumann, B. Büchner, Growth of carbon nanotubes from wet chemistry and thin film multilayer catalysts, Phys. Status Solidi Basic Res. 243 (2006) 3054–3057. doi:10.1002/pssb.200669175.

[67] R. Joshi, J.J. Schneider, O. Yilmazoglu, D. Pavlidis, Patterned growth of ultra long carbon nanotubes. Properties and systematic investigation into their growth process, J. Mater. Chem. 20 (2010) 1717. doi:10.1039/b919579c.

[68] G. Li, Synthesis of well-aligned carbon nanotubes on the NH3 pretreatment Ni catalyst films, Russ. J. Phys. Chem. A. 84 (2010) 1560–1565. doi:10.1134/S0036024410090219.

[69] T. Cui, R. Lv, F. Kang, Q. Hu, J. Gu, K. Wang, D. Wu, Synthesis and enhanced field-emission of thin-walled, open-ended, and well-aligned N-doped carbon nanotubes, Nanoscale Res. Lett. 5 (2010) 941–948. doi:10.1007/s11671-010-9586-1.

Chapter 3

CFD MODELS

The CVD process is highly complex and dependent on various parameters. In order to properly understand how the various components interact inside the tube during the synthesis phase, several computational models of the CVD process were set up, simulated and analyzed. As aforementioned in section 2.4, the most commonly used FEM/FVM codes are ANSYS FLUENT, ANSYS CFX, ANSYS FLOTRAN, ADINA, STAR-CD, COMSOL, FLOW3D, FIDAP and CFD-ACE. Within these software, the CFD code used in the study was ANSYS 15.0 CFX for being well-established [1–3], and for its technical specifications and modeling capabilities, namely laminar and turbulent flows, steady-state and transient simulations, ideal and real gases usage and heat transfer [4]. Moreover, results from comparisons to several CFD codes have shown that ANSYS CFX is less influenced by the generated mesh type and are faster at solving the same problem [5,6]. Figure 3.1 shows the designed computational models, which were based in physical setups used to synthesize CNTs and existent in both the IPC laboratory of the Polymer Engineer Department at the University of Minho and in the NECSTLab research group's main laboratory at the Massachusetts Institute of Technology (see Table 3.1, Figure 3.2 and Figure 3.3).

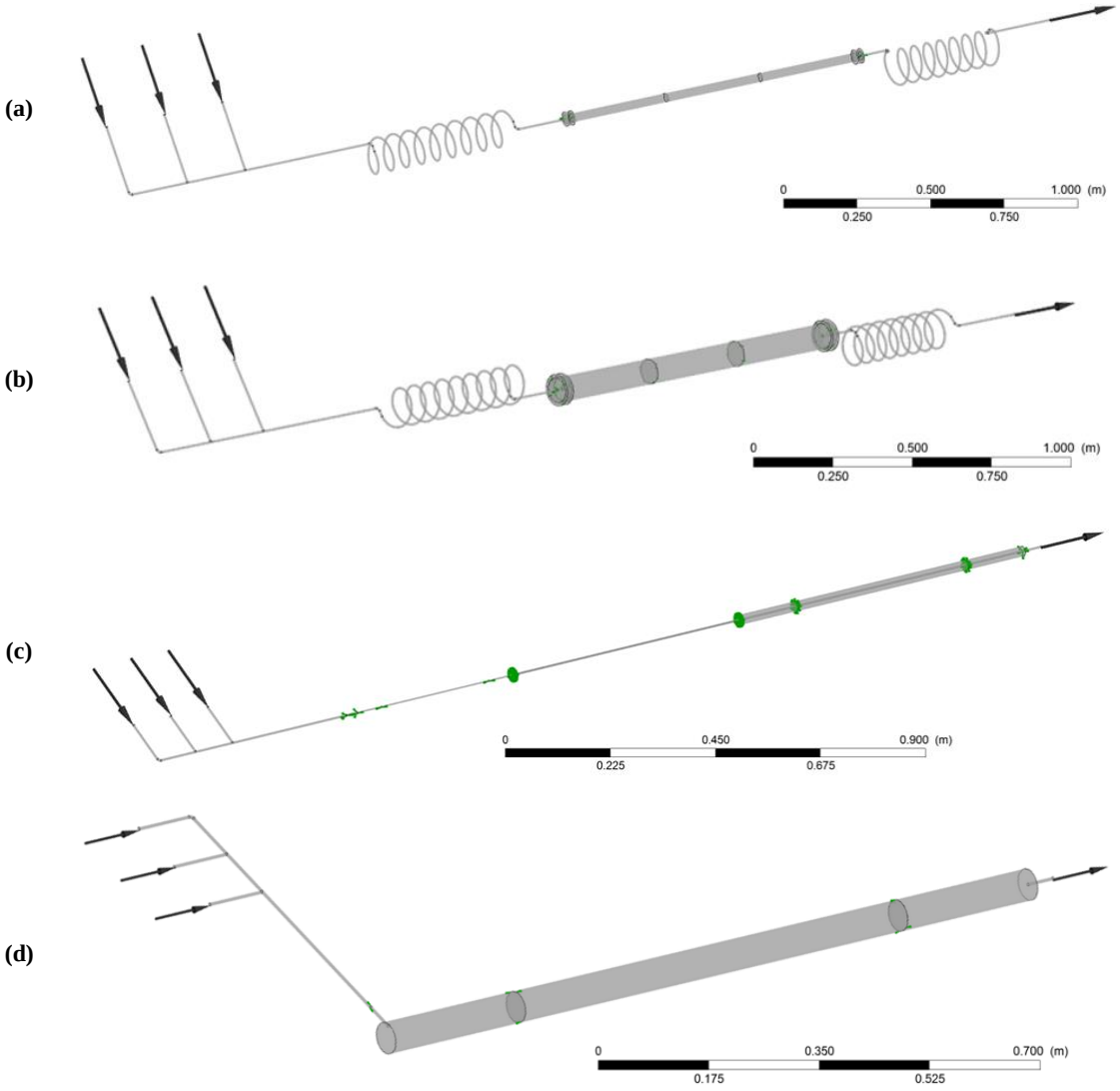

Figure 3.1: Designed computational models of the simulated CVD process tubes: (a) "30 mm", (b) "80 mm", (c) "1 Inch", and (d) "2 Inches" tubes.

These setups differ in various physical properties, depicted in Table 3.2:

- The tubes' length and inner diameter;
- The position of the tube's inlet in relation to its orientation;
- The existence or not of a pre-heater, i.e. a heating chamber prior to the main tube.

Moreover, the geometries depicted in Figure 3.2 represent the inner volumes of the tubes used for CNTs synthesis. Thus, there is no material allocated to each body, but instead a gas mixture, further detailed later, as a representation of the inner volume. The shaded areas depicted in these representations are the sections of the tubes which are heated by the

external furnace. They are positioned in the central section of the tubes.

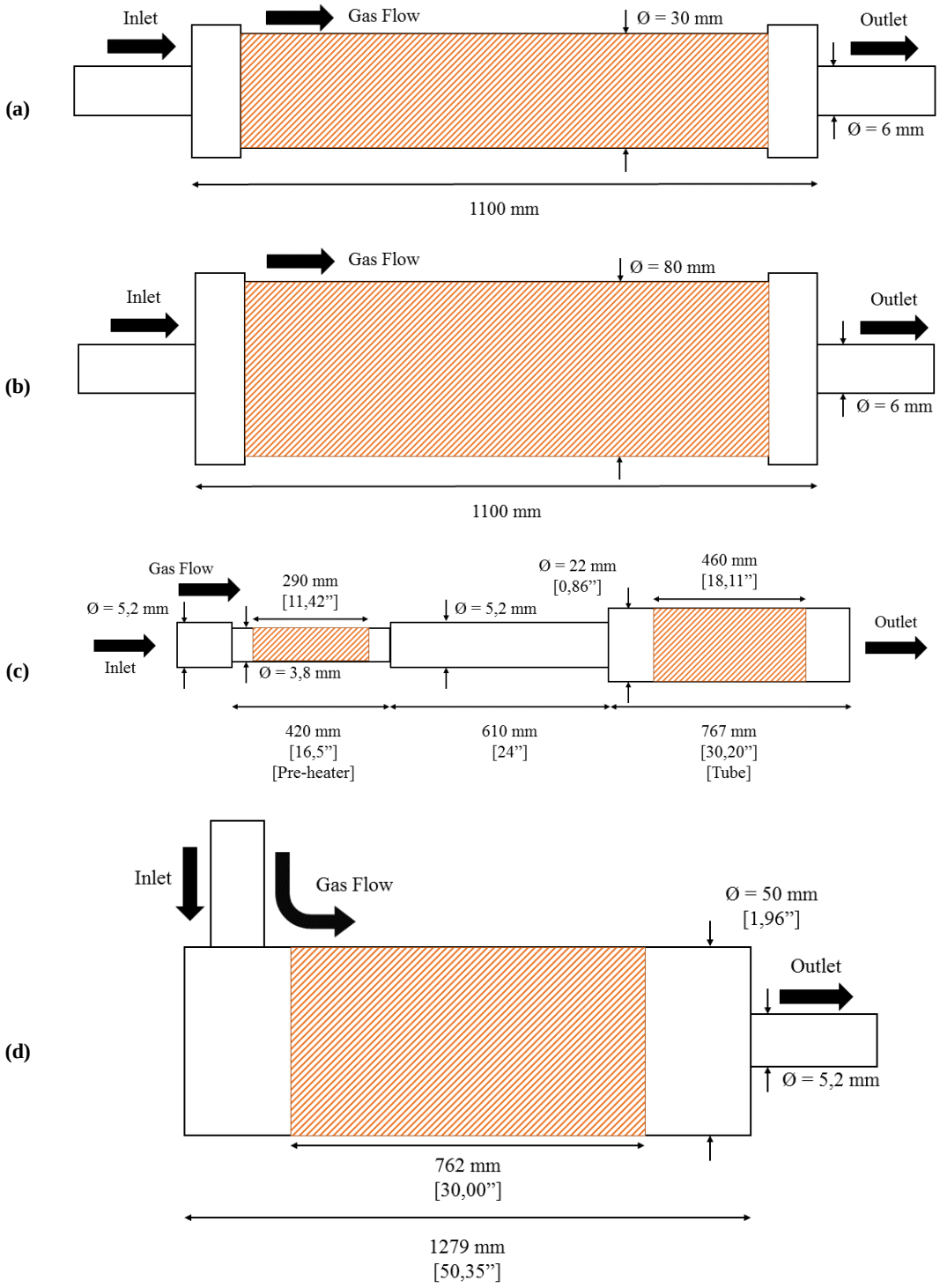

Figure 3.2: Graphical representation of the simulated CVD process tubes: (a) "30 mm", (b) "80 mm", (c) "1 Inch", and (d) "2 Inches" tubes. The shaded areas represent the tube sections where the heating furnace was placed.

(a)

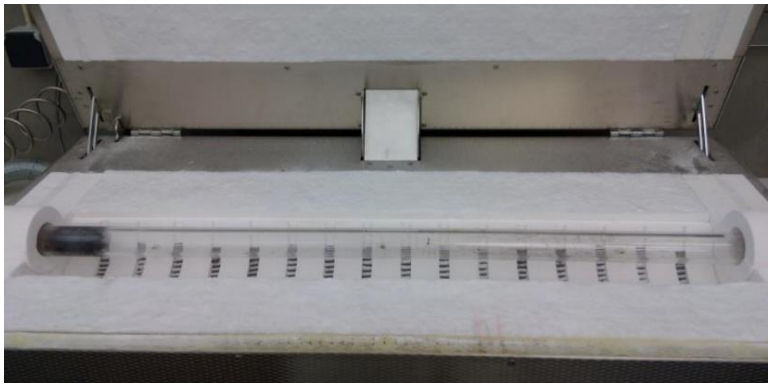

(b)

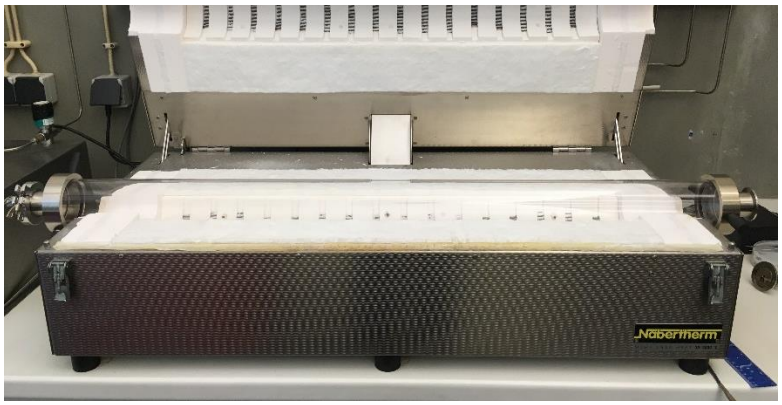

(c)

(d)

Figure 3.3: Photos of the simulated physical setups: (a) “30 mm”, (b) “80 mm”, (c) “1 Inch”, and (d) “2 Inches” tubes.

Table 3.1: Maker and model of the components of the addressed setups.

Name	Mass Flow Controllers	Furnace	Pre-heater Furnace
"30 mm"	MKS Instruments 1179	Nabertherm RS 80/750/11	-
"80 mm"	MKS Instruments 1179	Nabertherm RS 80/750/11	-
"1 Inch"	Aalborg Instruments & Controls, Inc. GFC17	Lindberg/Blue M HTF55122A	Lindberg/Blue M TF55035C1
"2 Inches"	Aalborg Instruments & Controls, Inc. GFC17	Lindberg/Blue M HTF55347C	-

Table 3.2: Physical properties and features of the addressed setups.

Setup		Tube dimensions [mm]		Setup features	
Name	Location	Length	Inner diameter	Entrance position	Pre-heater existence
"30 mm"	UM	1100	30	Concentric	No
"80 mm"	UM	1100	80	Concentric	No
"1 Inch"	MIT	460	22	Concentric	Yes
"2 Inches"	MIT	1279	50	Lateral	No

In order to model these CVD setups, the whole process used to synthesize CNTs was analyzed. Figure 3.4 illustrates typical temperature and gases flows profile during the previously described phases of the whole process to synthesize CNTs (see section 2.2.1): (1) cleaning; (2) reduction; (3) synthesis; (4) delamination; and (5) cooling. This data was collected from the "30 mm" setup used by the author at the University of Minho, where the used hydrocarbon, reducer and inert gases were ethylene (C_2H_4), hydrogen (H_2) and helium (He), respectively.

As aforementioned, the goal of the first analysis step - the sensitivity analysis - is to understand how the process parameters affect the synthesis conditions inside the tube. These conditions depend on how the various components interact inside the tube during the synthesis phase. Thus, despite the entire process chain illustrated, the simulations were set to model the synthesis phase (phase 3 in Figure 3.4). Since the process parameters do not change during each phase, the simulations were set as steady-state, enabling the analysis of how each set of process parameters would affect the synthesis conditions.

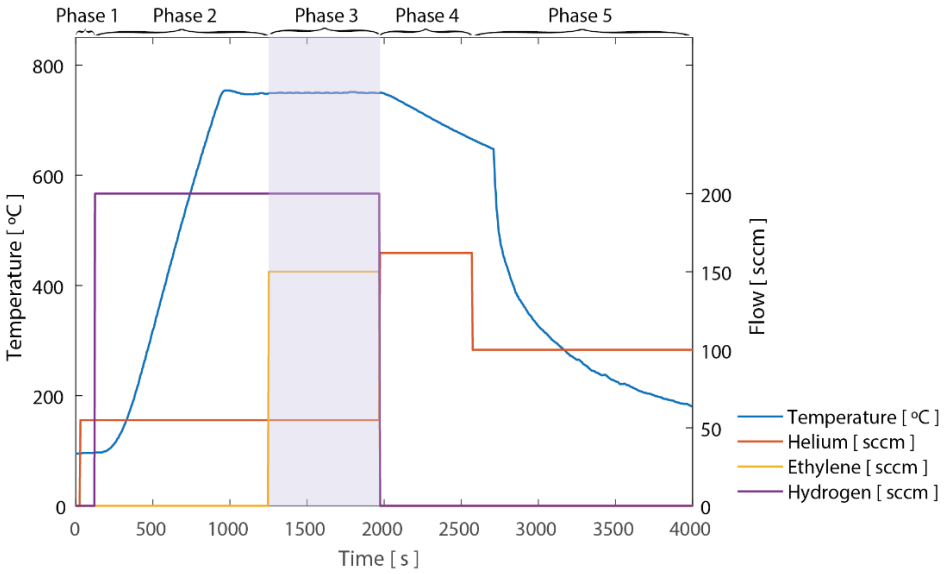

Figure 3.4: Typical temperature and gases flows profile during the various CVD Process phases.

3.1. Initial Conditions Definition

As known, one critical aspect about using computational tools is the correct setup of the simulation itself, namely the proper definition of the simulation conditions. Within the simulation conditions, it is critical: (i) the definition of the number of iterations to perform; and (ii) the mesh to use. The proper definition of these conditions ensures results' reliability with minimum computational effort and consumed time. In order to setup the simulation conditions, a simulation (see Table 3.3) was initially set. The gases were considered to be ideal and were imported from the Ansys *"Gas Phase Combustion"* library, where the gases specific heat property is defined by the National Aeronautics and Space Administration (NASA) format via Eq. 3.1. The used gases properties are presented in Table 3.4 [7].

$$\frac{C_p}{R_s} = a_1 + a_2 T + a_3 T^2 + a_4 T^3 + a_5 T^4 \qquad \textbf{Eq. 3.1}$$

Table 3.3: Simulation scenario used to define the simulation conditions to use.

Gas Inlets [sccm[1]]			Tube temperature [°C]	Gas mixture initially inside the tube[2] [%]	
C_2H_4	H_2	He		H_2	He
150	200	55	750	78.4	21.6

[1] Standard Cubic Centimeter per Minute.
[2] Based on the gases flows experimentally used during the second phase (see Figure 3.4).

Table 3.4: Gases properties used in the simulations.

		C_2H_4	H_2	He
	Lower	300	300	300
Temp. [K]	**Midpoint**	1,000	1,000	1,000
	Upper	5,000	5,000	5,000
Molar Mass [kg.k.mol^{-1}]		28.05	2.016	4
R_s [k.J.kg^{-1}.K^{-1}]		0.296	4.12	2.08
	a1 []	3.52842	2.99142	2.5
	a2 [K^{-1}]	0.0114852	0.000700064	0
	a3 [K^{-2}]	-4.41838e-06	-5.63383e-08	0
Upper coef.	**a4 [K^{-3}]**	7.8446e-10	-9.23158e-12	0
	a5 [K^{-4}]	-5.26685e-14	1.58275e-15	0
	a6 [K]	4,428.29	-835.034	-745.375
	a7 []	2.23039	-1.35511	0.915349
	a1 []	-0.861488	3.29812	2.5
	a2 [K^{-1}]	0.0279616	0.000824944	0
	a3 [K^{-2}]	-3.38868e-05	-8.14301e-07	0
Lower coef.	**a4 [K^{-3}]**	2.78515e-08	-9.47543e-11	0
	a5 [K^{-4}]	-9.73788e-12	4.13487e-13	0
	a6 [K]	5,573.05	-1,012.52	-745.375
	a7 []	24.2115	-3.29409	0.915349

In order to run the presented simulation, an initial mesh was required. The mesh targets the discretization of the model in triangular and quadrilateral elements. Table 3.5 shows the values used in the configuration parameters for the mesh sizing. In the CFX-Solver, the mesh size is mainly defined by the "Num. Cell Across Gap" parameter, which *"specifies the number of element layers to be generated in the gap sections (i.e. between features)"* [8]. Setting this parameter to a higher value results in more mesh elements in the same volume (gap), i.e. a denser mesh. Since the mesh size only interferes with the model discretization into individual elements and not with their value, it was initially set with 3 elements across a gap between model's features, which is the default value given by the CFX-Solver [8]. Other configuration parameters were set so that the mesh is dependent on the geometric key features, such as curves and sharp angles, with a smooth and slow transition between elements.

Table 3.5: Configuration parameters used in the mesh sizing.

Parameter	Value
Use Advanced Size Function	On: Proximity and Curvature
Relevance Center	Fine
Initial Size Seed	Active Assembly
Smoothing	High
Transition	Slow
Span Angle Center	Fine
Num. of Cells Across Gap	3

The CFX-Solver is an iterative process, which repeatedly solves a set of fluid dynamics equations until a maximum number of iterations is achieved [3]. In order to quantitatively assess the maximum number of iterations to perform for each model, the previously described scenario (Table 3.3) was simulated with different number of iterations. Table 3.6 depicts the minimum and maximum number of iterations, as well as the increment, used to define these simulations. Since the "30 mm" model was firstly assessed, a smaller increment, which defined the starting number of iterations, was used. Being based in the "30 mm" model, the "80 mm" model was thought to require more iterations, thus the higher starting point and increment. Lastly, since the same thought could not be inferred for the "1 Inch" and "2 Inches" models, these were simulated with a smaller increment.

These simulations were then evaluated by the percentual errors of certain variables inside the tube. The selected variables were the compounds concentrations and the temperature. The individual average of these variables throughout the concentric center line of the tube were computed for each simulation. Then, the percentual error (PE_i), between the consecutive pair of iterations $i-1$ and i, was computed using Eq. 3.2, where Var_i and

Table 3.6: Minimum and maximum iterations, as well as the increment, used in the simulations to define the number of iterations to perform for each model.

Name	Minimum	Increment	Maximum
"30 mm"	50	50	1300
"80 mm"	1000	500	3500
"1 Inch"	100	100	1400
"2 Inches"	100	100	2000

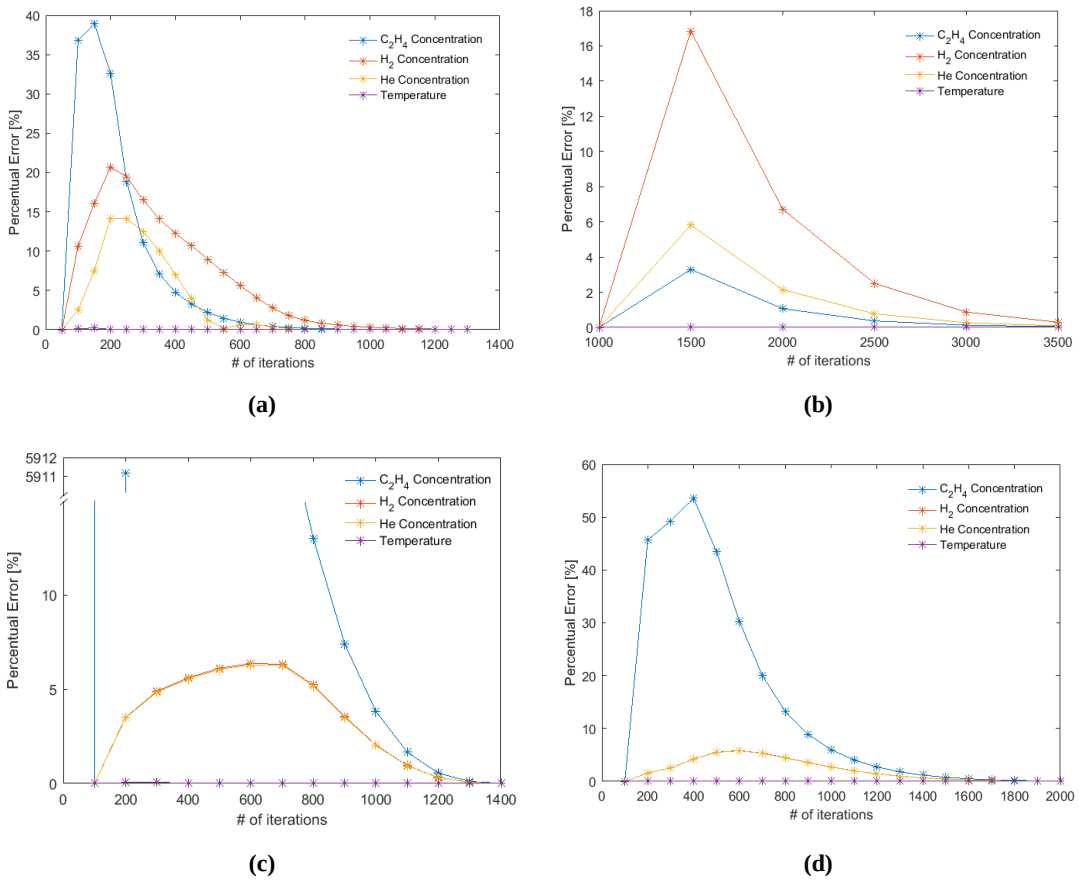

Figure 3.5: Evolution of the percentual errors of the variables addressed in the iterations analysis for the (a) "30 mm", (b) "80 mm", (c) "1 Inch" and (d) "2 Inches" models.

Var_{i-1} are the values of each previously calculated average for each corresponding iteration. The evolution of the computed percentual errors for each model are presented in Figure 3.5.

$$PE_i = 100 * \frac{|Var_i - Var_{i-1}|}{Var_{i-1}} \qquad \textbf{Eq. 3.2}$$

From these trends, considering a convergence of 98% (percentual error of 2%) to be the selection criteria, the maximum number of iterations for each model was selected as the minimum simulated point, where this criteria was fulfilled. Figure 3.6 depicts the zoomed sections, of the previously presented evolutions, where a 98% convergence occurs: 750, 3000, 1100 and 1300 iterations for the "30 mm", "80 mm", "1 Inch" and "2 Inches", respectively.

As for the mesh sizing, an analysis was performed to tune it in order to properly model the envisioned process. For such analysis, the "30 mm" setup was simulated for 750 iterations while using different mesh sizes. These differed from each other by the "Num. Cells Across Gap" parameter (see Table 3.5), which defines the number of elements to

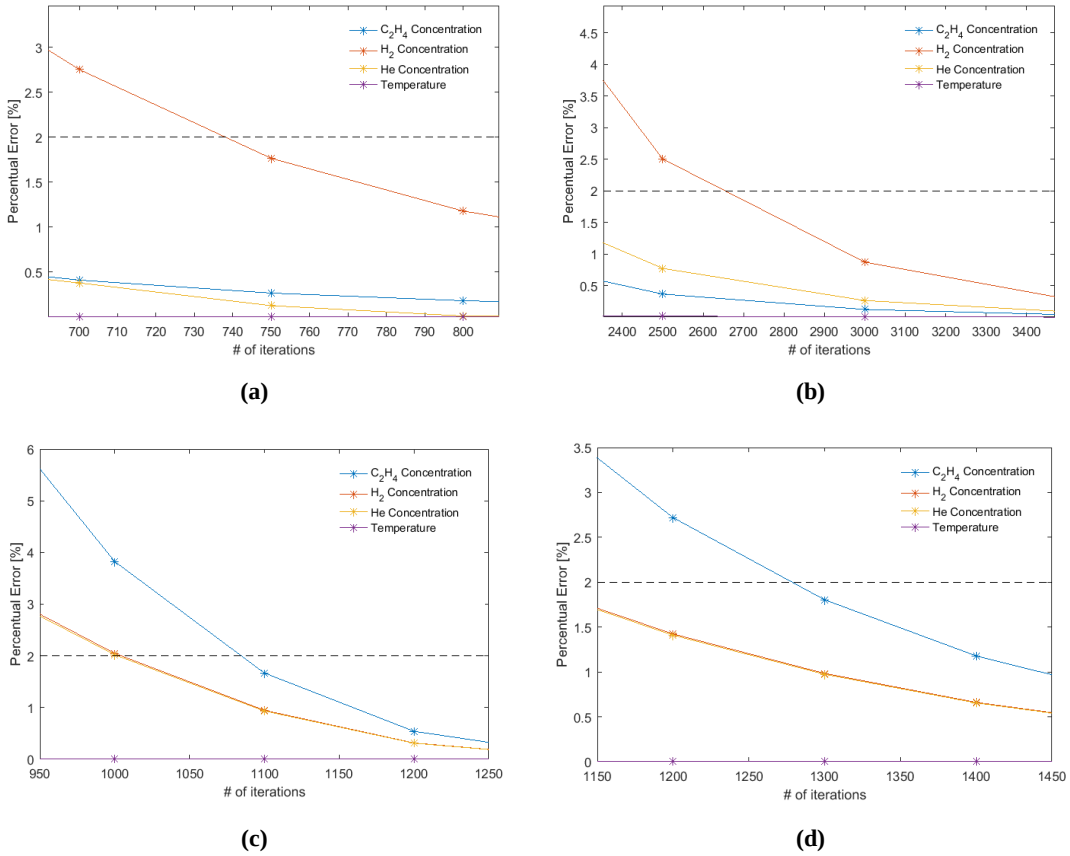

Figure 3.6: Evolution of the percentual errors of the variables addressed in the iterations analysis, for the (a) "30 mm", (b) "80 mm", (c) "1 Inch" and (d) "2 Inches" models, zoomed into the section where a 98% convergence occurs: 750, 3000, 1100 and 1300, respectively.

generate between geometric features. The setup was simulated using 10, 15, 20, 25 and 30 cells across gap. The performed analysis addressed the evolution of the compounds concentrations and temperature throughout the concentric center line of the tube. When compared, these evolutions did not differ from each other. For instance, Figure 3.7 depicts the temperature evolutions throughout the tube for the simulated mesh sizes. Since the mesh sizing only affects the model discretization into individual elements (see Figure 3.8), no difference exists between the depicted curves. Thus an approach independent of the variables' value needed to be used for this analysis.

Since varying the mesh size only affects the total number of elements, in which the model is discretize, an approach based in the distance between them was followed. Table 3.7 shows the time each simulation takes and the resulting average distance between mesh elements, for the addressed mesh sizes on the "30 mm" setup. As depicted, increasing the number of elements in the mesh, i.e. the number of cells across gap, not only reduces the average distance between elements, but also increases the computational time of each simulation. Thus, in order to select the mesh size, a trade-off methodology was followed.

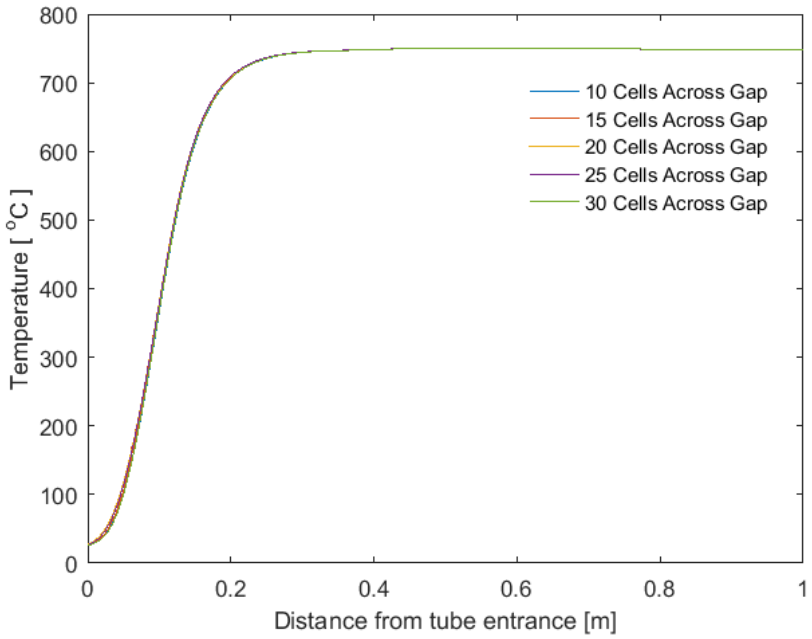

Figure 3.7: Evolution of the mixture's temperature throughout the concentric center line of the tube, while simulating the "30 mm" setup for different mesh sizes.

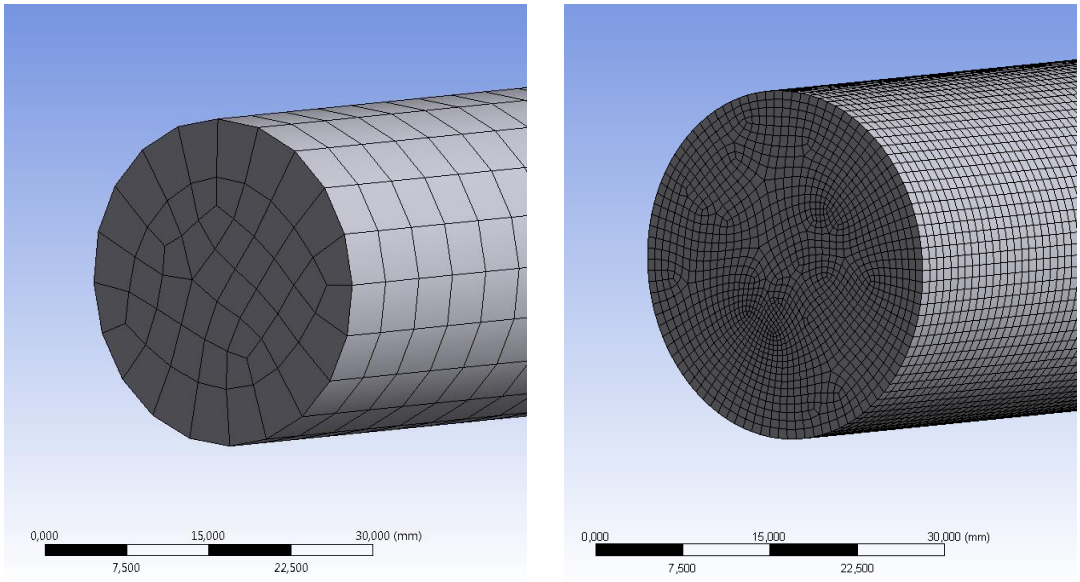

(a) **(b)**

Figure 3.8: Comparison of a (a) 3 and a (b) 30 cells per gap meshes of the same geometry.

Such trade-off methodology was performed by comparing consecutive mesh sizes, based on the additional simulation time (how many additional hours does it take to simulate) and the deducted distance between elements (how much closer consecutive elements are in the mesh). The analysis was performed by addressing the distance between elements won per additional computational time. From the results (see Table 3.8) a mesh

with 20 cells across gap was selected, since with an additional 1.38 hours still subtracts 0.5 mm to the distance between elements, which was considered valuable as such mesh results in a distance less than 1.5 mm (see Table 3.7). Moreover, the 0.08 mm/h achieved by selecting the 25 cells across gap mesh size was considered insufficient.

The same 20 cells across gap was considered for the other setups, since they will all be compared with each other in the following sensitivity analysis. Thus, Table 3.9 depicts the simulation conditions used in the presented research study.

Table 3.7: Time duration of each simulation and average distance between mesh elements, for different mesh sizes, in the "30 mm" setup.

Num. Cells Across Gap	Duration of each simulation [h]	Average distance between elements [mm]
10	6.80	2.6
15	7.80	1.8
20	9.18	1.3
25	12.98	1
30	24.34	0.9

Table 3.8: Distance reduction between mesh elements per additional simulation time.

Num. Cells Across Gap	Additional simulation time [h]	Deducted distance between elements [mm]	Deducted distance per additional time [mm/h]
10	-	-	-
15	0.99	0.8	0.8
20	1.38	0.5	0.36
25	3.79	0.3	0.08
30	11.36	0.1	0.01

Table 3.9: Obtained simulation conditions to be used in the research study.

Tube	Num. of Cells	Num. of Iterations
“30 mm”	20	750
“80 mm”	20	3000
“1 Inch”	20	1100
“2 Inches”	20	1300

3.2. Simulation Scenarios Selection

After defining the simulation conditions, a CFD-based sensitivity analysis was performed to understand the fluid dynamics that occur inside the tube reactor. Such sensitivity analysis addressed the effects of each process parameter in the inner tube synthesis conditions, and thus consists in a parameterization study.

As previously referred, the CVD synthesis process has various parameters. In the specific case of the setups addressed in this research, these process parameters are the three gas flows and the furnace temperature. In the most simple sensitivity analysis, where each parameter is tested for the maximum and minimum values allowed in the setups, a total of 16 simulations would be required. However, such simplified analysis would result in a low-detail comprehension of the process. Thus, each parameter should be tested for more values. However, increasing the number of tested values increases the total number of simulations to perform by a power of four, which would increase the sensitivity analysis' computational time.

Alternatively, the Taguchi method [9,10] was used to set the simulations scenarios to be considered in the study. It uses orthogonal arrays to stipulate a minimum number of experiments, which could give the complete information of all the factors affecting the performance parameter, saving time and resources. These arrays are selected given the number of parameters and levels, i.e. values. For the previously described case of 4 parameters and 2 levels, only a total of 8 simulation scenarios would be required (see Table 3.10).

Table 3.10: Taguchi orthogonal array, depicting the scenarios to simulate in a 4 parameter (a, b, c and d) and 2 levels (1 and 2) example.

	Parameter			
Run	**a**	**b**	**c**	**d**
1	1	1	1	1
2	1	1	1	2
3	1	2	2	1
4	1	2	2	2
5	2	1	2	1
6	2	1	2	2
7	2	2	1	1
8	2	2	1	2

Table 3.11: Number of simulations to run, depending of the number of parameters and levels, when following the Taguchi orthogonal arrays, as well as its percentual representation when compared to the total number of simulations if the Taguchi method was not considered.

		Number of Parameters			
		2	**3**	**4**	**5**
Number of Levels	**2**	4 (100%)	4 (50%)	8 (50%)	8 (25%)
	3	9 (100%)	9 (33%)	9 (11%)	18 (7%)
	4	16 (100%)	16 (25%)	16 (6%)	16 (1.5%)
	5	25 (100%)	25 (20%)	25 (4%)	25 (0.8%)

Moreover, Table 3.11 depicts the total number of simulations to perform, according to the Taguchi orthogonal arrays, for various combinations of parameters and levels. It also shows a percentual comparison between these values with the corresponding total number of simulations, which would be performed if the Taguchi method was not considered. For instance, for 5 parameters evaluated for 2 levels each, the total number of combinations is $2^5 = 32$. Thus, if the Taguchi method is considered, the resulting 8 simulations represent 25% of that number. Through this comparison, it is deductible that the Taguchi method always result in less simulations (except when there are only 2 parameters), and its efficiency is proportional to the number of levels or parameters. Thus, the Taguchi method was applied to select the scenarios for simulation.

In the following chapters, a description of the Taguchi orthogonal array, used in each performed sensitivity analysis, depicting the number or parameters and levels to be considered, is presented.

3.3. Post-Processing

The Taguchi orthogonal arrays significantly reduce the number of scenarios to be considered in each analysis. In order to obtain complete information about the analyzed system, a few mathematical equations must be followed. Such procedure is described in this section.

Once all values were obtained for each simulation, the analysis was performed addressing individual levels of each parameter. Since each parameter-level combination appears multiple times throughout the experiments, the value of a certain variable for such combination was computed as the average of the values of that variable for those scenarios. This procedure is represented by Eq. 3.3, where $V_{parameter}^{level}$ is the value of variable V for a

given parameter-level combination, and $V_{s_P}^{L}$ is the value of variable V, obtained in a simulation which scenario contains the $P-L$ combination.

$$V_{parameter}^{level} = average\left(\forall\, V_{s_{parameter}}^{level}\Big|_{P=parameter;L=level}\right) \quad \textbf{Eq. 3.3}$$

Considering a 4 parameters and 2 levels example, whose output of each run i is represented by V_i (see Table 3.12), the value of this variable when, for example, the parameter *b* has the value *2*, V_b^2, is computed as the average of the set $[V_3, V_4, V_7, V_8]$. Similarly, when the parameter *d* has the value *1*, V_d^1 is the average of the set $[V_1, V_3, V_5, V_7]$.

Moreover, in order to have a better perception on each gas influence in a certain variable, the maximum and minimum values for each combination were also computed and presented in the results for each variable. For example, Eq. 3.4 and Eq. 3.5 depict how the maximum and minimum values were calculated for the parameter-level combination, respectively.

$$max_{V_{parameter}^{level}} = max\left(\forall\, V_{s_{parameter}}^{level}\Big|_{P=parameter;L=level}\right) \quad \textbf{Eq. 3.4}$$

$$min_{V_{parameter}^{level}} = min\left(\forall\, V_{s_{parameter}}^{level}\Big|_{P=parameter;L=level}\right) \quad \textbf{Eq. 3.5}$$

Posteriorly, envisioning the analysis of how each parameter affects each variable, a ranking vector was computed for each variable. Since every parameter-level combination was tested the same amount of times, the computed means, i.e. the V_P^L values, were used to

Table 3.12: Scenarios to simulate in a 4 parameter (a, b, c and d) - 2 (1 and 2) levels example with an output variable.

	Parameter				Output
Run	***a***	***b***	***c***	***d***	
1	1	1	1	1	V_1
2	1	1	1	2	V_2
3	1	2	2	1	V_3
4	1	2	2	2	V_4
5	2	1	2	1	V_5
6	2	1	2	2	V_6
7	2	2	1	1	V_7
8	2	2	1	2	V_8

create this ranking. Considering X_P^V as the set containing all values of variable V calculated for parameter P, the variation caused by P in V, Δ_P^V, can be calculated by Eq. 3.6.

$$\Delta_P^V = \max(X_P^V) - min(X_P^V) \quad \textbf{Eq. 3.6}$$

Considering the previous example (see Table 3.12), X_b^V is the set which includes all values of the variable V for the parameter b, i.e. $[V_b^1, V_b^2]$. This is the set used to calculate the variation Δ_b^V via Eq. 3.6.

Finally, the effects of how each parameter affect each variable were addressed as a percentual ranking, where the parameter with the highest percentage would be the one, which produces the highest variation in each variable. Thus, the percentual dependency of variable V on parameter P, D_P^V, can be calculated by Eq. 3.7.

$$D_P^V = \frac{\Delta_P^V}{\sum \Delta_i^V} \quad \textbf{Eq. 3.7}$$

In the example, to calculate the dependency of the variable V on parameter b, D_b^V, Eq. 3.7 is re-written as follow.

$$D_b^V = \frac{\Delta_b^V}{\Delta_a^V + \Delta_b^V + \Delta_c^V + \Delta_d^V} \quad \textbf{Eq. 3.8}$$

Following this methodology, it is possible to analyze which process parameter has higher impact in the process conditions inside the tube. Since the conditions' dependency on each parameter is calculated as a fraction of all the variations, a higher percentual dependency is related with a higher impact that a parameter has in a specific variable.

3.4. Variables selection

Since the Taguchi method only allows the analysis of certain process characteristics [9,10], these were selected taking into account previous observations on typical variables' curves throughout the tube. For instance, Figure 3.9 depicts typical evolutions of the mixture's temperature and velocity throughout the tube. The selected process characteristics to be analyzed are related with the variables' convergence point (point A in Figure 3.9), which was defined as the smallest distance from the tube entrance (i) that ensures a convergence of 98% (see Eq. 3.9, where f_i^{end} is the vector containing all values of a certain variable for indexes greater or equal to index i).

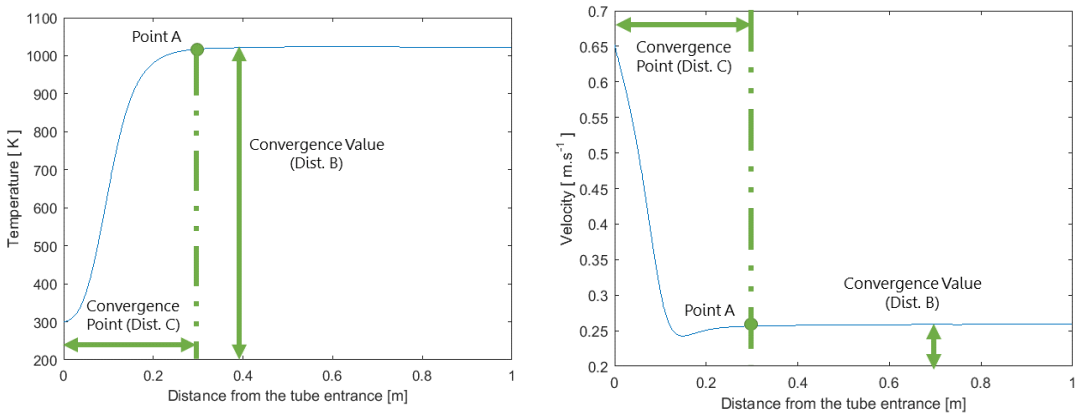

(a) **(b)**

Figure 3.9: Typical curve of the mixture's (a) temperature and (b) velocity evolutions throughout the tube, depicting the convergence parameters used in the sensitivity analysis.

$$\frac{max\left(\left\|f_i^{end} - \overline{f_i^{end}}\right\|\right)}{\overline{f_i^{end}}} < 0.02 \qquad \textbf{Eq. 3.9}$$

The process characteristics addressed in this sensitivity analysis were selected by evaluating how each variable's evolution changes for different gas flows. For variables which tend to converge, at different rates, to the same value (the mixture's temperature, for instance), the distance from the tube entrance where it reaches the convergence value was selected (Dist. C in Figure 3.9). On the other hand, for variables which converge towards different values (such as the mixture's velocity), the mean value of convergence was evaluated (Dist. B in Figure 3.9). Finally, if the variable's profile throughout the tube is uniform, i.e. it does not converges to a specific value, the mean value of the variable throughout the tube was used.

3.5. Final Considerations

The methodology here described is followed throughout the following chapters to perform several sensitivity analysis of the CVD setups. However, each sensitivity analysis is performed with a different purpose. Thus, each one has its own sets of simulation scenarios and of selected variables to analyze, which are described individually in detail for each sensitivity analysis.

References

[1] J. Tu, G. Yeoh, C. Liu, Computational fluid dynamics: A practical approach, 3rd ed., Elsevier B.V., Oxford, UK, 2018.

[2] H.K. Versteeg, W. Malalasekera, An Introduction to Computational Fluid Dynamics - The Finite Volume Method, 2nd ed., Pearson Education, 2007.

[3] T. Norton, D.-W. Sun, Computational fluid dynamics (CFD) - an effective and efficient design and analysis tool for the food industry: A review, Trends Food Sci. Technol. 17 (2006) 600–620. doi:10.1016/j.tifs.2006.05.004.

[4] ANSYS Inc, ANSYS CFX 13.0 - Technical Specifications, Contract Hold. (2010).

[5] W. Jeong, J. Seong, Comparison of effects on technical variances of computational fluid dynamics (CFD) software based on finite element and finite volume methods, Int. J. Mech. Sci. 78 (2014) 19–26. doi:10.1016/j.ijmecsci.2013.10.017.

[6] T. Glatzel, C. Litterst, C. Cupelli, T. Lindemann, C. Moosmann, R. Niekrawietz, W. Streule, R. Zengerle, P. Koltay, Computational fluid dynamics (CFD) software tools for microfluidic applications – A case study, Comput. Fluids. 37 (2008) 218–235. doi:10.1016/j.compfluid.2007.07.014.

[7] J. Mcbride, A. Reno, Coefficients for Calculating Thermodynamic and Transport Properties of Individual Species, Nasa Tech. Memo. 4513 (1993) 98. http://ntrs.nasa.gov/archive/nasa/casi.ntrs.nasa.gov/19940013151_1994013151.pdf.

[8] ANSYS Inc, [Lecture 4] Introduction to ANSYS Mechanical: Meshing, (2010). http://inside.mines.edu/~apetrell/ENME442/Labs/1301_ENME442_lab3.pdf.

[9] R.K. Roy, A Primer on the Taguchi Method, Second, SME, 2010.

[10] I.N. Vuchkov, N.L. Boyadjieva, Quality improvement with design of experiments: a response surface approach, 7th ed., Springer Science & Business Media, 2013. doi:10.1017/CBO9781107415324.004.

Chapter 4

SENSITIVITY ANALYSIS

A CFD-based sensitivity analysis was the starting point, and aimed at understanding the fluid dynamics which occur inside the tube reactor. Such sensitivity analysis addresses the effects of each process parameter in the inner tube synthesis conditions. By identifying and understanding these effects through numerical tools, it becomes then possible to target and achieve specific synthesis conditions by adjusting the process parameters.

4.1. Methodology

The presented analysis consisted in a parametrization study, where the addressed process parameters were the gases flows. In the analysis, each gas was tested for various flows and their effects on several process characteristics was evaluated. As mentioned in chapter 3, the Taguchi method was used to set the simulations scenarios to be considered in the study.

The sensitivity analysis addressed all three gases (ethylene, hydrogen and helium), tested for five different flows (50, 250, 500, 750 and 1000 sccm), resulting in detailed information on the synthesis conditions' dependency on the process parameters. These flow

Table 4.1: Gas flows, presented in sccm, used in the simulation scenarios that constitute the sensitivity analysis.

Exp.	C_2H_4	H_2	He
1	50	50	50
2	50	250	250
3	50	500	500
4	50	750	750
5	50	1,000	1,000
6	250	50	250
7	250	250	500
8	250	500	750
9	250	750	1,000
10	250	1,000	50
11	500	50	500
12	500	250	750
13	500	500	1,000
14	500	750	50
15	500	1,000	250
16	750	50	750
17	750	250	1,000
18	750	500	50
19	750	750	250
20	750	1,000	500
21	1,000	50	1,000
22	1,000	250	50
23	1,000	500	250
24	1,000	750	500
25	1,000	1,000	750

values were selected taking into account the Mass Flow Controllers' maximum flow available in the lab (1000 sccm), and the equidistance between them. Since a non-zero flow is always intended, the lower value (50 sccm) is the only non-equidistant one. For this sensitivity analysis with 3 parameters and 5 levels, a total of 25 simulation scenarios should be performed according to the Taguchi method (see Table 4.1).

In this sensitivity analysis, the studied variables were:

- Mean of each gas concentration throughout the tube;
- Convergence value of the mixture's, temperature and velocity;

- Distance to tube entrance (convergence point) where the mixture's temperature and velocity reach convergence.

These variables were measured throughout the tube's center line, coaxial to the mixture's flow (see Figure 4.1). Once all values were obtained for each simulation, the analysis was performed by following the methodology presented in section 3.3, where the percentual dependencies of each synthesis condition on each process parameter are calculated. These dependencies reflect the impact of each parameter in each variable and thus, can be used as a metric to determine the parameter which influence most of the variables.

4.2. Results and Discussion

The sensitivity results for the addressed variables are presented in this section, which is organized based on the variables' nature. The various subsections are: (i) gases concentrations; (ii) mixture's velocity; (iii) mixture's temperature; (iv) temperature dependent properties; and (v) comparison between tubes.

4.2.1. Gases Concentrations

Since the varied parameters are the compounds flows, the most directly affected variables are their concentrations. Figure 4.2, Figure 4.3 and Figure 4.4 depict the sensitivity analysis results for the C_2H_4, H_2 and He concentrations, respectively, for all

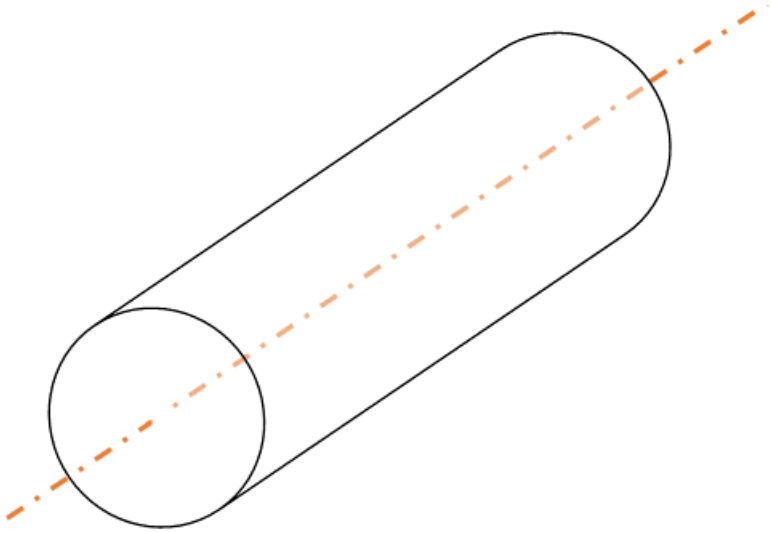

Figure 4.1: Graphical representation of the tube's center line, where measurements were made.

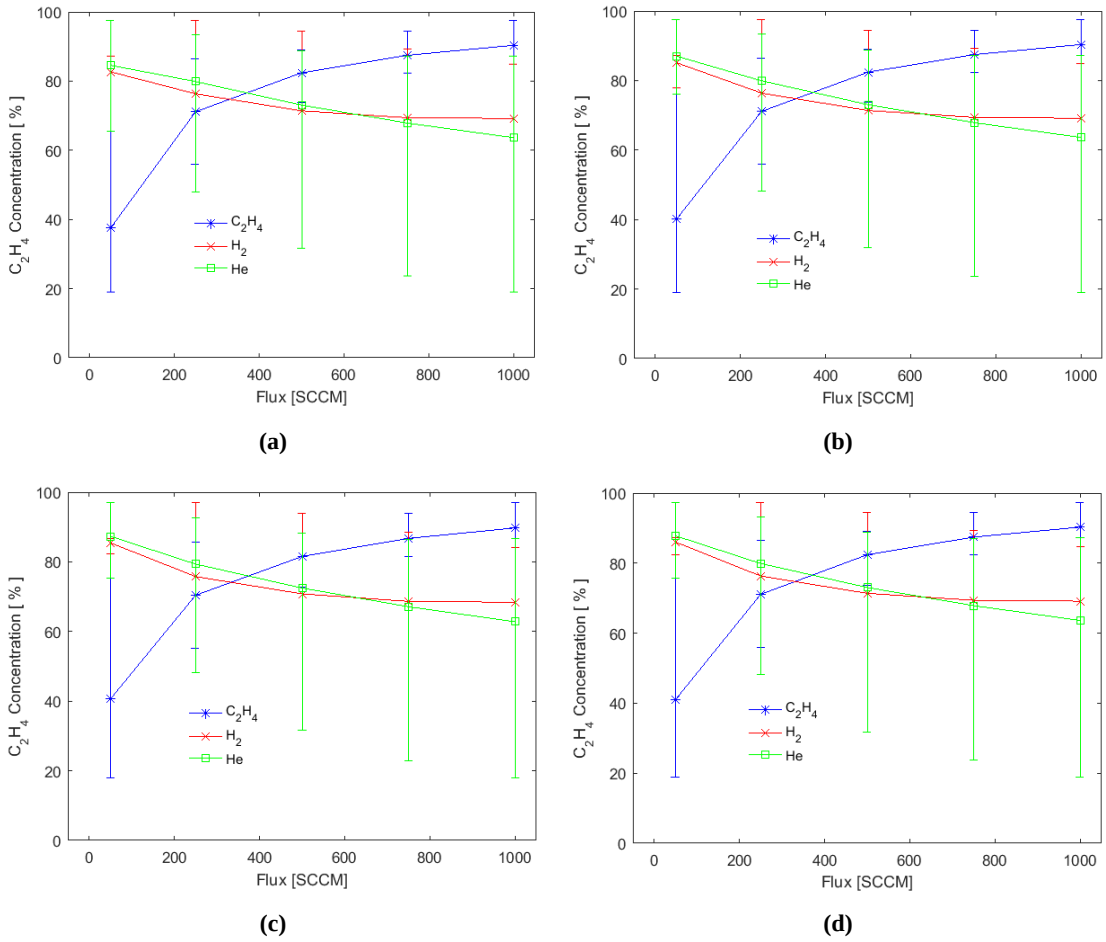

Figure 4.2: Sensitivity analysis of the ethylene concentration, for the (a) "30 mm", (b) "80 mm", (c) "1 Inch" and (d) "2 Inches" tubes.

addressed tubes. As stated in section 3.3, for each gas-flow combination, in addition to the mean value (V_P^L), the maximum and minimum points were also computed and are presented as error bars. As expected, each compound concentration increases with its own flow and decreases with the increase of the other gases' flows.

Nonetheless, the ethylene gas flow is the parameter which causes more variation in the compounds' concentrations' mean values. Having a higher molar mass (see Table 3.4), ethylene is the compound which most affect the mixture's behavior inside the tube, leading to its higher concentration and, consequently, a lower concentration of the other gases. For the same reason, ethylene also has influence in the difference between the maximum and minimum points of other gases concentrations. The simulations where the ethylene flow is maximum (or minimum), are the ones which result in the maximum (or minimum points) for the other compound curves. This means that simulations that limit the H_2 and He concentration values, for any given tested flow, are the ones where the ethylene flow is the highest or the lowest. Thus, although data was collected for the other gases, only the

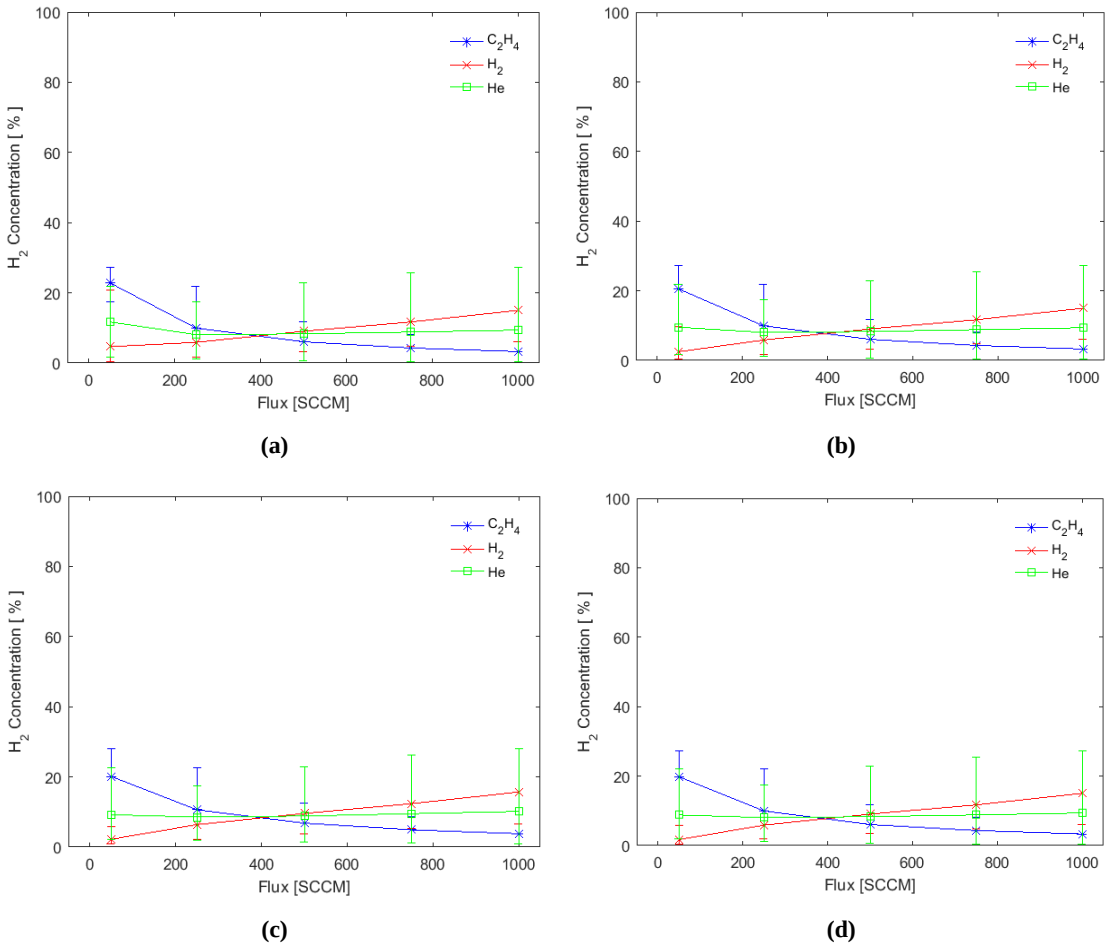

Figure 4.3: Sensitivity analysis of the hydrogen concentration, for the (a) "30 mm", (b) "80 mm", (c) "1 Inch" and (d) "2 Inches" tubes.

ethylene's effects on the addressed variables are presented this point onward.

Moreover, these results are consistent for the different setups, assessed in this analysis. In fact, the obtained error bars are equal for all four setups, meaning that the setups' distinguishable features do not affect the concentrations inside the tube. These are only affected by the gases flows.

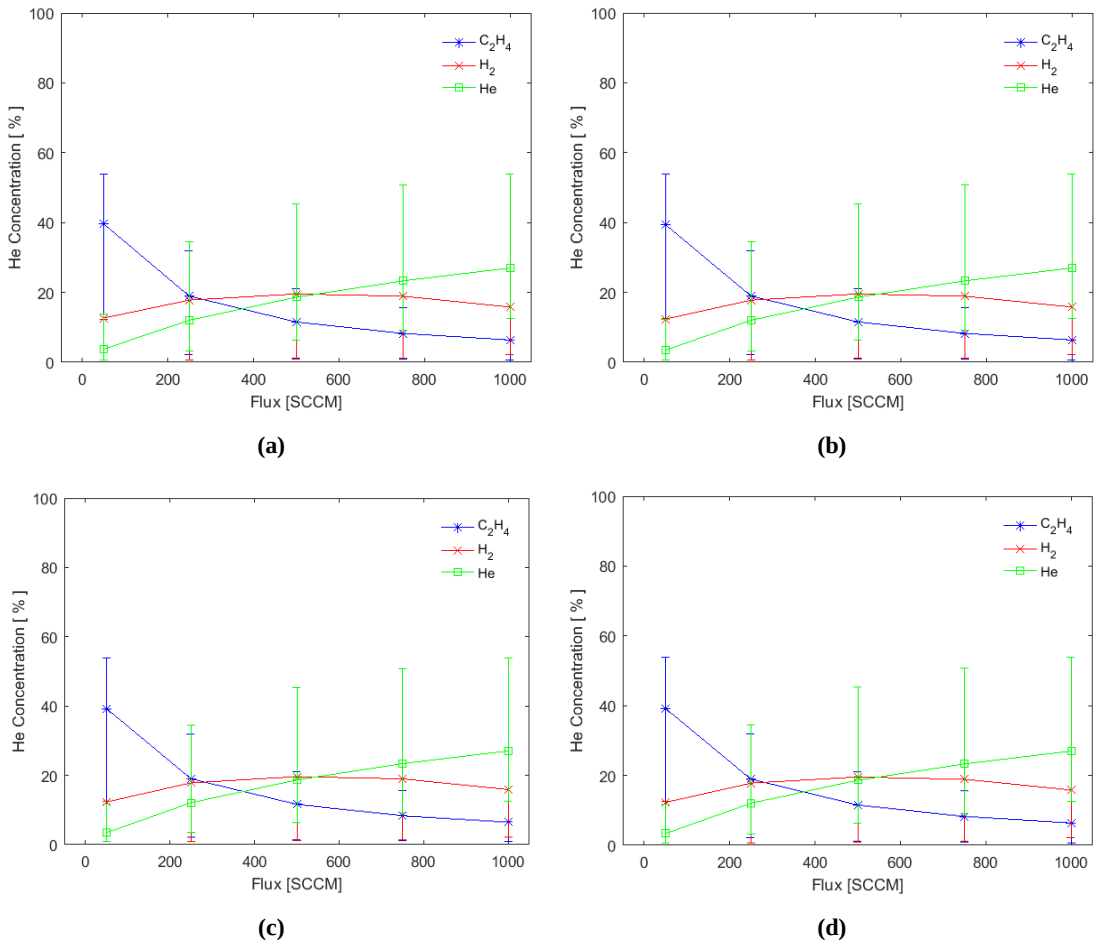

Figure 4.4: Sensitivity analysis of the helium concentration, for the (a) "30 mm", (b) "80 mm", (c) "1 Inch" and (d) "2 Inches" tubes.

4.2.2. Mixture's Velocity

The variable which most directly depends on the total flow is the mixture's velocity profile throughout the tubes. Figure 4.5 depicts a typical velocity profile throughout the tube in the 30 mm setup. After entering the tube, the mixture's velocity decreases due to the difference between the diameters of the setup lines and tube. Inside the tube, the mixture has a greater area to flow and, in order to maintain the same volumetric flow, its velocity is reduced. The mixture's velocity is also influenced by its viscosity, which defines the mixture's resistance to its own flow. Due to this property, the particles nearer the tube walls slow down and, to maintain the volumetric flow, particles nearer the tube center have to speed up. Moreover, in gases, the viscosity increases with temperature [1–3]. Compared to liquids, gases have a weaker intermolecular force and, the increase of temperature causes

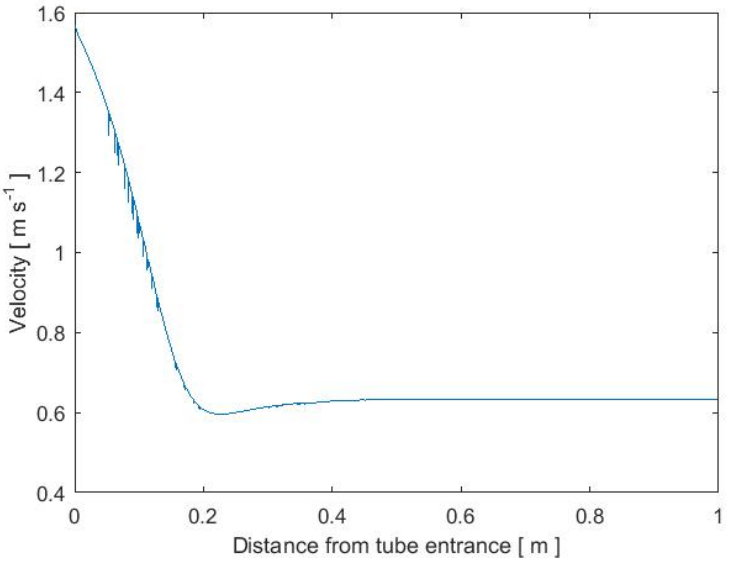

Figure 4.5: Velocity profile throughout the tube for the experiment with ethylene, hydrogen and helium flows of 250-250-500 sccm, in the "30 mm" setup.

the molecules to travel more freely and randomly, causing more collisions between them, increasing the viscosity and intensifying the referred velocity increase.

Both these phenomenon affect the mixture's velocity. Closer to the tube entrance, the velocity reduction effects are greater, and, further away, the velocity increase is still occurring until a constant velocity is achieved and maintained throughout the tube. Thus the mixture's velocity is a parameter whose evolution converges to a certain value, being defined by its convergence value and point. These variables were assessed in the sensitivity analysis and the results are shown in Figure 4.6. As expected, a higher flow induces a higher mixture velocity (see Figure 4.6a). Such phenomenon can be seen when comparing the gases' streamlines and velocity throughout the 30 mm tube in experiments with a low and

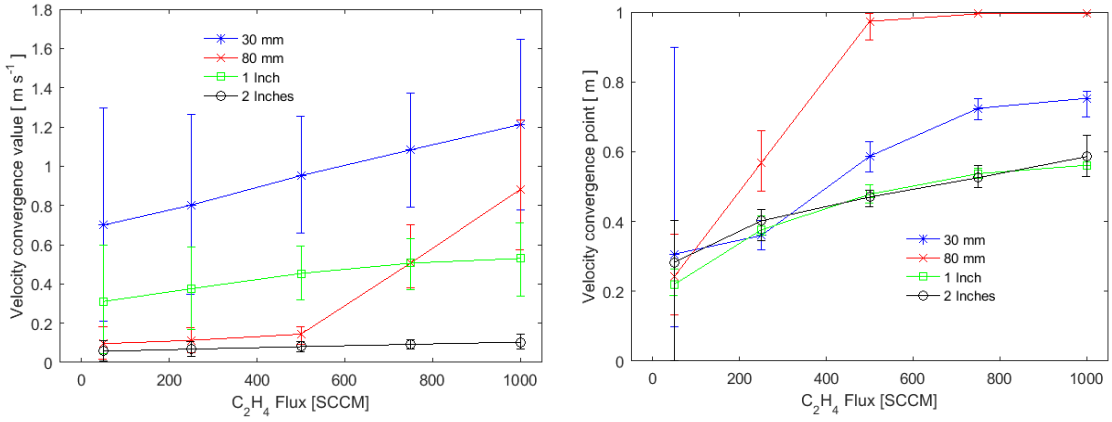

(a) **(b)**

Figure 4.6: Sensitivity analysis, while varying the C_2H_4 flow, of the velocity's convergence (a) value and (b) point, for all setups.

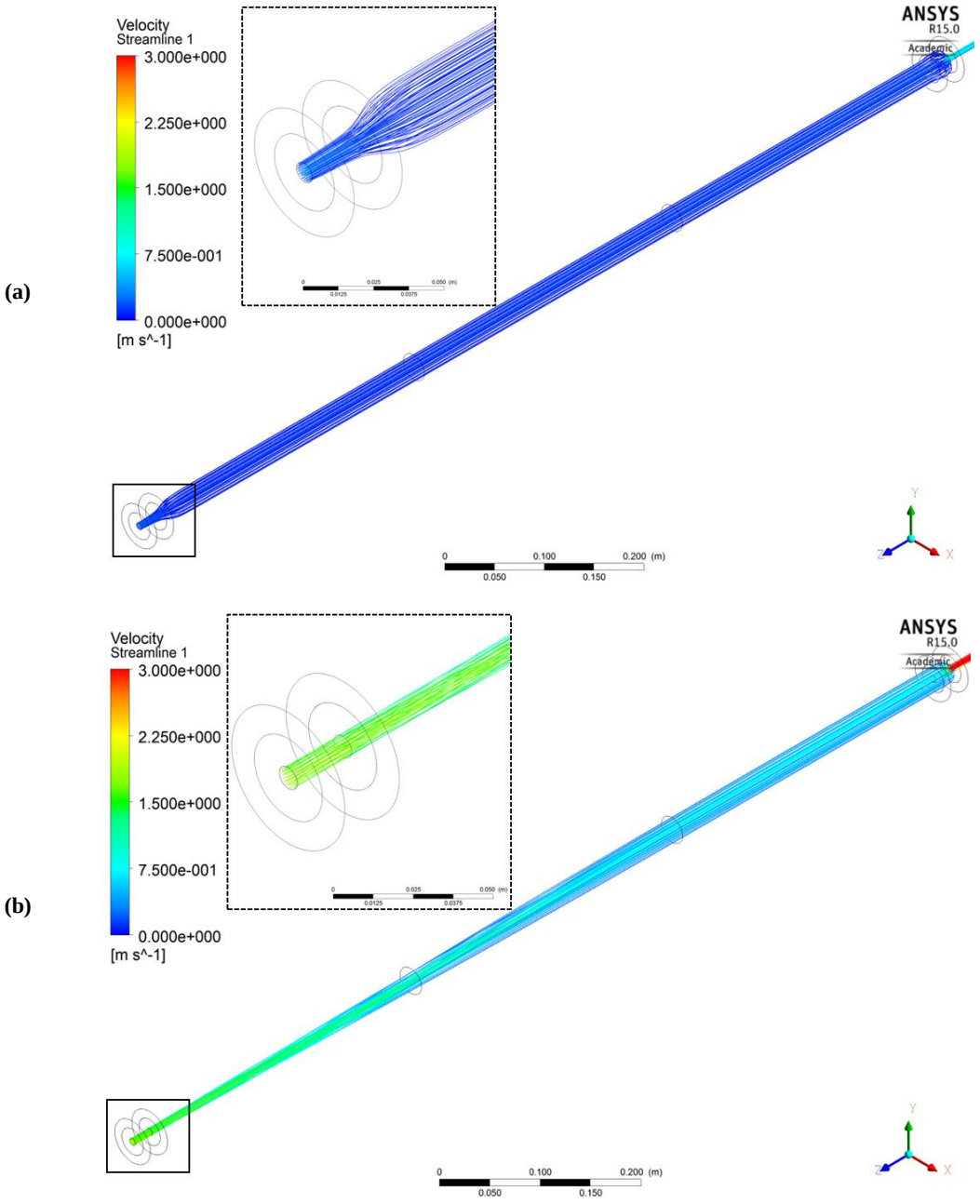

Figure 4.7: Comparison of the gases mixture's velocity streamlines across the "30 mm" tube for experiments with ethylene, hydrogen and helium flows of (a) 50-50-50 and (b) 1000-250-50 sccm.

a high ethylene flow (see Figure 4.7). Moreover, in the later scenario, since the total flow is greater, it requires more time for the velocity to stabilize. Thus a higher ethylene flow also increases the distance from the tube entrance where the mixture's velocity converges at (see Figure 4.6b).

In the 80 mm setup, due to its higher radius, the mixture is more dispersed than in the 30 mm tube, for the same flow, leading to a smaller converge values. Such phenomenon can be seen in Figure 4.8, which depicts the velocity profiles, for the same experiment, in

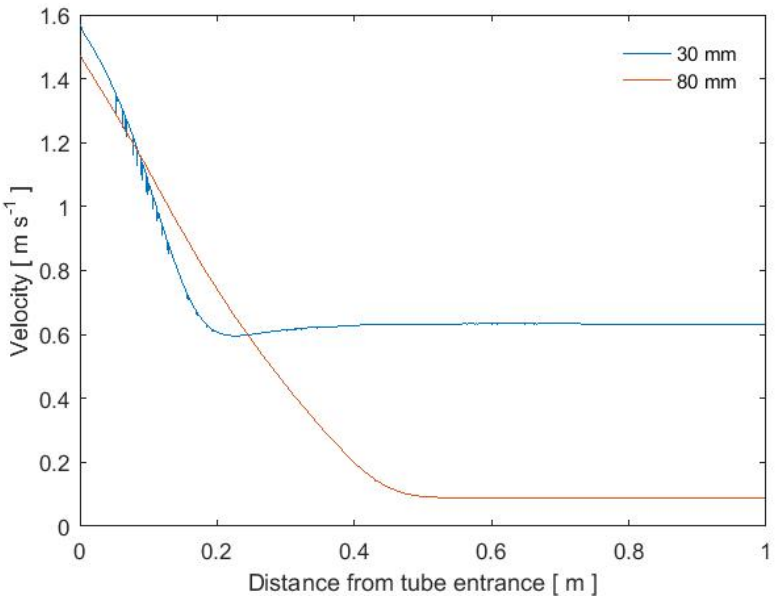

Figure 4.8: Velocity profile throughout the tube for the experiment with ethylene, hydrogen and helium flows of 250-250-500 sccm, in the "30 mm" and the "80 mm" setups.

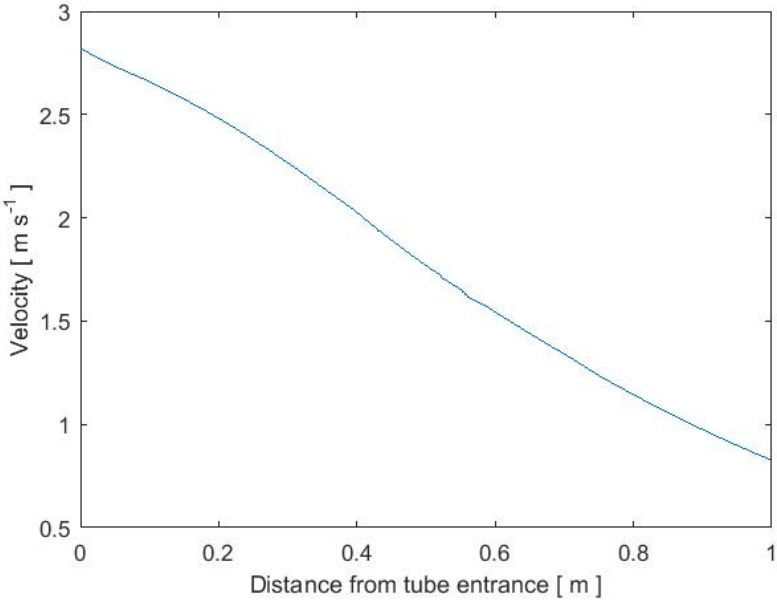

Figure 4.9: Velocity profile throughout the tube for the experiment with ethylene, hydrogen and helium flows of 1000-50-1000 sccm, in the "80 mm" setup.

both setups. Thus in the 80 mm setup, for the same flow, the mixture's velocity converges to a smaller value and also requires more tube distance to reach that convergence (see Figure 4.6). Moreover, for ethylene flows higher than 500 sccm, the tube length is not sufficient for the mixture to converge properly (see Figure 4.9), resulting in a convergence point saturation and convergence values which do not follow the trend of the experiments with lower flows (see Figure 4.6).

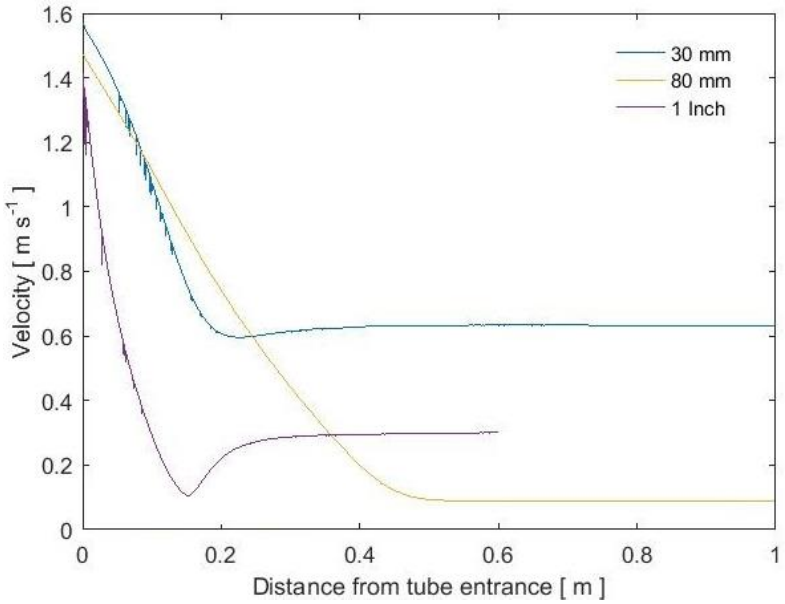

Figure 4.10: Velocity profile throughout the tube for the experiment with ethylene, hydrogen and helium flows of 250-250-500 sccm, in the "30 mm", the "80 mm" and the "1 inch" setups.

In the 1 inch setup, on the contrary to the previous setups, the furnace is not placed directly at the tube entrance (see Figure 3.2). Thus, when entering the tube, the mixture's velocity is only affected by the reduction caused by the tube's bigger radius. Figure 4.10 depicts a comparison between the velocity profiles, for the same experiment, in these three setups. In the 1 inch tube, since the mixture is not being heated right after entering tube, the previously referred velocity increase due to the increased dynamic viscosity does not occur. Thus, the velocity reduction effects due to the different radius are more noticeable. The velocity increase effects due to the increased viscosity only occur later in the tube, when the mixture enters the tube section heated by the furnace, resulting in a velocity convergence value between the 30 mm and the 80 mm curves (see Figure 4.6).

The fact that the 2 Inches setup's entrance is positioned sideways in relation to the main tube alters the gases' diffusion through it. The particles collide with the tube wall, directly opposite to the tube entrance (see Figure 4.11). Such collision causes the mixture particles to slow down abruptly, stabilizing before flowing through the tube (see Figure 4.12). It is this phenomenon that causes the velocity convergence value to be smaller than in the other setups and to suffer almost no alteration when varying the ethylene flow (see Figure 4.6a).

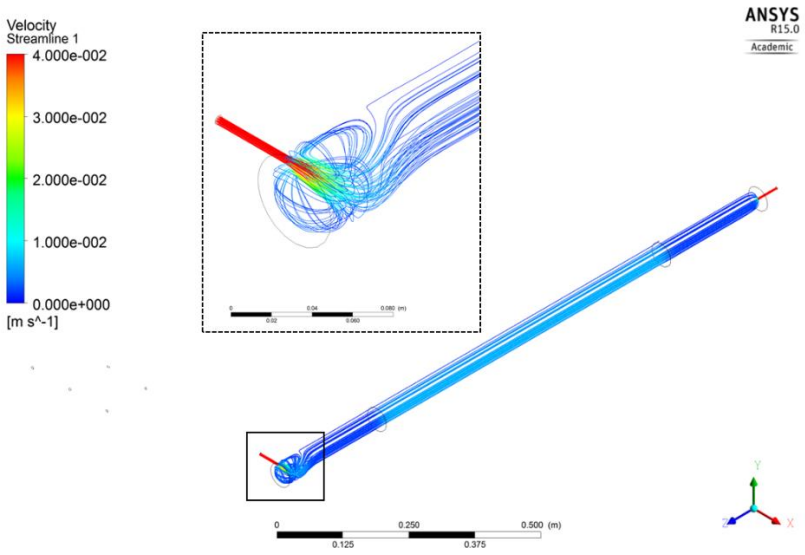

Figure 4.11: Mixture's velocity streamlines across the "2 Inches" setup for the experiment with ethylene, hydrogen and helium flows of 250-250-500 sccm.

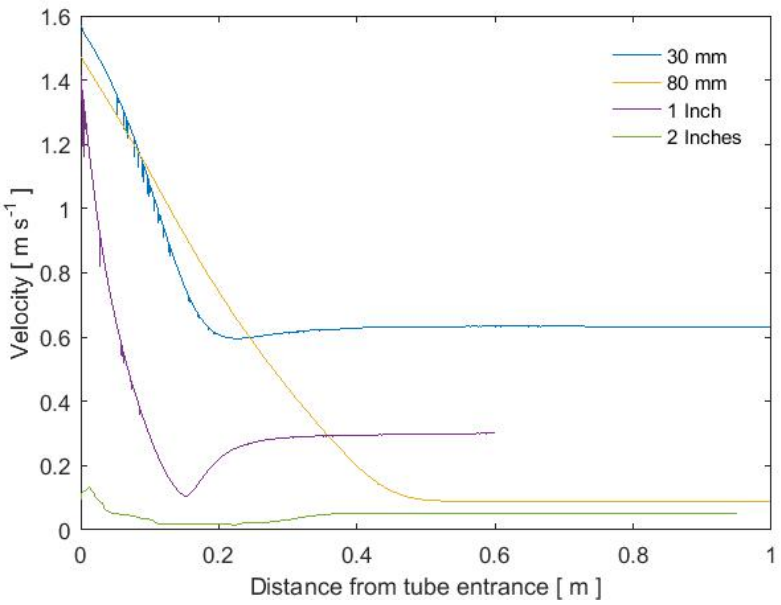

Figure 4.12: Velocity profile throughout the tube for the experiment with ethylene, hydrogen and helium flows of 250-250-500 sccm, in all setups.

Moreover, since the furnace is placed in the middle of the tube, when the mixture reaches the heated section, it is already flowing at a uniform velocity, and, as in the 1 inch setup, it speeds up a bit (see Figure 4.12). As for the velocity convergence point, it increases with the ethylene flow, as in the other setups (see Figure 4.6a).

The physical features and differences between setups play a significant role in the mixture's velocity profile throughout the tubes. For instance, only by increasing the tube radius or even by changing the tube entrance result in a completely different velocity profile

throughout the tube, for the same gases flows. Moreover, such effects also alter how the velocity-related variables are affected by different gas flows. Such profiles affect other mixture's properties, which are presented in the next sections.

4.2.3. Mixture's Temperature

The CVD process consists on compounds flowing through a heated tube, thus, the mixture's temperature profile depends on the amount of heat transferred from the tube walls to the mixture. Such heat transfer rate is mainly influenced by the mixture's velocity and by the tube temperature, which was constant in this sensitivity analysis. Figure 4.13 depicts a typical temperature profile in the 30 mm setup. As the mixture enters the tube, it starts

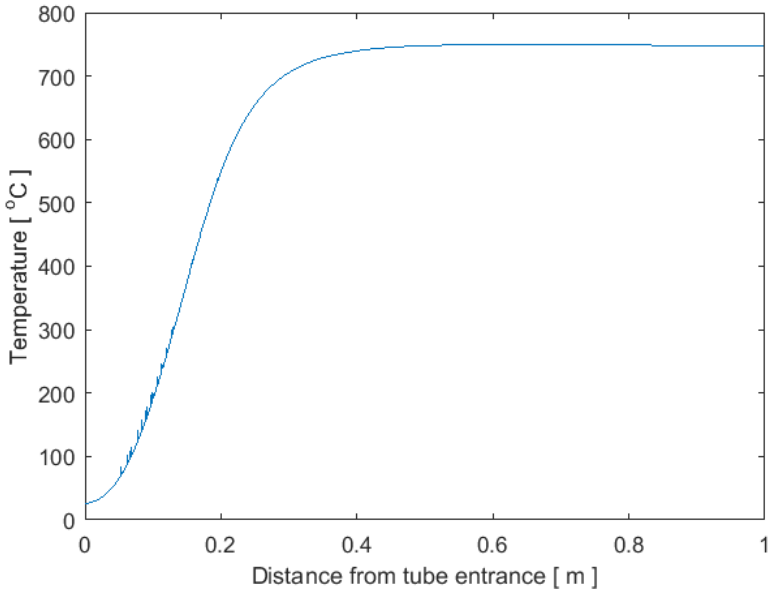

Figure 4.13: Temperature profile throughout the tube for the experiment with ethylene, hydrogen and helium flows of 250-250-500 sccm, in the "30 mm" setup.

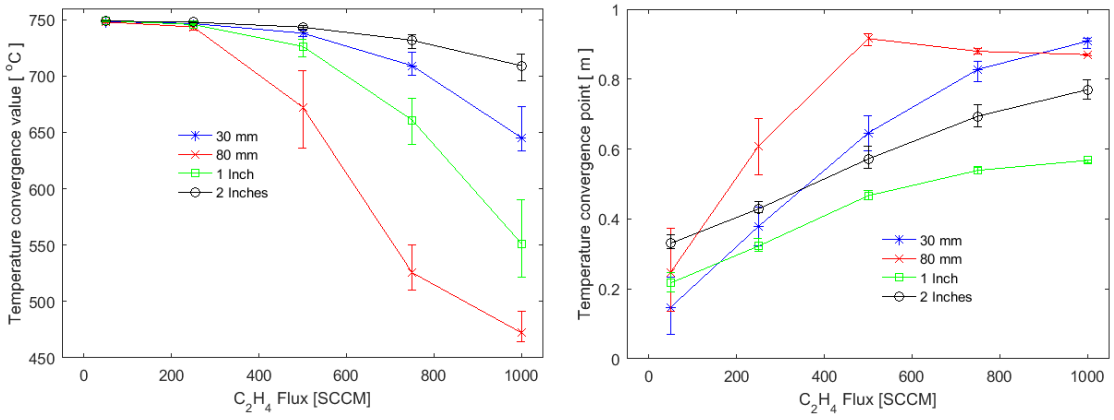

(a) **(b)**

Figure 4.14: Sensitivity analysis, while varying the C_2H_4 flow, of the temperature's convergence (a) value and (b) point, for all setups.

heating up and, as it travels throughout the tube, its temperature keeps increasing converging to the same value as the tube walls temperature (750 ºC, in this case). Thus, the mixture's temperature profile throughout the tube can be expressed by its convergence value and point (see Figure 4.14).

As previously stated, the mixture's temperature is influenced by the heat transferred to its particles. If the mixture is travelling at a bigger velocity, these particles require less time to travel the whole tube length, and consequently, more tube distance to reach the same temperature as the tube. This can be seen in Figure 4.15, where the temperature profile of the simulation with greater flows required more tube distance to reach the temperature of 750 ºC. Thus, it is conclusive that the temperature convergence point increases with the gas flows (see Figure 4.14b). As shown in Figure 4.15, such relation is transversal to all setups, as it is a consequence of the velocity at which the mixture travels throughout the tube. In this figure, it is also noticeable the furnace position in relation to the tubes, in the

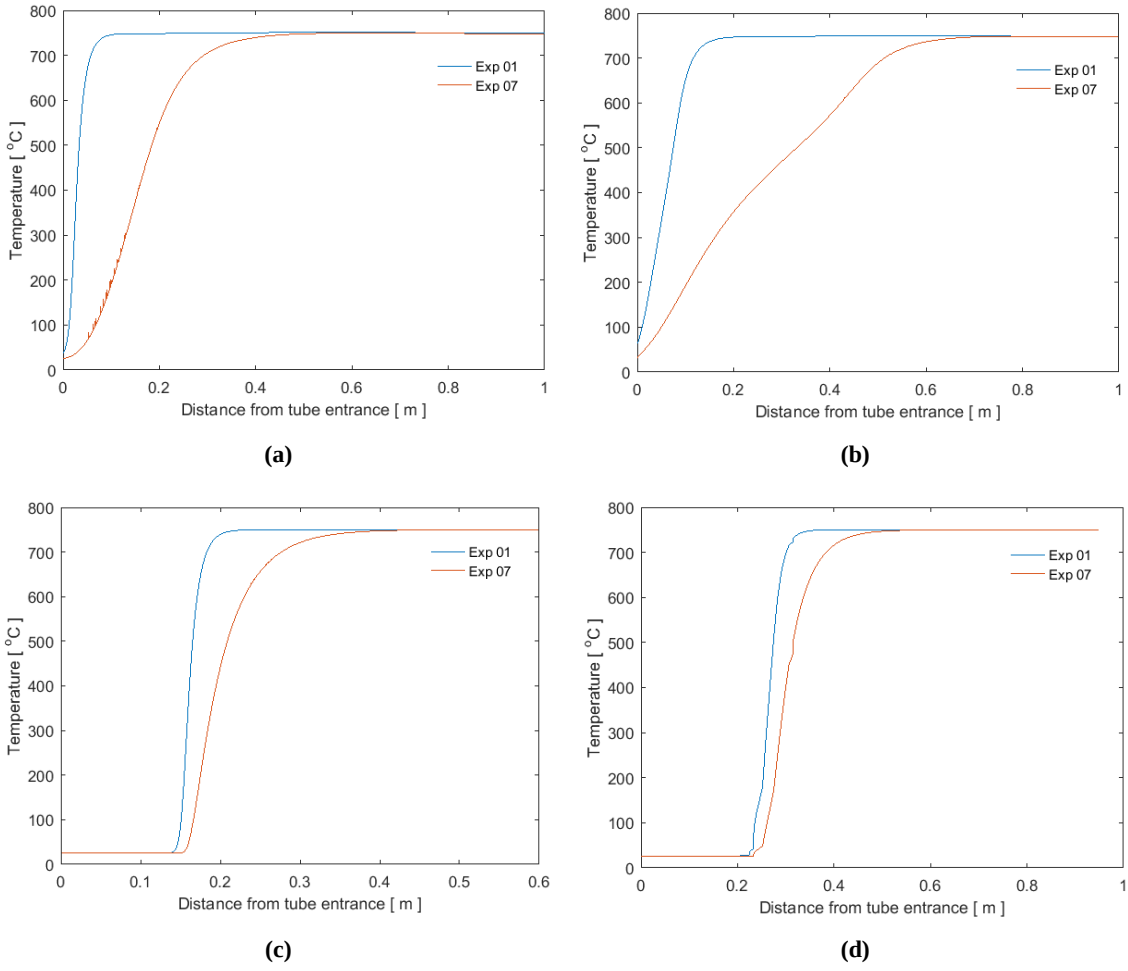

Figure 4.15: Temperature profiles throughout the tube for the experiment with ethylene, hydrogen and helium flows of 50-50-50 and 250-250-500 sccm, in the (a) "30 mm", (b) "80 mm", (c) "1 Inch" and (d) "2 Inches" tubes.

1 inch and 2 inches setups.

As the mixture's velocity increases, more tube length is required for its temperature to reach the desired one. Consequently, if the mixture is travelling too fast, it might occur that the existent tube total length is no sufficient for the desired temperature to be reached. Comparing the streamlines and temperature throughout the 30 mm tube in experiments with a low and a high ethylene flow (see Figure 4.16), it is noticeable that, in the latter, the mixture's velocity is too big for the temperature to reach the desired value. This means that,

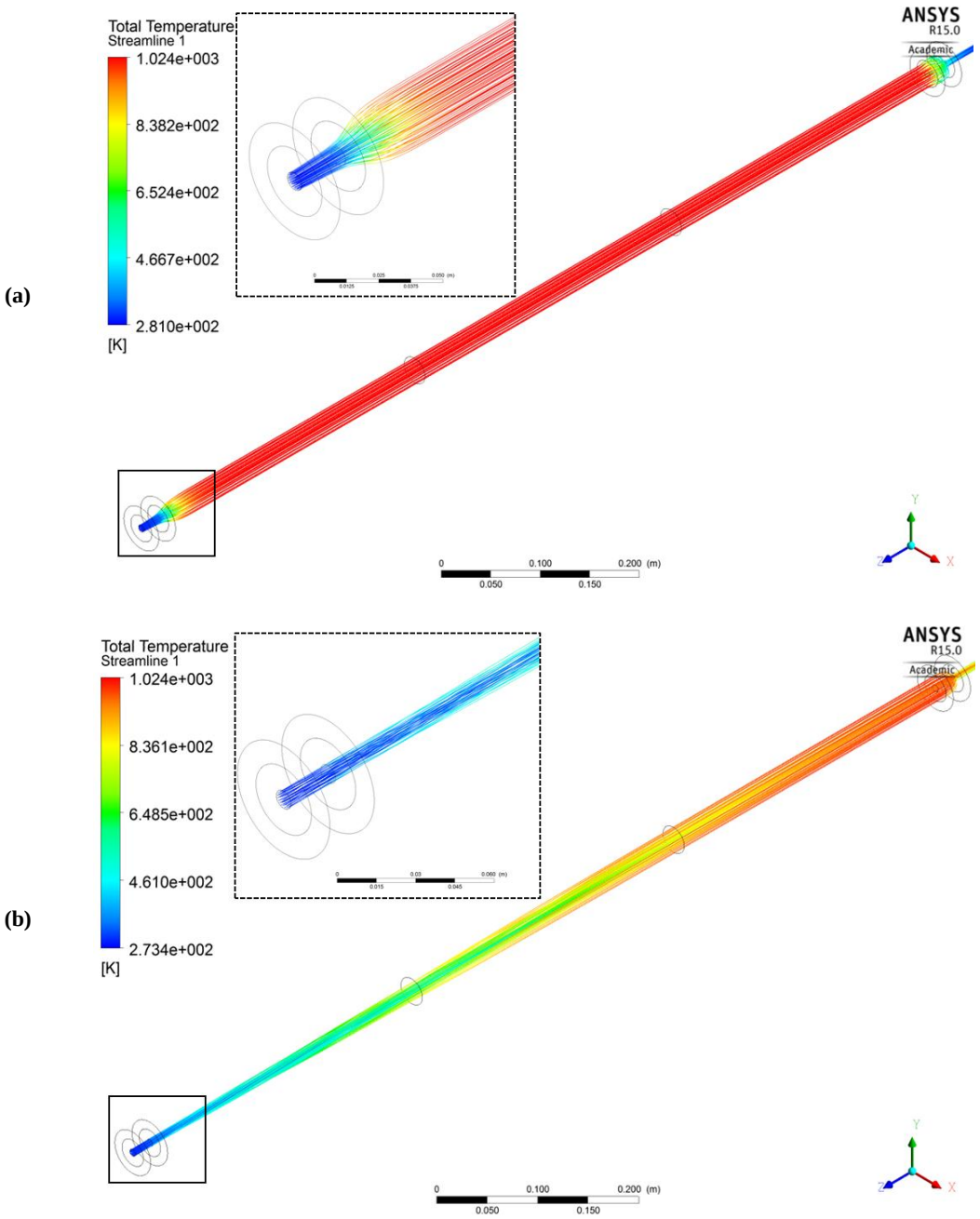

Figure 4.16: Comparison of the gases mixture's temperature streamlines across the "30 mm" setup for experiments with ethylene, hydrogen and helium flows of (a) 50-50-50 and (b) 1000-250-50 sccm.

as the flow is increased, the temperature convergence value is reduced (see Figure 4.14a).

However, when comparing results for different setups, there is not a direct relation between their velocity and temperature convergence values (see Figure 4.6a and Figure 4.14a). For instance, the 30 mm setup is the one which achieved higher velocity values, but is not the one with the lowest temperature values. This is due to the total length of the setups' heated section. For instance, the 30 mm tube has a longer heated section (110 cm) than the 1 inch's one (46 cm). Thus, the 30 mm tube has more length for the mixture's temperature to evolve and converge to the desired value.

In the case of the 80 mm tube, although having the same heating section as the 30 mm one, it has a bigger radius, meaning that it takes more time for the heat transferred to reach the particles travelling in the tube center line, where the measurements were performed. This results in a smaller temperature convergence value than the other setups.

As for the 2 inches setup, the mixture's velocity is always smaller than the other setups due to its lateral entrance. Consequently, the obtained temperature convergence value, although also suffering a reduction with bigger flows, such reduction is small, when compared to the other setups (see Figure 4.14a).

4.2.4. Percentual Rankings

As stated in the methodology, following Eq. 3.6 and Eq. 3.7, it is possible to compute the percentual dependency of a given variable V on a given parameter P, D_P^V. Such procedure was followed for every addressed setup and, posteriorly, an overall percentual ranking of the addressed variables was constructed based on the average of each individual dependency. In other words, considering $D_{P\,S}^V$ the percentual dependency of the variable V on the parameter P in setup S, the overall percentual ranking, R_P^V, can be computed following Eq. 4.1. Following such methodology, the overall percentual rankings were computed and are presented in Figure 4.17, which depicts how each addressed variable is influenced by each parameter.

$$R_P^V = average\left(\forall D_{P\,S}^V\right) \quad \textbf{Eq. 4.1}$$

Table 4.2 shows the mean and standard deviation of each gas' overall ranking, across all addressed variables and, with an overall mean and standard deviation of 61.76% and 14.11%, respectively, ethylene is the gas whose flow most influences the addressed

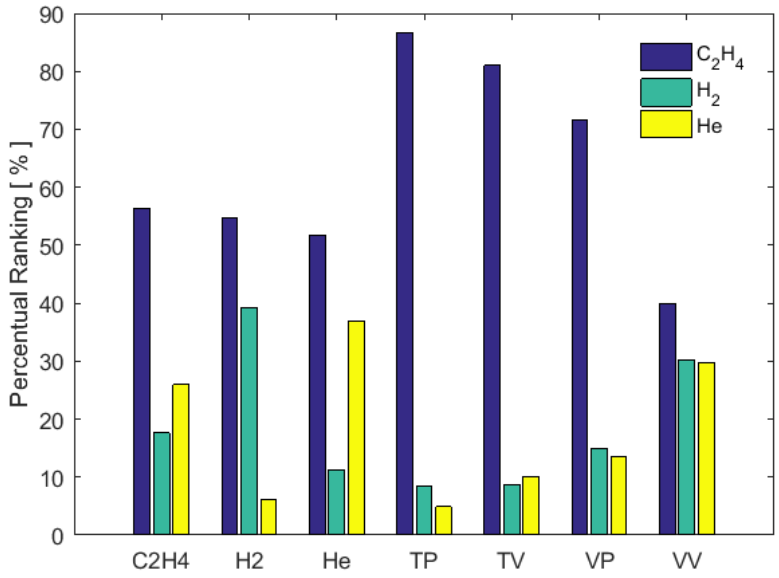

Figure 4.17: Percentual ranking of each gas' effect in each variable, for all setups. Variables: ethylene (C2H4), hydrogen (H2) and helium (He) concentrations, temperature convergence point (TP) and value (TV), velocity convergence point (VP) and value (VV)

Table 4.2: Mean and standard deviation values of the overall percentual rankings for each addressed parameter.

	C_2H_4	H_2	He
Mean [%]	61.76	18.67	19.57
Std. [%]	14.11	10.59	12.08

variables, being only surpassed by both the other flows in the helium's concentration and in the mixture's dynamic viscosity. Such results suggest that, when envisioning a transition methodology between different setups, ethylene is the gas, whose flow requires more attention.

4.1. Final Considerations

In this chapter, a sensitivity analysis, based on a parameterization study, was performed. Each gas was tested for various flow values and several characteristics of the CVD process to synthesize CNTs were evaluated. Measuring such characteristics for various gas flows allowed the analysis of each gas' effects on the address characteristics, resulting in a better understanding of the fluid dynamics, occurring inside the tube reactor during the synthesis phase of the CVD process.

Since each gas was intended to be tested for various flows, resulting in a high number of simulation scenarios, the Taguchi orthogonal arrays were used to select the set of scenarios, which would still result in relevant information regarding the CVD process sensitivity to changes in the gases' flows.

After performing the scenarios, several process characteristics, such as gas concentrations and velocity, were measured and then analyzed for variation of the inlet gases. Such analysis resulted in a percentual ranking for each address characteristic, depicting the gas flow which most influence each variable. With a mean percentual ranking of 55%, ethylene was the gas, whose flow most influence most characteristics. These findings suggest that, when envisioning certain process characteristics, ethylene is the gas, whose flow requires more attention.

References

[1] D.R.K. Bansal, A Textbook of Fluid Mechanics and Hydraulic Machines, 1st Editio, Laxmi Publications, New Dehli, 1983.

[2] A.J. Smits, J.-P. Dussauge., Turbulent Shear Layers in Supersonic Flow, Springer Science & Business Media, 2006.

[3] D. Halliday, R. Resnick, J. Walker, Fundamentals of physics extended, John Wiley & Sons, 2010.

Chapter 5

TRANSITION MODEL

A CFD-based analysis was applied to the CVD synthesis process of CNTs to understand the fluid dynamics, which occur inside the tube reactor, and to evaluate the effect of each parameter in the inner tube conditions. Such CFD analysis was then explored to support the transition between two distinct setups. The development of a transition methodology is crucial to ease knowledge transfer between labs, and is proposed as an alternative to the time-consuming trial-and-error process when addressing yield scale-up. This transition was defined as the process of mimicking the conditions obtained in one setup in the other. The proposed methodology was based in an optimization problem, where the metric to minimize is the error between the conditions at a certain point and the desired ones.

5.1. Conditions Measurement

This section envisions the design and validation of a CFD-based methodology to support the transition between two different CVD setups to synthesize CNTs. Such transition consists on achieving the same synthesis conditions, i.e. C_2H_4 concentration and both mixture's temperature and velocity, in both setups. As a first approach, in order to

Table 5.1: Simulated scenario used to compare both setups.

Gas Inlets [sccm]			Tube temperature [ºC]	Gas mixture initially inside the tube [%]	
C_2H_4	H_2	He		H_2	He
150	200	55	750	78.4	21.6

have a better understanding on how different are these conditions between both setups, they were measured and compared for the same scenario (see Table 5.1).

However, due to the mixture's viscosity, the evolution of certain variables throughout the tube varies with the measurement distance to its center. In other words, considering a vertical cross-section of a cylindrical tube (see Figure 5.1), the value of some variables, measured in a certain point (Point A), varies with its distance to the tube center (Point C) - Dist. B. For instance, due to the mixture's viscosity, particles nearer the tube walls (a higher Dist. B) travel slower than the ones further away (see Figure 5.2). When entering the tube, particles within the tube entrance radius (in both cases 3 mm), have much higher velocity than the ones at higher distances from the tube center. Then, the overall velocity starts being more well distributed, meaning that the particles closer to the tube center start losing velocity, which is transferred to the ones outside the tube entrance radius. However, due to the mixture's viscosity, the closer a particle is to the tube walls, the harder it is for it to gain velocity, since it is also being slowing down by friction. This leads to a smaller convergence velocity than the one achieved by the particles nearer to the tube center.

Moreover, the way each particle travels throughout the tube has influence in its own temperature. For instance, since they are traveling more slowly, particles nearer the walls

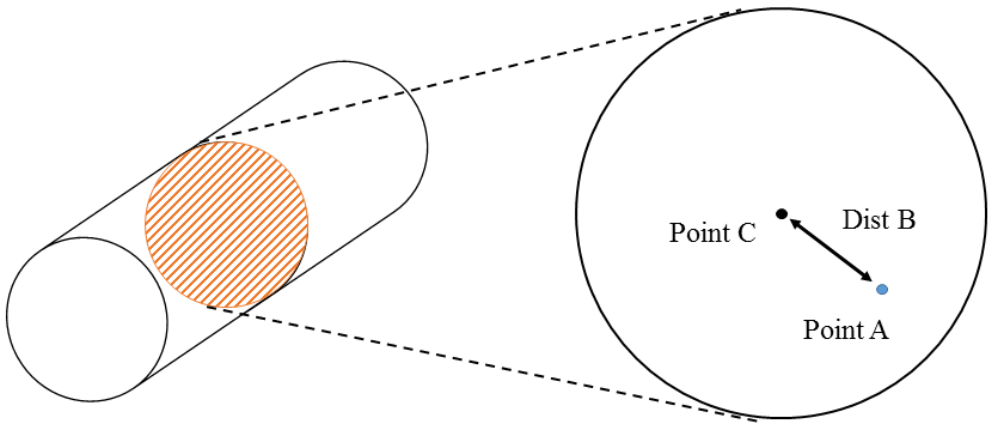

Figure 5.1: Typical vertical cross-section of a cylindrical tube, perpendicular to the flow's direction.

(a)

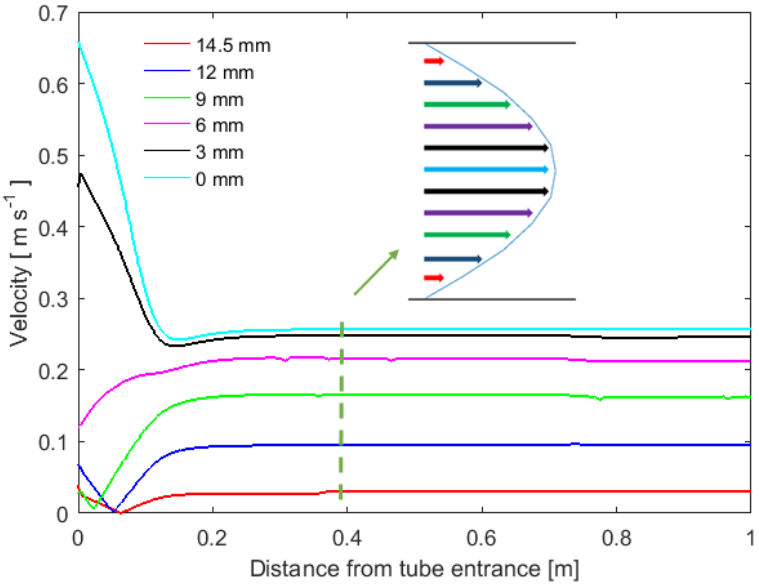

(b)

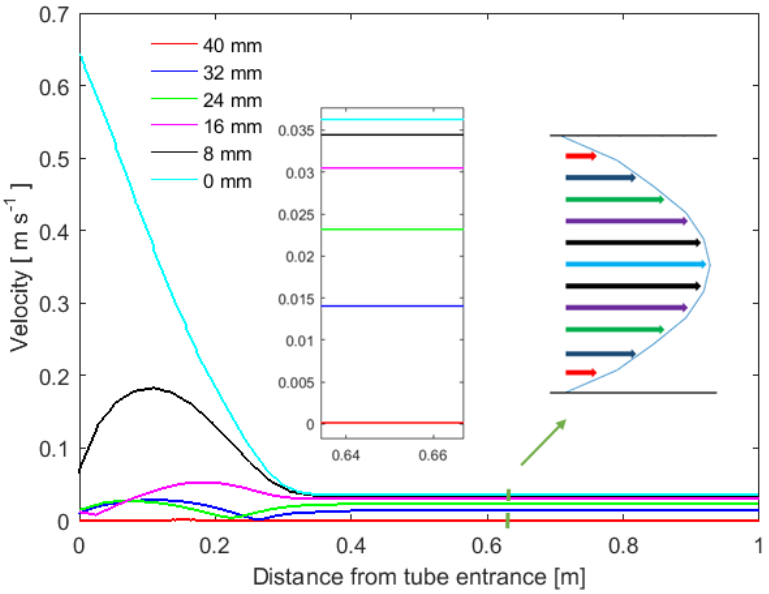

Figure 5.2: Velocity profiles, for various distances from the tube center, throughout the (a) 30 mm and the (b) 80 mm tubes.

suffer a higher heat transfer than the others, leading to a temperature's profile whose convergence is achieved nearer to the tube entrance (see Figure 5.3). On the other hand, particles closer to the tube center are travelling faster, achieving temperature convergence further away from the tube entrance.

Both these phenomenon suggest that the distance to the center, at which the substrate is positioned, should be taken into consideration when measuring the conditions to mimic. Furthermore, these effects of the mixture's viscosity on its velocity and temperature profiles are more noticeable in a tube with a smaller diameter. For instance, in the 80 mm tube, although the mixture's velocity is smaller than in the 30 mm tube, it takes more time to

(a)

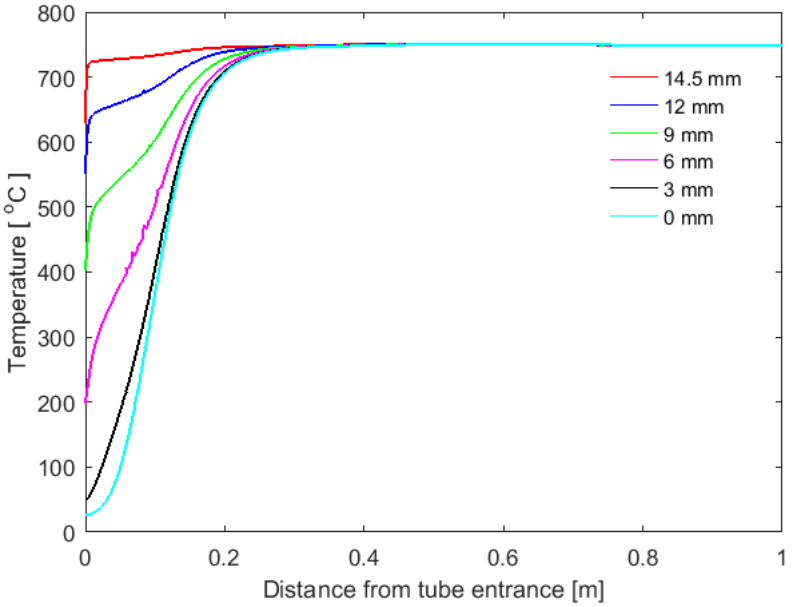

(b)

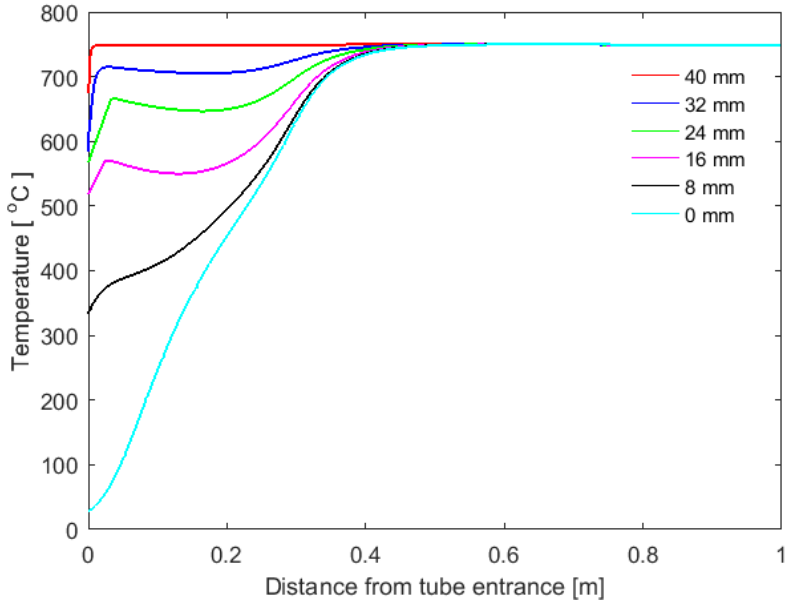

Figure 5.3: Temperature profiles, for various distances from the tube center, throughout the (a) 30 mm and the (b) 80 mm tubes.

stabilize, i.e. farther convergence point (see Figure 5.2). As a consequence, the mixture's temperature's convergence point also increases for tubes with higher diameter (see Figure 5.3).

As suggested by Figure 5.2 and Figure 5.3, certain variables, namely the mixture's velocity and temperature, have different evolutions throughout the tube. Particles closer to the walls have lower temperature's convergence point and velocity's convergence value than the ones nearer to the tube center. Thus, envisioning the transition between two tubes, the substrate position in relation to the tube center should be taken into consideration when measuring, in one tube, the conditions (i.e. ethylene concentration and mixture's

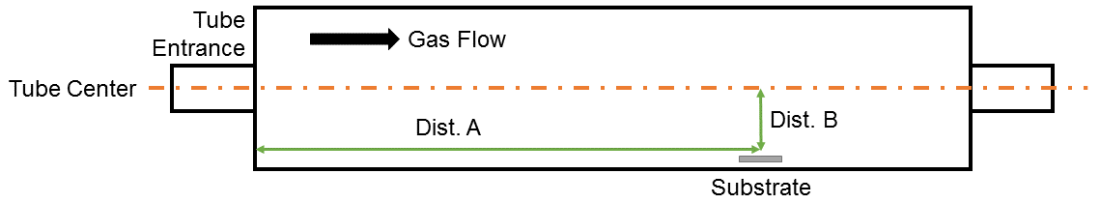

Figure 5.4: Typical horizontal cross-section of a cylindrical tube, depicting the variables that define the substrate position.

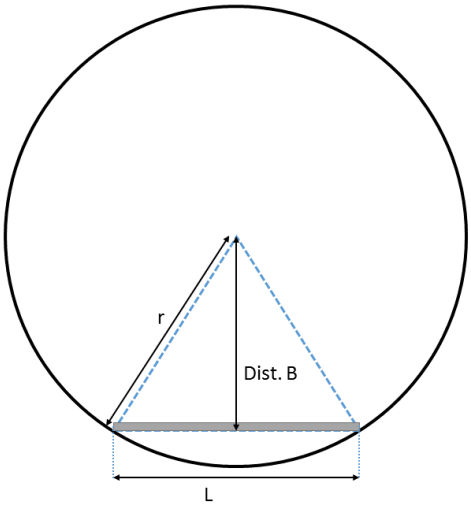

Figure 5.5: Scheme to compute the height at which the substrate is placed.

temperature and velocity) to mimic in the second tube.

As depicted in Figure 5.4, the substrate position is defined by its distance to the tube entrance (Dist. A), and by the distance to the tube center (Dist. B). In previous synthesis performed in the 30 mm tube (see [1]), the substrate was positioned without additional structures, being its distance to the tube center (Dist. B) defined only by its wafer piece size. Moreover, considering a vertical cross-section of a typical cylindrical tube (Figure 5.5), it is possible to define the relationship between the width of the substrate (L) and its distance to the tube center ($Dist\ B$) by Eq. 5.1, where r is the radius of the tube and h_2 is the distance between the substrate and the tube center.

$$Dist\ B = \left|\sqrt{r^2 - (L/2)^2}\right| \qquad \textbf{Eq. 5.1}$$

Since previous CNTs synthesis were performed in 10 mm square substrates [1], it is possible to evaluate the evolutions of each condition (ethylene concentration and mixture's temperature and velocity) throughout the tubes, when considering or not the substrate's distance to the tube center. A comparison between these profiles is depicted in Figure 5.6.

(a)

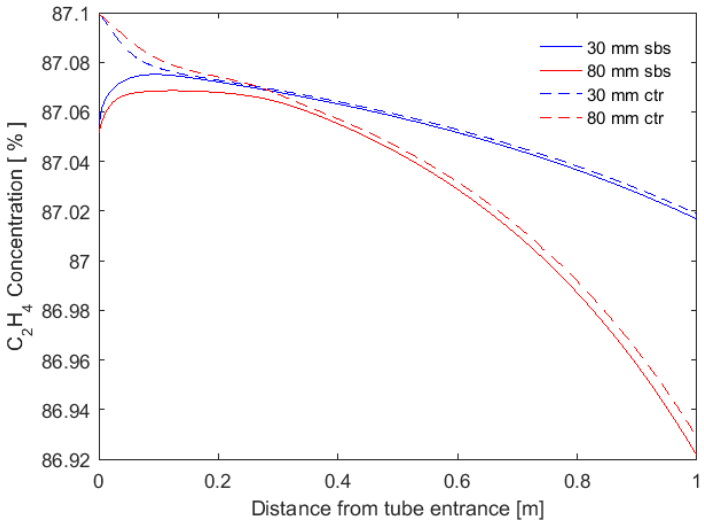

(b)

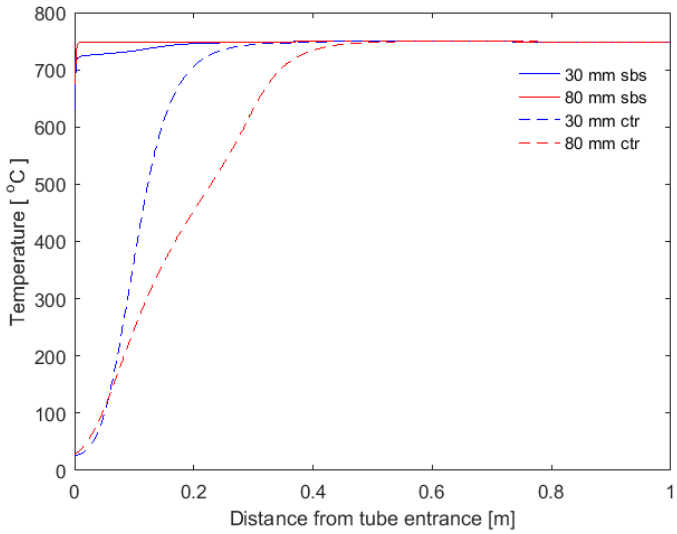

(c)

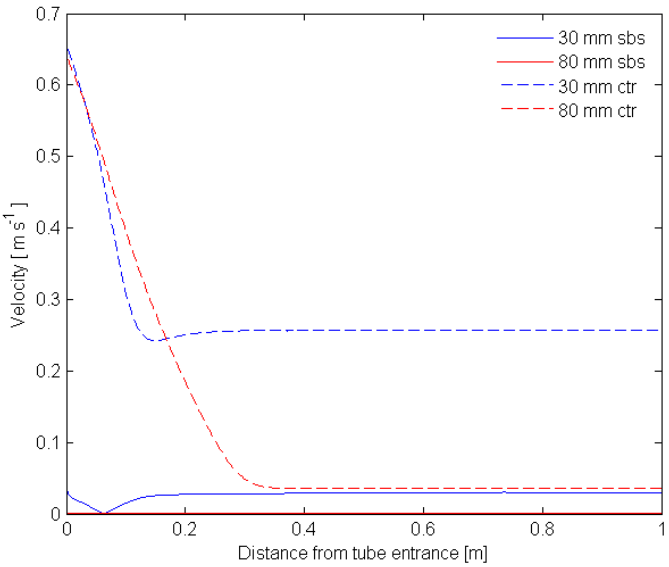

Figure 5.6: Profiles of the (a) ethylene concentration, (b) mixture's temperature and (c) velocity throughout both tubes at the tube center (ctr) and at a height, at which a 10 mm square substrate would be according to Eq. 5.1 (sbs).

Firstly, the ethylene concentration's variation with the height of measurement is

Table 5.2: Relation between the 30 mm and the 80 mm tubes' area and velocity ratios.

	Area [mm^3]	Velocity [m^{-1}]
30 mm tube	706.8583	0.2571
80 mm tube	5026.5	0.0362
30 mm / 80 mm ratio	0.1406	0.1408

negligible (see Figure 5.6a). As depicted, nearer the tube entrance, there is a higher concentration of ethylene in the center of the tube than nearer its walls, for both tubes. This occurs since the inlet lines have a smaller diameter than the tube and are positioned concentrically with it, making the center of the tube nearer its entrance the tube section which more directly receives the ethylene inlet.

Secondly, as for the mixture's temperature, a few conclusions are noticeable from Figure 5.6b. As aforementioned, the particles nearer the walls absorb more heat from them, leading to a faster temperature convergence at the substrate height. Due to their distance to the tube center, where the mixture's velocity is higher (see Figure 5.2), the temperature at the substrate height converges farther in the 30 mm tube (see Figure 5.6b). Moreover, due to the greater tube radius, the temperature increase nearer the center is slower in the 80 mm tube.

Lastly, the mixture's velocity in the 80 mm tube is always smaller than in the 30 mm tube (see Figure 5.6c). In fact, the ratio between the velocities at the tubes' center is equal to their area ratio (see Table 5.2).

5.2. Methodology

From Figure 5.6, it is conclusive that the mixture's velocity is the condition which most differs when comparing both tubes. As previously referred, the variation of the ethylene concentration is negligible (see Figure 5.6a), and the mixture's temperature always converges to the same value (750 ^{o}C), nearer or further away from the tube entrance (see Figure 5.6b). As for its velocity, it converges to different values, depending of the tube and the substrate position (see Figure 5.6c). In fact, without changing the height at which the substrate is positioned, the desired mixture's velocity is not achievable in the 80 mm tube. Moreover, such achievement is still not possible while varying only the ethylene flow from 50 to 500 sccm (see Figure 5.7). Nevertheless, as depicted in Figure 5.2, one way to

overcome this issue is to place the substrate at a higher height. Figure 5.8 depicts how the velocity convergence value varies for various positioning heights in the 80 mm tube, and pertains the hypothesis to achieve the desired velocity by changing the substrate's position.

Summing up, the transition from the 30 mm to the 80 mm tube can be seen as a third order system with three inputs (ethylene concentration and both mixture's temperature and

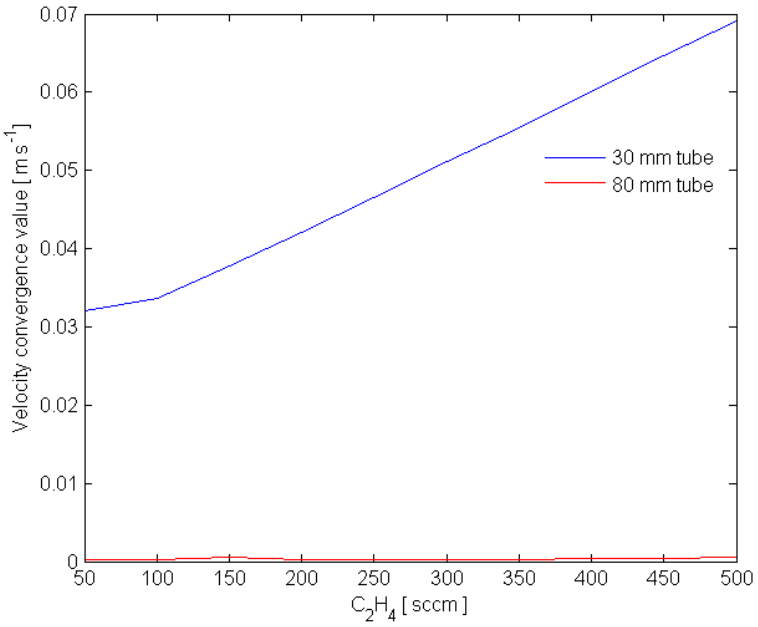

Figure 5.7: Evolution of the velocity convergence value, for both tubes, when varying the ethylene flow and considering a substrate positioning height when it is placed in the bottom of the tubes.

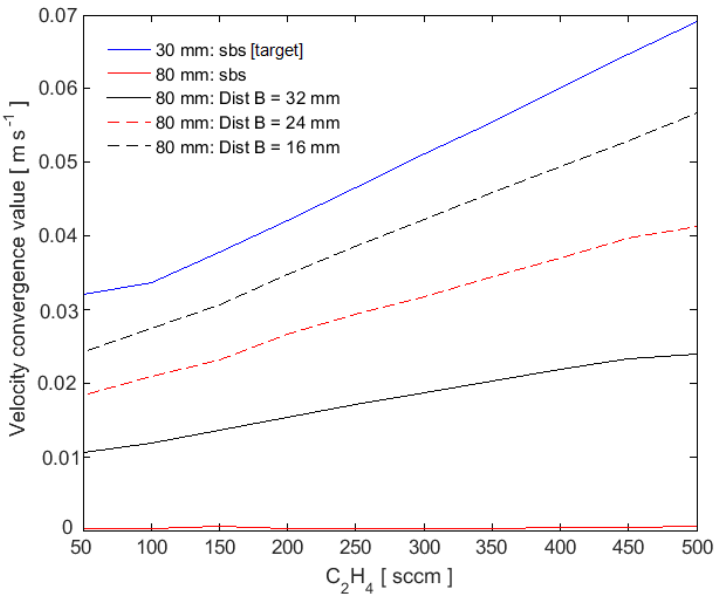

Figure 5.8: Evolution of the velocity convergence value, varying the ethylene flow, for the desired 30 mm tube conditions and various heights in the 80 mm tube.

velocity) and three output variables (ethylene flow, and the height and distance from the tube entrance at which the substrate should be positioned).

In fact, the described problem can be seen as an optimization one, where the objective function to minimize (i.e. metric) is the error between the conditions at a certain point and the desired ones. Considering the error of each addressed variable as a vector, the total error is the norm of the sum of those vectors (see Eq. 5.2). Moreover, Eq. 5.3 depicts how the percentual error was computed.

$$Error_{Position} = \sqrt{{Error_{C2H4}}^2 + {Error_{Temp}}^2 + {Error_{Veloc}}^2} \quad \textbf{Eq. 5.2}$$

$$Error_{Variable} = \frac{|Desired_{Value} - Position_{Value}|}{Desired_{Value}} \quad \textbf{Eq. 5.3}$$

However, as a first approach to this problem, the substrate's positioning height in the second setup is defined a priori to 16 mm below the tube center. This height was selected since it was the one with least error when compared to the value measured at the substrate height, in the 30 mm tube (depicted as the target in Figure 5.8). A previously defined height in the second setup narrows the search to only two variables: the C_2H_4 flow and the substrate position in relation to the tube entrance (Dist. A in Figure 5.4).

Thus, it is possible to map the described problem with three dimensions: (i) ethylene flow; (ii) distance from the tube entrance; and (iii) the value of $Error_{Position}$ at that specific point. With such configuration, the transition process can be described as finding the minimum point of $Error_{Position}$ and return the synthesis process parameters, i.e. ethylene flow and distance from the entrance, which result in such value.

5.3. Results and Discussion

5.3.1. Fixed Height Search

As aforementioned, the first approach to the described transitioning problem was to mimic in the 80 mm tube the conditions obtained in the 30 mm tube during the synthesis phase of the recipe depicted in Table 5.1. In the author's experimental setup, when synthesizing CNTs in the 30 mm tube, a 1 cm squared substrate is positioned at 60 cm from

Table 5.3: Conditions measured at the substrate position on the 30 mm tube for the simulated scenario.

Variable	C_2H_4 Con. [%]	Temp. [ºC]	Vel. [m s $^{-1}$]
Value	86.934	750.05	0.036752

the tube entrance. Taking this substrate position into account, as well as its height according to Eq. 5.1, the scenario described in Table 5.1 was simulated and the synthesis conditions, which should be achieved in the 80 mm tube, where measured and are presented in Table 5.3.

With such conditions, it is possible to apply the proposed methodology to target the process parameters and substrate position which would minimize described metric, i.e. better mimic these synthesis conditions in the 80 mm tube. As aforementioned, the search in the 80 mm tube was firstly performed at a single substrate positioning height ($Dist\ B$) of 16 mm. Moreover, the search was performed using data collected in the simulations

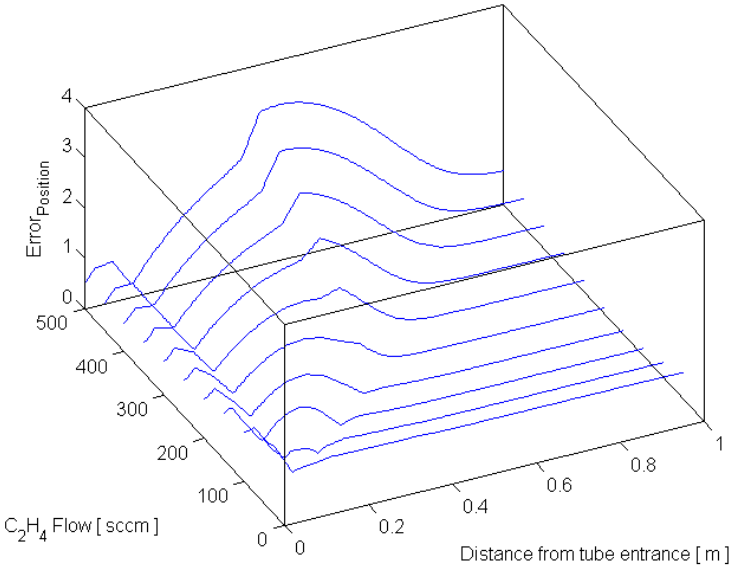

Figure 5.9: Relation of all three dimensions when searching, in the 80 mm tube, for the conditions obtained in the 30 mm tube.

Table 5.4: Recipe which mimics best, in the 80 mm tube, the conditions obtained in the 30 mm tube.

Variable	C2H4 Flow [sccm]	Distance from entrance [cm]	C_2H_4 Con. [%]	Temp. [ºC]	Vel. [m s $^{-1}$]
Value	200	69.258	89.961	749.55	0.034955
Desired	-	-	86.934	750.05	0.036752
Error [%]	-	-	3.48	0.05	4.89
Metric [%]	-	-		6.00	

where the C_2H_4 flow was varied from 50 to 500 sccm in 50 sccm steps, while keeping the H_2 and He flows at 200 and 55 sccm, respectively. Using this simulation domain, it is possible to map the relation between all three dimensions, i.e. ethylene flow, distance from the tube entrance; and the value of $Error_{Position}$ (see Figure 5.9). Using the proposed methodology, this domain was searched for the process parameters, which result in the minimum metric. These are shown in Table 5.4, which, resulting in a total percentual error of 6%, are validated to mimic the desired conditions.

For any given set of desired synthesis conditions, measured in the 30 mm tube, the 80 mm tube simulations' domain can be scanned and searched for the conditions, which better mimic the desired ones, i.e. the ones with the lowest percentual error (metric).

Since the desired conditions can be measured for any simulation scenario on the 30 mm tube, this fixed-height search methodology was followed for every simulated scenario[1]. For each scenario, the desired conditions were measured and compared with the 80 mm tube's simulations domain, thus resulting in the minimum percentual error for each scenario in the 30 mm tube (presented in Figure 5.10). Moreover, the obtained process parameters, substrate positioning and individual percentual errors are presented in Table 5.5.

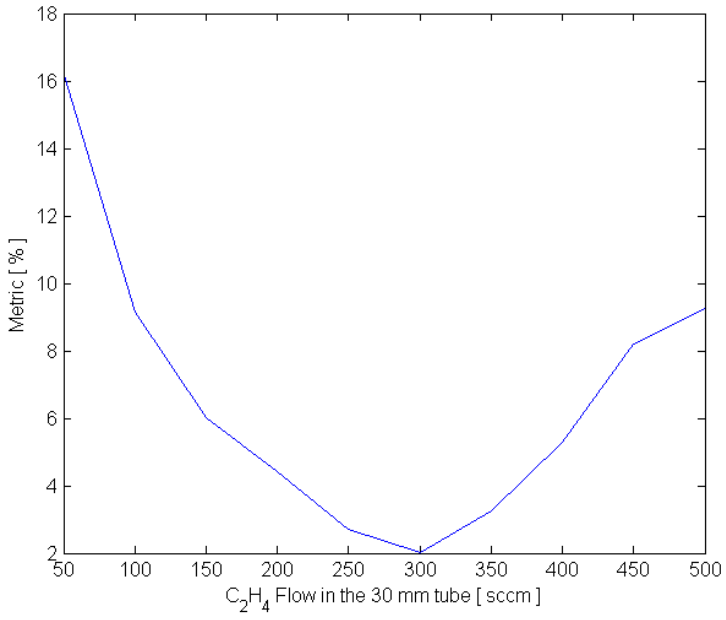

Figure 5.10: Obtained metric when transitioning from the 30 mm tube to the 80 mm one. Here the synthesis conditions to mimic are measured in a 10 mm square substrate positioned 60 cm from the tube entrance and the search in the 80 mm is fixed to a height of 16 mm below the tube center.

[1] Defined by varying the ethylene flow from 50 to 500 sccm, in steps of 50 sccm.

Table 5.5: Results obtained when transitioning between both tubes, by searching on a fixed height methodology.

C_2H_4 Flow [sccm]		Position	Errors [%]			Metric
30 mm	80 mm	[m]	C_2H_4	Temp.	Vel.	[%]
50	50	0.107742	7.21	11.96	8.22	16.21
100	150	0.994037	6.97	0.20	5.93	9.16
150	200	0.692581	3.48	0.05	4.89	6.00
200	300	0.74828	3.50	0.93	2.56	4.43
250	350	0.899463	2.40	0.78	1.03	2.73
300	400	0.998925	1.75	0.91	0.37	2.01
350	450	0.998925	1.34	2.08	2.13	3.26
400	500	0.998925	1.06	4.17	3.08	5.29
450	500	0.891506	0.47	7.96	1.84	8.19
500	500	0.859678	0.01	9.20	1.20	9.27

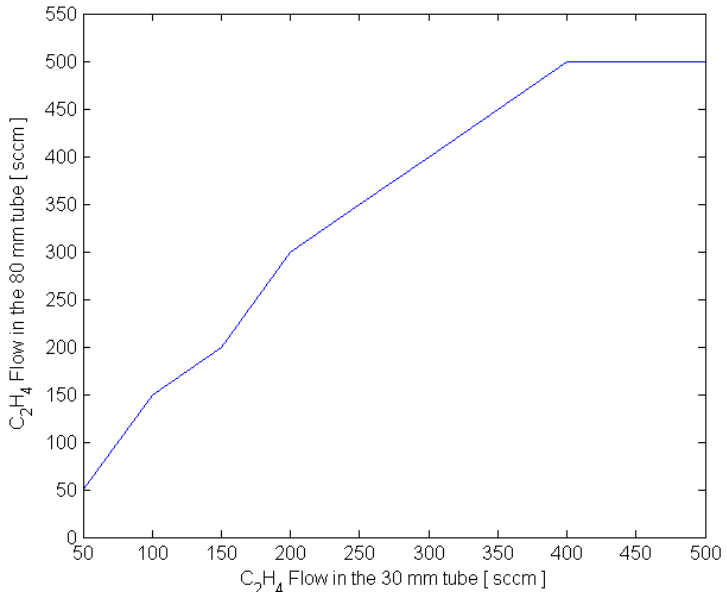

Figure 5.11: Relation between the flows in the 30 and the 80 mm tubes.

Due to the tube diameter increase, the obtained ethylene flow in the 80 mm tube is always greater than the one used in the 30 mm tube (see Figure 5.11). As depicted, the relation between the ethylene flows on both tubes is quasi-linear until a 30 mm tube ethylene flow of 400 sccm. Beyond this point, the increasing trend stops at an 80 mm ethylene flow of 500 sccm since no simulation was performed with a higher value. Such relation comes in accordance with the results depicted in Figure 5.8, where a linear relation was obtained between the 30 mm tube at substrate height and the 80 mm tube at the tested substrate height. Moreover, the result's saturation also occurs in the substrate position,

which result in an increase of the metric for flows higher than 300 sccm (see Figure 5.10). Such saturation is due to two phenomenon:

1. With the flow increase, the mixture is less affected by the heat transfer from the tube walls, thus reducing the temperature's convergence value (see Figure 5.12);
2. With a higher flow, the mixture requires more time to reach a constant velocity, increasing its convergence point (see Figure 5.13).

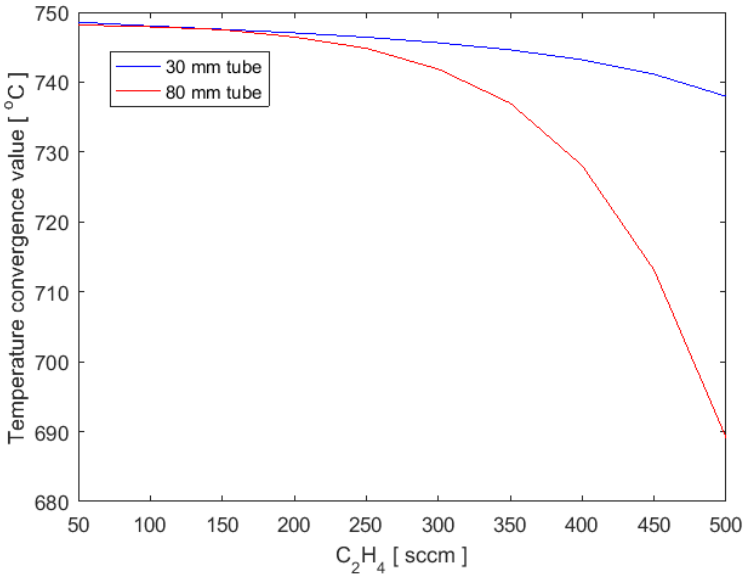

Figure 5.12: Temperature's convergence value for various ethylene flows at the evaluated substrate heights.

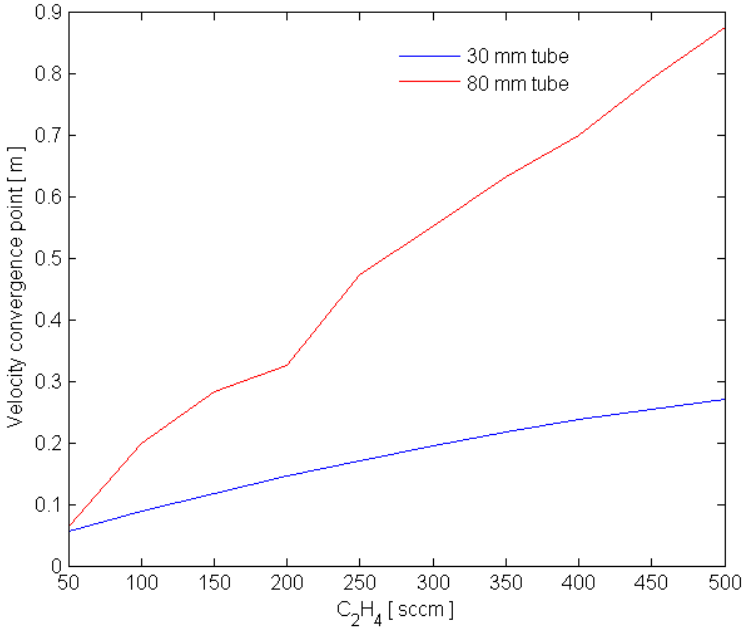

Figure 5.13: Velocity's convergence point for various ethylene flows at the evaluated substrate heights.

Both these phenomenon lead to an increase of the metric for higher ethylene flows. One hypothesis to tackle both these issues would be extending the search for other substrate heights. Moreover, the former one could also be tackled by increasing the temperature at which the tube is heated, resulting in a higher heat transfer. Thus, widening the search for other height, as well as performing a sensitivity analysis tackling the tube temperature's effects on the conditions were the next steps to achieve transition between both tubes.

5.3.2. Non-fixed Height Search

Results previously presented addressed the search problem by narrowing it to a single substrate positioning height. This was considered as one of the issues, which could lead to higher error when transitioning between both tubes. Thus, the proposed methodology was extended to a four dimensions searching problem. Besides the three previously presented variables (ethylene flow, substrate distance to the tube entrance, and the total error between the measured conditions), the height at which the substrate could be positioned in the second tube was also taken into account.

This non-fixed height search methodology was followed for the same simulations as previously, and the resulting metric is depicted in Figure 5.14. Table 5.6 depicts the obtained process parameters, substrate positioning in the 80 mm tube and the individual percentual errors. As expected, following a non-fixed height methodology leads to smaller

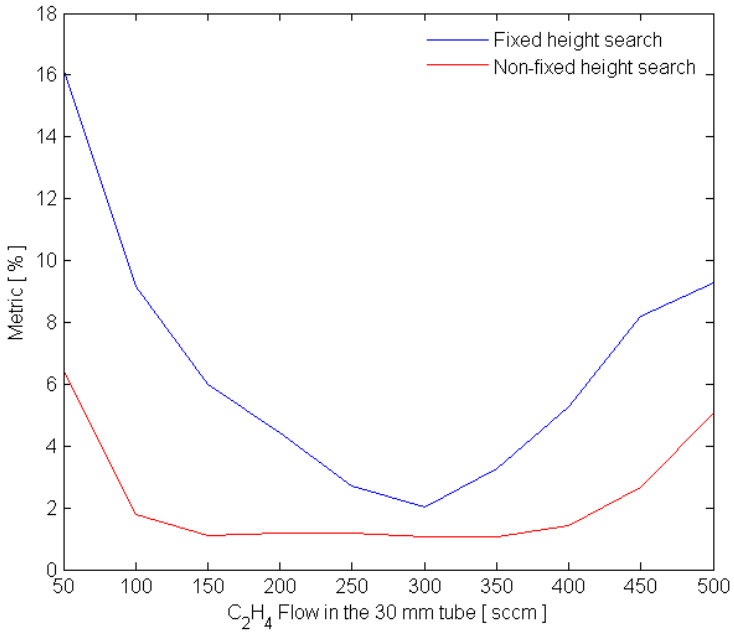

Figure 5.14: Obtained metric when transitioning between the tubes, following a fixed height (at 16 mm below the tube center) and a non-fixed height search.

Table 5.6: Results obtained when transitioning between both tubes, by searching on a non-fixed height methodology.

C_2H_4 Flow [sccm]		Position	Height	Errors [%]			Metric
30 mm	80 mm	[m]	[m]	C_2H_4	Temp.	Vel.	[%]
50	50	0.998925	1.71E-04	2.80	0.22	5.84	6.48
100	100	0.994947	1.71E-04	0.11	0.20	1.78	1.79
150	150	0.991394	-3.69E-04	0.00	0.20	1.10	1.11
200	200	0.688603	-1.11E-04	0.03	0.07	1.16	1.17
250	250	0.994947	1.71E-04	0.01	0.19	1.17	1.19
300	300	0.983011	1.71E-04	0.01	0.23	1.06	1.08
350	350	0.998925	1.71E-04	0.01	0.41	0.97	1.05
400	400	0.998925	1.71E-04	0.01	1.04	0.95	1.41
450	450	0.998925	1.71E-04	0.01	2.53	0.82	2.66
500	500	0.998925	-6.10E-03	0.01	5.07	0.31	5.08

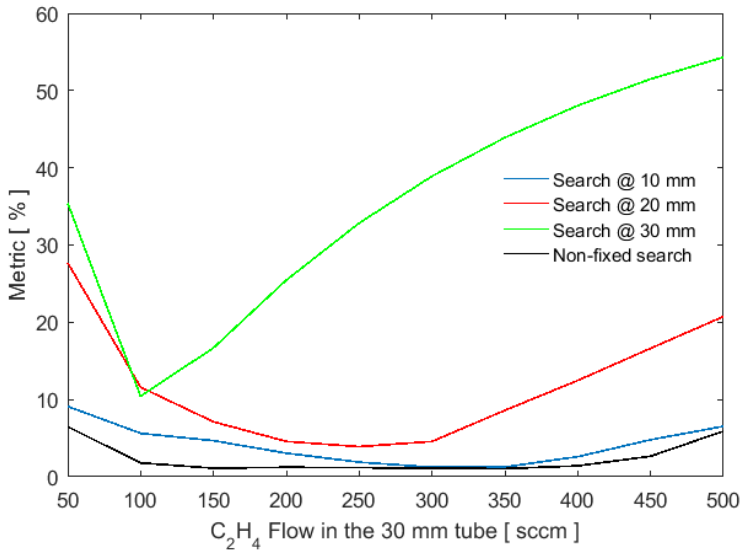

Figure 5.15: Comparison between the metrics achieved while following a non-fixed height search and the ones achieved when fixing the searching height at the 80 mm tube at other values.

percentual errors and, consequently, metric values (see Figure 5.14), which were obtained for a wider range of simulation scenarios, being lower than 2% for 30 mm ethylene flows between 100 and 400 sccm (see Table 5.6). Moreover, for other flows, the percentual error was never greater than 7%. Such findings are also true when comparing the non-fixed height search results with percentual errors achieved, when fixing the search in the 80 mm tube at other substrate positioning heights (see Figure 5.15).

Moreover, analyzing Table 5.6, the mixture's temperature's individual percentual error increases with the ethylene flow, reaching a final value of 5%. This comes in

accordance with the fact that heat transfer between the tube and the mixture reduces with the flow increase, and emphasizes the previously referred hypothesis to improve the methodology by also considering changes in the furnace temperature.

5.4. Transition Improvement by Temperature Effects

An error-minimization based methodology was proposed to search the synthesis parameters, which would better mimic, in the 80 mm tube setup, certain conditions measured in the 30 mm tube. This procedure resulted in a percentual error below 2% for most of the considered simulated scenarios in the 30 mm tube. Nonetheless, one synthesis condition, whose error can be improved, is the mixture's temperature, especially for higher ethylene flows, where the mixture does not have time to absorb sufficient heat to reach the desired temperature. Thus, a hypothesis to increase the heat transfer between the tube walls and the mixture by varying the furnace's temperature, and thus reduce the overall percentual error, was suggested. This section describes the methodology followed to validate such hypothesis. First, a sensitivity analysis regarding both the tube's temperature and the ethylene flow effects on the synthesis conditions was performed. Since this analysis validated the proposed hypothesis, the previously defined simulations' domain was increased by simulating more scenarios, where both the ethylene flow and the furnace temperature were varied. Lastly, the previously defined search methodology was followed for such domain, and results showed that the implementation of such improvement leads to higher percentual reductions when the search is fixed to a certain height.

5.4.1. Furnace Temperature Effects

Methodology

Similarly to the previously performed sensitivity analysis (see section 4.1), the study presented here consisted in a parameterization one, where each addressed parameter was tested for various values. As aforementioned, such analysis comprised changes in the ethylene flow and in the tube's temperature. These were tested for 50, 500 and 1000 sccm; and 750, 975 and 1200 ^{o}C, respectively. The ethylene values were selected based on the minimum, middle and maximum flow values previously tested (see Chapter 4). As for the tube's temperature, the values were the one typically used experimentally (750 ^{o}C), the maximum temperature allowed by the setup's furnace (1200 ^{o}C) and a middle point

Table 5.7: Simulations scenarios considered in the sensitivity analysis.

Ethylene Flow [sccm]	Tube Temperature [ºC]
50	750
50	975
50	1,200
500	750
500	975
500	1,200
1,000	750
1,000	975
1,000	1,200

(975 ºC). The Taguchi method's orthogonal arrays were used to set up the simulations scenarios to be considered in the study, which are presented in Table 5.7.

Since this sensitivity analysis is comprised in the improvement of a previously performed transition methodology, the assessed variables were the same synthesis conditions addressed by it:

- Ethylene's mean concentration throughout the tube;
- Value of convergence of the mixture's temperature and velocity;
- Distance to the tube entrance where the convergence values are reached.

After measuring these variables for each simulation, the sensitivity analysis was performed by following the methodology presented in section 3.3, allowing the evaluation of how each parameter affects each variable. Since this analysis is performed to complement and improve the methodology to transition between the 30 and the 80 mm tubes, it was performed for both cases and the results are shown as follow.

Results and Discussion

Figure 5.16 depicts how the ethylene concentration is affected by each parameter, for both tubes. As expected, it is majorly affected by the ethylene flow, being the values from the ethylene flow line that impose the variance in the temperature line. For example, the simulations where the ethylene flow is 50 sccm are the ones which give the minimum values in the temperature line variance, and vice-versa. Thus there is no significant effect of the tube temperature in the ethylene concentration.

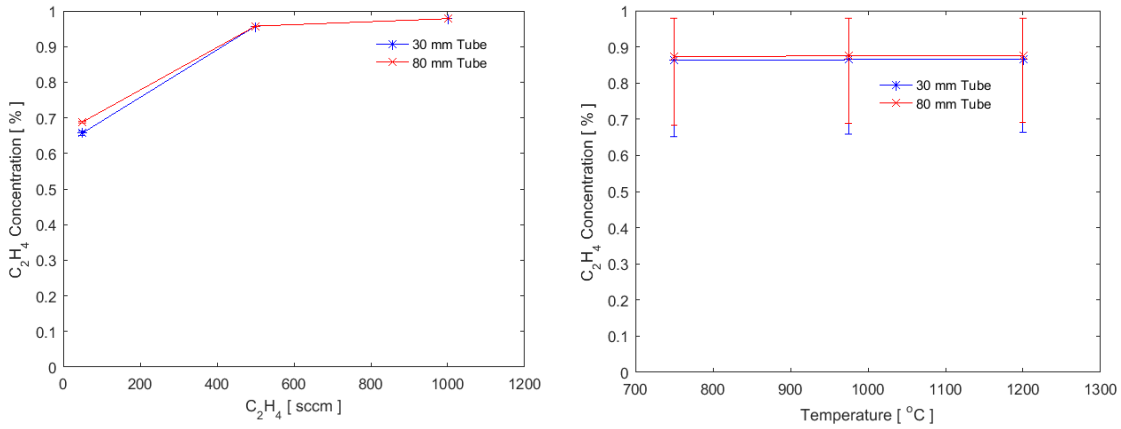

(a) **(b)**

Figure 5.16: Sensitivity analysis of the ethylene concentration, for the 30 and 80 mm tubes, depending on the (a) ethylene flow and the (b) tube temperature.

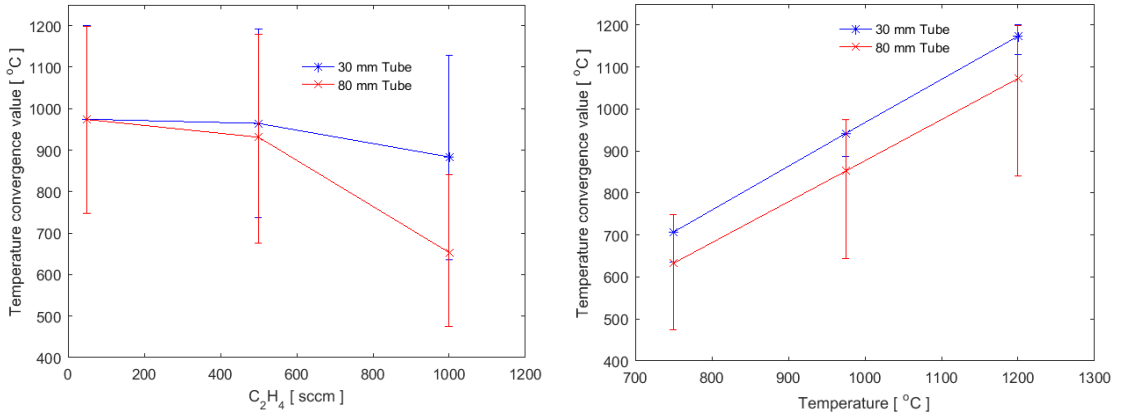

(a) **(b)**

Figure 5.17: Sensitivity analysis of the temperature's convergence value, for the 30 and 80 mm tubes, depending on the (a) ethylene flow and the (b) tube temperature.

On the other hand, the tube's temperature is the parameter which most influences the mixture's temperature's convergence value (see Figure 5.17). Increasing the tube temperature induces a higher heat transfer between the tube walls and the mixture, leading to greater temperature increases and, consequently, higher convergence values. Alternatively, increasing the ethylene flow increases the mixture's velocity (see Figure 5.18), which decreases the time during which the mixture receives heat from the tube walls, leading to a smaller temperature convergence value (see Figure 5.17).

As for the temperature's convergence point, it merely depends on the heat transfer rate from the tube walls to the mixture. As previously stated, a higher ethylene flow decreases the time where the mixture receives heat, thus increasing the temperature's convergence point (see Figure 5.19). On the other hand, increasing the tube temperature leads to a higher heat transfer rate, thus reducing the temperature's convergence point.

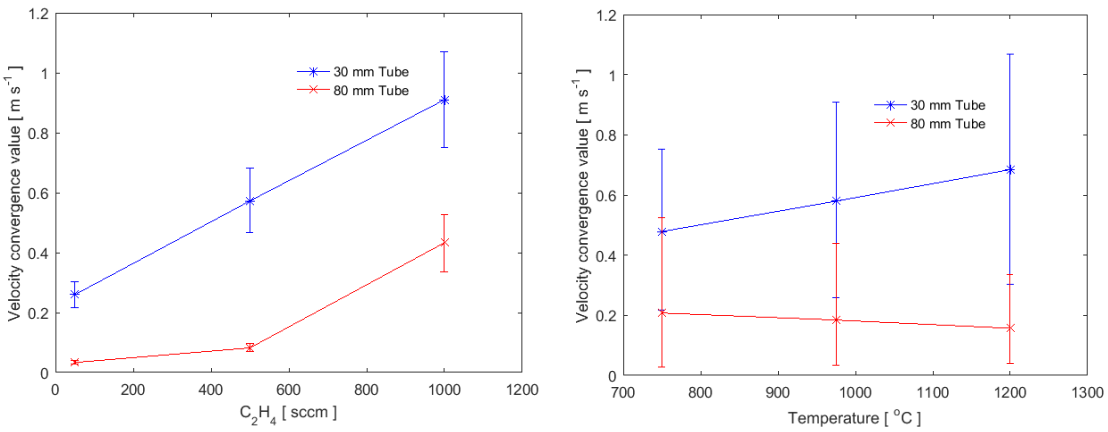

(a) **(b)**

Figure 5.18: Sensitivity analysis of the velocity's convergence value, for the 30 and 80 mm tubes, depending on the (a) ethylene flow and the (b) tube temperature.

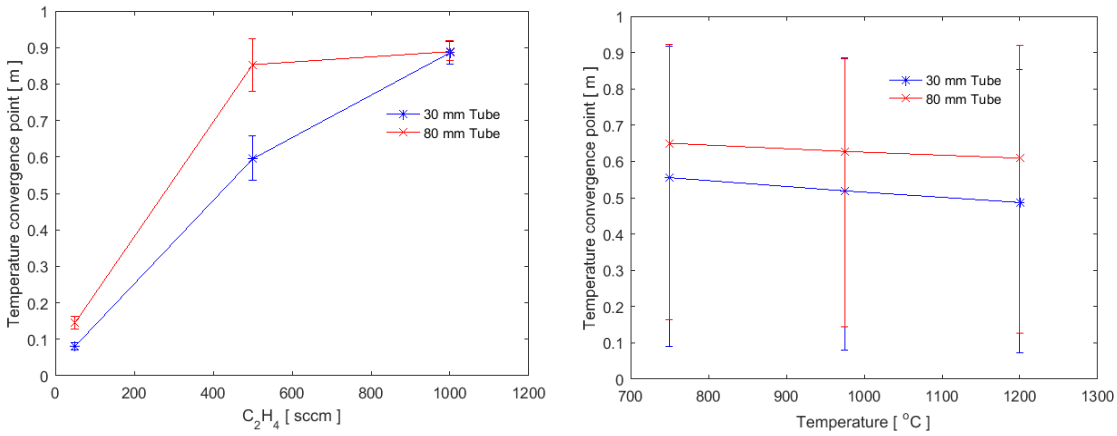

(a) **(b)**

Figure 5.19: Sensitivity analysis of the temperature's convergence point, for the 30 and 80 mm tubes, depending on the (a) ethylene flow and the (b) tube temperature.

However, as depicted in Figure 5.19, the temperature's convergence point effects by the tube temperature are minimal, when compared to the ones caused by the ethylene flow.

In order to analyze the furnace temperature effects on the mixture's velocity, it is crucial to understand how a mixture's temperature affects its motion. This effect is expressed as a relation between the mixture's temperature and its dynamic viscosity, which defines the mixture's resistance to its own flow. In gaseous fluids, on the contrary to liquid ones, their dynamic viscosity increases with their temperature [2]. This difference between gases and liquids is related with the space between molecules. Being more spacious, gases' molecules have a weaker intermolecular force. With the increase of temperature, molecules travel more freely and randomly causing more collisions between them, and thus increasing the gas dynamic viscosity. In liquids, the intermolecular forces are stronger and thus the molecules tend to stick together, which results in less collisions and thus a smaller viscosity.

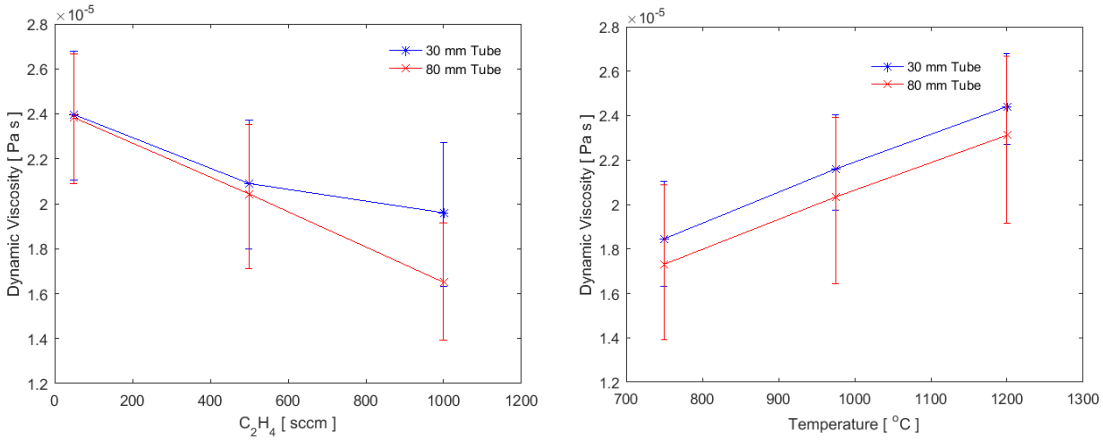

(a) **(b)**

Figure 5.20: Sensitivity analysis of the dynamic viscosity, for the 30 and 80 mm tubes, depending on the (a) ethylene flow and the (b) tube temperature.

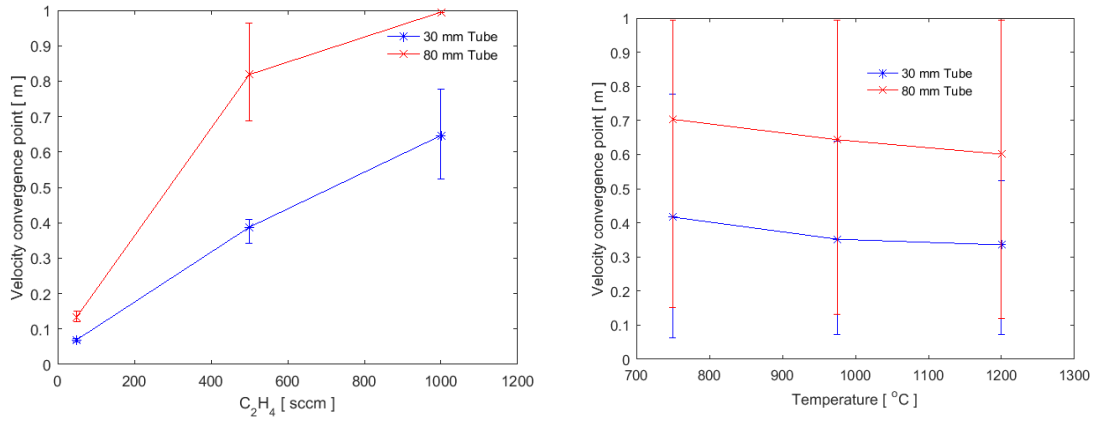

(a) **(b)**

Figure 5.21: Sensitivity analysis of the velocity's convergence point, for the 30 and 80 mm tubes, depending on the (a) ethylene flow and the (b) tube temperature.

After entering the tube, the mixture slows down, not only due to its transition to a bigger tube, but also due to being heated up. Such phenomenon increases the mixture's dynamic viscosity, which defines the mixture's resistance to its own flow, dampening its velocity. Since a lower temperature's convergence point is induced, both higher tube temperatures and smaller ethylene flows lead to higher dynamic viscosity (see Figure 5.20). This produces more resistance to the mixture's flow, leading to a smaller velocity's convergence point. Thus, both convergence points are related, in the sense that the velocity's convergence point also increases with the ethylene flow increase or with the tube temperature decrease (see Figure 5.21).

Although the velocity's decrease ceases with the dynamic viscosity increase stopping, there is another viscosity-related phenomenon that induces variation in the

velocity's evolution. Just for being a viscous fluid, the mixture's particles slow down, starting from the ones nearer the tube walls and continuing to the adjacent ones in a continuous process. However, to make up for this effect and maintaining the average velocity, the particles further away from the tube walls, in its mid-section, start accelerating [3]. Moreover, the distance required for this phenomenon to stabilize (cease the velocity increase) is proportional to the mixture's velocity and the tube diameter, and inversely proportional to the mixture's dynamic viscosity. As referred, higher tube temperatures makes the mixture more viscous, which, consequently, leads to shorter stabilizing distance, which comes in accordance with the results depicted in Figure 5.21.

In order to compare the tube temperature effects on the velocity's convergence value, several typical velocity profiles throughout the tube, whose simulation scenarios only vary on the tube temperature, were analyzed (see Figure 5.22). Since the mixture's velocity and temperature, at the tube entrance, are the same in the analyzed scenarios, the depicted velocity profiles are not affected by the ethylene flow. As aforementioned, as the mixture heats up, it slows down. However this velocity decrease only happens during the heating phase, which is smaller for higher tube temperatures (shorter velocity's convergence point). In those scenarios, the velocity stabilizing phase starts and, consequently, ends at higher velocity values. Thus, the velocity convergence value increases with the tube temperature (see Figure 5.18).

However, the results obtained for the 80 mm are not coherent with this relation between the tube temperature and the velocity's convergence value (see Figure 5.18). As

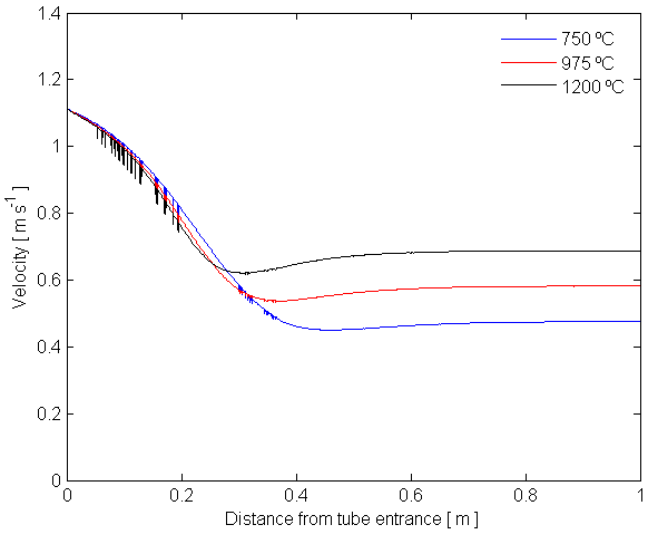

Figure 5.22: Typical velocity profiles throughout the 30 mm tube when C_2H_4 = 500 sccm.

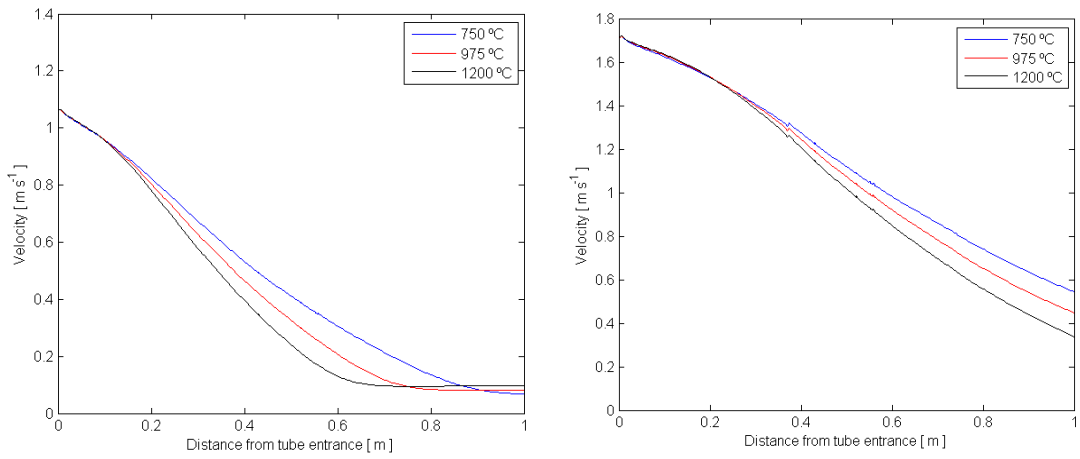

Figure 5.23: Velocity profiles throughout the 80 mm tube for an ethylene flow of (a) 500 and (b) 1000 sccm.

previously stated, the velocity's stabilizing distance increases with the tube's diameter. Thus, for the 80 mm tube, the velocity's convergence point occurs later in the tube and, for higher ethylene flows, it does not fully stabilizes within the tube length (see Figure 5.23). Such phenomenon is depicted in the velocity's convergence point (Figure 5.21), where the results for the simulation scenarios, whose ethylene flow is of 1000 sccm, are maximum.

5.4.2. Transition Considering the Temperature Effects

In the previous section, a sensitivity analysis addressing the effects of both the ethylene flow and the furnace temperature was performed. The achieved results have validated the hypothesis to improve the previously described transition model by also considering changes to the furnace temperature. This section describes the methodology followed to implement such improvement, as well as the obtained results.

Methodology

The improvement of the transition model was implemented upon the previously described methodology. Since the improvement is based on considering another tunable process parameter of the second setup, it only affects its simulation domain, being the synthesis conditions to mimic and the search methodology the same as before.

Previously, the search domain was defined as a set of simulation scenarios, where only the ethylene flow varied, from 50 to 500 sccm in steps of 50 sccm, while maintaining the hydrogen and helium flows as 200 and 55 sccm, respectively. These simulations were performed for a furnace temperature of 750 ºC. For the envisioned improvement, the domain was increased by including scenarios where the same ethylene flows were also

simulated for furnace temperatures of 975 ºC and 1200 ºC. Considering this set of simulation scenarios as the new domain, the previously described search methodology (see section 5.2) was followed and the obtained results are presented in the next section.

Results and Discussion

As previously, the fixed height search was first performed for a substrate positioned 16 mm below the tube center, and results are presented in Figure 5.24 and Table 5.8. In this

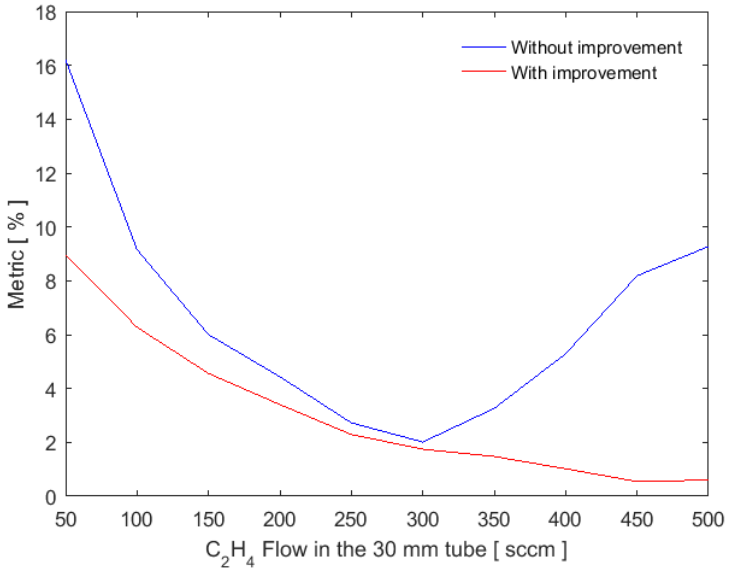

Figure 5.24: Comparison between the percentual errors, i.e. metric, obtained for a fixed height search at 16 mm below the tube center, with and without the suggested domain improvement.

Table 5.8: Obtained results - ethylene flow, furnace temperature and substrate position - in the 80 mm setup for the fixed height search, at 16 mm below the tube center, with the suggested improvement and the comparison between the percentual errors, i.e. metric, obtained with and without the improvement.

30 mm	**80 mm**			**Metric [%]**	
C_2H_4 Flow [sccm]	**C_2H_4 Flow [sccm]**	**Furnace Temp. [ºC]**	**Substrate Position [m]**	**Without Improv.**	**With Improv.**
50	50	1200	0.0441	16.21	8.95
100	100	975	0.0640	9.16	6.27
150	150	975	0.0799	6.00	4.56
200	250	975	0.0998	4.43	3.40
250	300	975	0.1117	2.73	2.29
300	350	975	0.1237	2.01	1.75
350	400	975	0.1356	3.26	1.48
400	450	975	0.1396	5.29	1.02
450	450	975	0.1515	8.19	0.55
500	500	975	0.1555	9.27	0.60

case, considering the furnace temperature in the performed search leads to smaller metric values, especially for higher ethylene flows where the improvement is higher (see Figure 5.24).

Table 5.9 presents a comparison between the ethylene flows and the individual percentual errors obtained while considering or not the improvement. Moreover, the errors obtained with the improvement are shaded in green or red if they were decreased or increased, respectively. These values suggest that most error reductions occurred in the ethylene concentration and the mixture's velocity, especially for scenarios in the 30 mm tube with smaller ethylene flows, whereas the mixture's temperature error was mostly improved for higher ethylene flows in the 30 mm tube (≥ 350 sccm).

The previously performed sensitivity analysis concluded that the furnace temperature has direct effects on the mixture's temperature, by increasing the heat transfer (see section 5.4.1). For scenarios with higher ethylene flows, this heat transfer increase leads to a higher mixture temperature, being the desired one achieved.

A higher furnace temperature also affects the mixture's velocity profile, by increasing its viscosity (see section 5.4.1). These effects are more noticeable for scenarios with smaller ethylene flows. With a higher furnace temperature, similar temperature as the ones without improvement can be achieved with smaller ethylene flows in the 80 mm, which allows the

Table 5.9: Comparison between the flows, errors and metrics, obtained for the fixed height search, at 16 mm below the tube center, with and without the furnace temperature based improvement. The improvement errors are shaded in green or red if they were reduced or increased, respectively.

C_2H_4 Flow [sccm]	Without Improvement					With Improvement				
	Flow [sccm]	Errors [%]			Metric [%]	Flow [sccm]	Errors [%]			Metric [%]
		C_2H_4	Temp.	Veloc.			C_2H_4	Temp.	Veloc.	
50	50	7.21	11.96	8.22	16.21	50	7.34	5.13	0.10	8.95
100	150	6.97	0.20	5.93	9.16	100	0.68	6.06	1.48	6.27
150	200	3.48	0.05	4.89	6.00	150	0.19	4.47	0.87	4.56
200	300	3.50	0.93	2.56	4.43	250	2.11	2.24	1.45	3.40
250	350	2.40	0.78	1.03	2.73	300	1.41	1.56	0.90	2.29
300	400	1.75	0.91	0.37	2.01	350	1.01	1.07	0.93	1.75
350	450	1.34	2.08	2.13	3.26	400	0.76	0.7	1.05	1.48
400	500	1.06	4.17	3.08	5.29	450	0.59	0.13	0.82	1.02
450	500	0.47	7.96	1.84	8.19	450	0.005	0.43	0.33	0.55
500	500	0.01	9.20	1.20	9.27	500	0.005	0.13	0.59	0.60

Table 5.10: Comparison between searches performed in different heights when considering the furnace temperature based improvement, depicting which synthesis conditions were improved or not, shaded in green or red, respectively.

C_2H_4 Flow [sccm]	Searched Height											
	4 mm			8 mm			16 mm			32 mm		
	C_2H_4	Temp	Veloc	C_2H_4	Temp	Veloc	C_2H_4	Temp	Veloc	C_2H_4	Temp	Veloc
50												
100												
150												
200												
250												
300												
350												
400												
450												
500												

search methodology to explore other combinations of synthesis conditions with a better overall percentual error (see Table 5.9).

The same methodology was followed for different substrate positioning heights and results are presented in Figure 5.25. For each height, it is depicted the obtained minimum metric, for each 30 mm simulation scenario, when considering or not the temperature based improvement. It is clear that the effects of the improvement depend on the searching height. For instance, for substrate positioning nearer the tube walls, there is no improvement at all. At these heights, there is more heat transferred than nearer the tube center, thus the effects of changing the furnace temperature in the mixture's temperature are none. Moreover increasing the furnace temperature would increase the mixture's viscosity and thus its velocity profile. So, although not having effects on the mixture's temperature, performing the suggested improvement would alter the other synthesis conditions, and thus the overall metric. In order to understand what occurs in the other heights, Table 5.10 was constructed, depicting which conditions' percentual errors are improved or not in each addressed height.

From this table, it is conclusive that the main effect of altering the furnace temperature is in the mixture's temperature, especially for scenarios in the 30 mm tube with higher ethylene flows. As aforementioned, this is due to the increased heat transferred to the mixture. As for the other synthesis conditions, when searching at heights near the tube center, altering the furnace temperature would mostly affect the mixture's velocity profile,

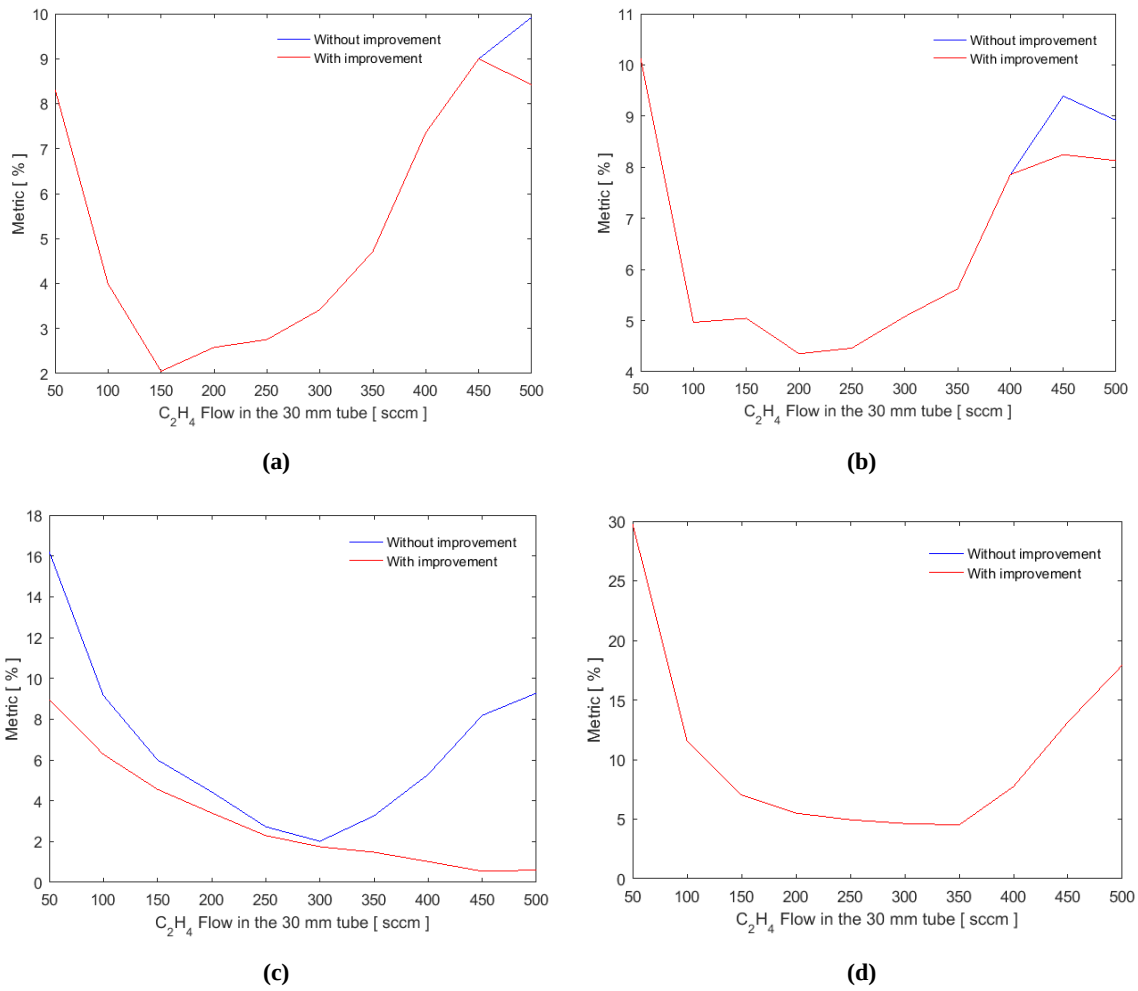

Figure 5.25: Comparison between the percentual errors, i.e. metric, obtained for a fixed height search, with and without the suggested improvement, for a substrate positioning height of (a) 4 mm, (b) 8 mm, (c) 16 mm, and (d) 32 mm below the tube center.

due to the increase of its viscosity. Moreover, the transferred heat takes longer to reach the particles traveling at this heights, resulting in a combination of effects which will not improve the overall percentual error.

In conclusion, nearer the tube center, only the scenarios with higher ethylene flow are improved, due to a reduced temperature percentual error. As the analysis is performed further away from the tube center, this effect starts occurring for scenarios with smaller ethylene flows. On the other hand, when nearer the tube walls, the effects of the temperature are no longer noticeable and, due to the mixture's viscosity, effects on its velocity start occurring, which is translated in no improvements at all. Nonetheless, for searching heights between these cases, altering the furnace temperature has positive effects in all addressed synthesis conditions. As previously described, the temperature ones occur for scenarios with higher ethylene flows, whereas the other effects occur for lower ethylene flows.

Finally, an analysis of the furnace temperature based improvement was performed when the positioning height is not fixed, and results are presented in Figure 5.26 and Table 5.11. In this case, since there is no height constraints to the searches, the percentual error is reduced for scenarios with higher ethylene flow, due to the effects on the mixture's temperature.

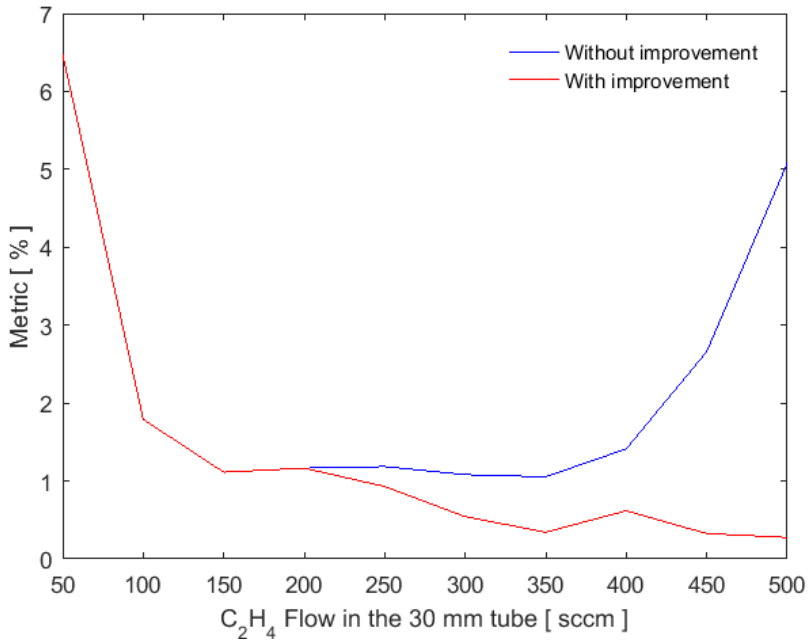

Figure 5.26: Comparison between the percentual errors, i.e. metric, obtained for a non-fixed height search, with and without the suggested improvement.

Table 5.11: Obtained results - ethylene flow, furnace temperature and substrate position - in the 80 mm setup for the non-fixed height search with the suggested improvement and the comparison between the percentual errors, i.e. metric, obtained with and without the improvement.

30 mm	**80 mm**				**Metric [%]**	
C_2H_4 Flow [sccm]	**C_2H_4 Flow [sccm]**	**Furnace Temp. [ºC]**	**Substrate**		**Without Improv.**	**With Improv.**
			Position [m]	**Height [m]**		
50	50	750	0.9989	2E-4	6.48	6.48
100	100	750	0.9949	2E-4	1.79	1.79
150	150	750	0.9914	-4E-4	1.11	1.11
200	200	750	0.6886	-1E-4	1.17	1.17
250	250	975	0.2072	-0.02	1.19	0.93
300	300	975	0.2390	-0.02	1.08	0.54
350	350	975	0.2589	-0.02	1.05	0.34
400	400	975	0.2708	-0.02	1.41	0.62
450	450	975	0.0719	-0.01	2.66	0.32
500	500	975	0.2868	-0.02	5.08	0.27

Table 5.12: Comparison between the flows, errors and metrics, obtained for the non-fixed height search, with and without the furnace temperature based improvement. The improvement errors are shaded in green or red if they were reduced or increased, respectively.

C_2H_4 Flow [sccm]	Without Improvement					With Improvement				
	Flow [sccm]	Errors [%]			Metric [%]	Flow [sccm]	Errors [%]			Metric [%]
		C_2H_4	Temp.	Veloc.			C_2H_4	Temp.	Veloc.	
50	50	2.80	0.22	5.84	6.48	50	2.80	0.22	5.84	6.48
100	100	0.11	0.20	1.78	1.79	100	0.11	0.20	1.78	1.79
150	150	0.00	0.20	1.10	1.11	150	0.00	0.20	1.10	1.11
200	200	0.03	0.07	1.16	1.17	200	0.03	0.07	1.16	1.17
250	250	0.01	0.19	1.17	1.19	250	0.03	0.60	0.71	0.93
300	300	0.01	0.23	1.06	1.08	300	0.02	0.38	0.39	0.54
350	350	0.01	0.41	0.97	1.05	350	0.01	0.28	0.19	0.34
400	400	0.01	1.04	0.95	1.41	400	0.006	0.16	0.60	0.62
450	450	0.01	2.53	0.82	2.66	450	0.005	0.06	0.32	0.32
500	500	0.01	5.07	0.31	5.08	500	0.005	0.26	0.08	0.27

The furnace temperature increase effects are depicted with more detail in Table 5.12. Similar to the previous analyzed searches (see Figure 5.25), the improvements occur in scenarios of the 30 mm tube with a higher ethylene flow. As before, this is due to the effects of an increased heat transferred to the mixture, which increases its temperature and alters its velocity profile. Moreover, this later effect is also responsible for the improvements in both the 250 and 300 sccm scenarios. As before, for the other scenarios, the increase in the furnace temperature affects the mixture's viscosity, which alters its velocity profile and, thus, the gases dispersion through the tube. Consequently, in these cases, the suggested improvement does not reduce the overall metric. Overall, considering the temperature-based improvement to the transition methodology resulted in total percentual errors lower than 1%, for scenarios with an ethylene flows higher than 250 sccm. For scenarios with an ethylene flow lower than 250 sccm, considering the furnace temperature in the transition methodology did not resulted in any improvement.

5.5. Final Considerations

In this chapter, a methodology to support the transition between different CVD setups to synthesize CNTs was designed and evaluated. After measuring the desired synthesis conditions in the 30 mm tube, various simulations performed in the 80 mm tube were

searched for the process parameters whose conditions would better mimic the desired ones. This mimicking was evaluated by calculating a percentual error.

The search was performed while considering or not a pre-defined fixed height to position the substrate and better results were achieved when not narrowing the search to a specific height, where a percentual error less than 2% was achieved for most of the considered scenarios.

Posteriorly, the methodology was improved by considering variations to the furnace temperature. Such changes have effect in the mixture's temperature, by increasing the heat transfer rate, and in the mixture's velocity, by affecting its viscosity. This temperature-based search was followed for various fixed heights and without fixing the searching height. As before, the un-fixed height search was the one which achieved the lowest percentual errors, being less than 1% for more than half of the analyzed 30 mm simulation scenarios. When fixing the search to a specific height, the results depend on the selected one, being better for heights further away from both the tube center and the tube walls.

The results presented in this chapter were an evaluation of the designed transition methodology. Achieving percentual errors between both setups inferior to 2% or 1%, depending on whether the furnace temperature is considered, pertains the usage of the methodology as a support tool to experimentally transition between setups.

References

[1] C.A. Coelho, A.T. Sepúlveda, L.A. Rocha, A.F. Silva, Carbon nanotubes: The challenges of the first syntheses trials, in: BIODEVICES 2015 - 8th Int. Conf. Biomed. Electron. Devices, 2015: pp. 95–102. doi:10.5220/0005201000950102.

[2] D.R.K. Bansal, A Textbook of Fluid Mechanics and Hydraulic Machines, 1st Editio, Laxmi Publications, New Dehli, 1983.

[3] E. Pasche, M. Rada, M. Toppel, A. Kilic, Fundamentals of fluid mechanics, (2004). doi:10.1016/0378-3804(88)90174-X.

Chapter 6

CFD WITH CHEMICAL REACTIONS

Throughout the previous sections, the development of a CFD-based tool to support the transition between different CVD processes to synthesize CNTs was performed. Such tool took advantage of the CFD capabilities to analyze how different compounds would flow through a specific tube to estimate how the synthesis conditions would vary for different process parameters. However, such transition tool has its limitations. Since one of the synthesis conditions to mimic between setups is the concentration of the used hydrocarbon, the transition methodology is only applicable if the addressed setups use the same gases. As depicted in section 2.2, there are various possible compounds combinations that result in CNT synthesis. Thus, how could the transition tool be adapted in order to tackle transition between setups, which use different compounds? Further CFD capabilities can be used to tackle these and other issues related with the CNTs synthesis. For instance, chemical reactions can be included in the designed model to evaluate how those compounds react and interact with each other [1].

Therefore, with the intention to study how these capabilities could help solving experimental issues, a model of a CVD process including chemical reactions, which occur during the CNTs synthesis, was designed and assessed. The model was based on an experimental CVD setup to synthesize CNTs, existent in the Institute for Soldier Nanotechnology (ISN) at the Massachusetts Institute of Technology (MIT), mainly operated by the NECSTLab research group.

The issues tackled in this case study were related with CNT growth uniformity in a carbon fiber weave, when using a sodium-based catalyst. The usage of CFD tools to address such issues had already been attempted by modeling the synthesis phase of the CVD process. Nonetheless, further experimental work suggested that the issues were due to poor catalyst particles formation during the reduction phase. Thus, the CFD model was altered to address the chemical reactions occurring in that phase. Posteriorly, a sensitivity analysis, assessing the growth uniformity inside the weave, was performed, and the results gave some insights on the next steps to perform experimentally in order to solve the addressed issues.

Moreover, considering the main objective of this thesis work is to develop a CFD-based model to support the transition between CVD setups, it was thought that the chemical reactions kinetics could be an add-on feature of the model in order to extend the transition between setups, whose synthesis is based in different hydrocarbons, and not limited to different equipment geometries.

6.1. Case Study Description

As aforementioned, in order to analyze the CFD chemical reactions capabilities in tackling experimental issues, these reactions were included in the design of the computational model of a CVD setup, existent in the ISN at the MIT (see Figure 6.1 and Table 6.1).

In this setup, CNTs are synthesized using acetylene (C_2H_2) and carbon dioxide (CO_2) as the precursors, hydrogen (H_2) as the reducer, and argon (Ar) as the inert gas. Each gas flow is controlled by a mass flow controller, which can flow them directly to the quartz tube (blue line) or through a water bubbler, used to flow water molecules into the tube, in order to increase the process humidity (yellow line). The quartz tube is 762 mm long, has an inner diameter of 22 mm, and is placed inside a furnace. The pressure inside the tube is

(a)

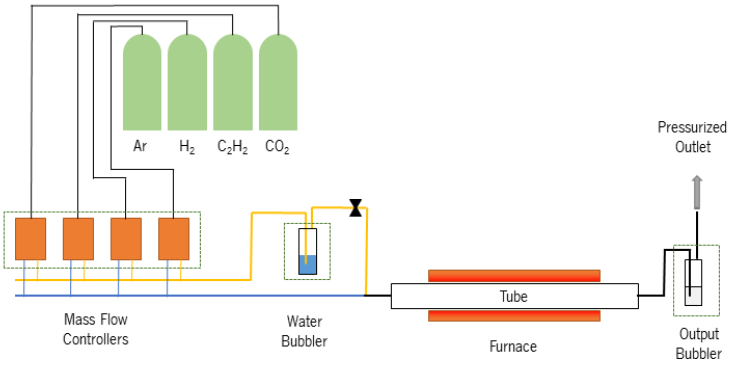

(b)

Figure 6.1: Experimental setup (a) schematic and (b) photo.

Table 6.1: Maker and model of the components of the CVD setup.

Mass Flow Controllers	Furnace
Aalborg Instruments & Controls, Inc. GFC17	Lindberg/Blue M TF55035C1

maintained by an output bubbler, containing medium viscosity mineral oil. After passing through this bubbler, the gases flow through a pressurized outlet to the building's exhaustion system.

Over the last years, the group has been focusing in the CNT inter and intra-laminar growth on carbon fibers [2,3]. Lately, the possibility to synthesize CNTs by following an acetylene-based protocol in a sodium-based catalyst has been studied, due to the protocol's capability of growing CNTs at lower temperatures (480 ^{o}C), as well as the catalyst even adhesion in the carbon fibers [4–6]. However, the on-going study of this catalyst had revealed some uniformity issues on the CNT synthesis [3].

Figure 6.2 shows a graphical representation of the Carbon Fiber (CF) weave placed

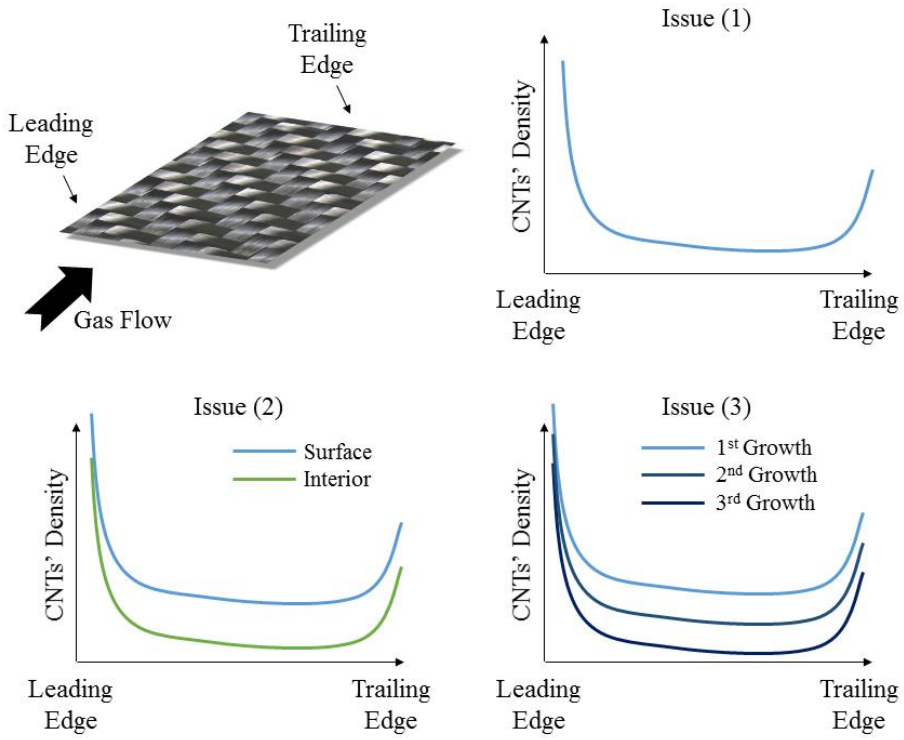

Figure 6.2: Schematic of the CVD setup to synthesize CNTs in a Carbon Fiber (CF) weave, depicting the noticed uniformity issues: (1) throughout the weave; (2) inside the weave; and (3) throughout the growths performed during the day.

in respect to the gas flow direction, depicting its leading and trailing edges. Figure 6.2 also shows the three main uniformity issues, depicted through adimensional representations of typical curves of the CNTs synthesis throughout the weave. These three issues are:

(1) Throughout the weave: CNTs grow more in the CF leading edge than in the rest of the weave;

(2) Inside the weave: CNTs grow more at the surface of the CF, when compared to its inside;

(3) Throughout the day: if the same experiment is repeated throughout the day, it has been shown that the synthesis quality reduces from growth to growth.

In order to tackle the first two of these issues, a chemical reaction based CFD model of the case study CVD setup was designed and analyzed.

6.2. Methodology

The main goal of this case study was to use chemical reactions based CFD models to

support the experimental work to solve uniformity issues when synthesizing CNTs in a carbon fiber weave. Prior to the analysis presented in this section, a model of the chemical reactions which occur during the growth phase of the CNT synthesis was designed and analyzed by a researcher in the NECSTLab group [3]. Such model was used as a starting point to the work presented here.

6.2.1. Previously Designed Model

As aforementioned, the NECSTLab research group has previously designed a chemical reaction based CFD model to analyze the growth phase in the synthesis of CNTs in a carbon fiber weave [3]. Such model was designed and analyzed using the ANSYS FLUENT CFD software. Figure 6.3 shows a graphical representation of the tube, and Figure 6.4 illustrates its previously designed model, which only included the quartz tube, neglecting the end caps, which resulted in a length of 660 mm [3]. Moreover, in order to reduce the number of mesh elements and, consequently, the simulation time, the tube is modeled as a half-tube with a symmetry wall. The weave was modeled as rectangle with a width of 19 mm, length of 51 mm, and a thickness of 0.5 mm.

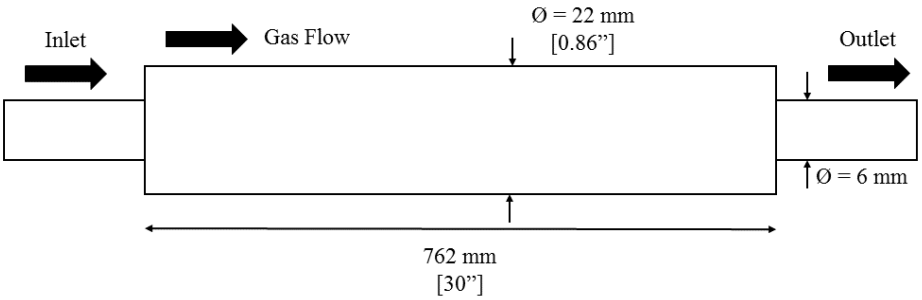

Figure 6.3: Graphical representation of the case study CVD tube.

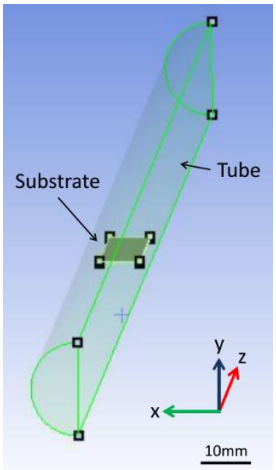

Figure 6.4: Illustration of the CVD tube and substrate previously designed and analyzed (taken from [3]).

Since this model addresses the growth phase of an acetylene-based CNT synthesis, the implemented chemical reaction (see Eq. 6.1) reflects the acetylene and carbon dioxide breakdown into carbon atoms, which create bonds with other carbon atoms existent in the CNTs' structure, and both carbon monoxide and water vapor, which exits the tube.

$$C + C_2H_2 + CO_2 \rightarrow CO + H_2O + 3C \qquad \textbf{Eq. 6.1}$$

This model was used to perform a sensitivity analysis on how the compounds' dispersion at the surface and inside the weave vary with process parameters, such as the output pressure and the weave structure, during the growth phase. Results have shown that the weave structure, more specifically, its surface area to volume ratio, had great influence on the gases concentrations throughout the weave. The resulting higher concentrations in the weave's leading edge compared to the rest of the weave were considered to be a potential cause for the decrease of CNTs throughout the weave. Moreover, when addressing the weave's interior, inconstant concentrations suggested that the weave structure might not allow the gas depletion through it. More insights on the whole analysis and results can be found in [3].

6.2.2. Analysis of New Hypothesis: Reduction Phase

The previously constructed reaction model of the case study CVD setup was focused in the growth phase of the CNT synthesis process, being independent of the used catalyst [3].

In the work presented in this chapter, envisioning to synthesize CNTs using a sodium-based catalyst, the first approach was to evaluate if the reduction phase was properly done - premise upon which the previously model was constructed - by analyzing if the catalyst was properly reduced into particles. If the reduction phase is not properly done, i.e. if the particles are not properly created, the uniformity issues existent with the CNT synthesis are no longer due to the growth phase, but instead due to the reduction phase.

In order to perform such analysis of the reduction phase, a set of experiments, where the synthesis process would stop immediately before the growth phase, were performed. Posteriorly, the resulting carbon fiber samples were analyzed via Scanning Electron Microscope (SEM) in search for the catalyst particles.

Samples preparation

To prepare the samples for the reduction phase analysis, the following steps were performed:

- The carbon fiber was cut in 20 x 25 mm samples;
- The samples were cleaned via submersion in distilled water;
- The samples were cured in a vacuum oven at 120 ^{o}C for 20 min;
- The samples were submerged in a 125 g distilled water and 0.9 g sodium hydroxide (NaOH) solution for 5 min;
- The samples were then dried in ambient conditions for a minimum of 5 hours.

Performed experiments

As stated before, in order to evaluate the catalyst reduction into particles, a set of experiments were thought. Being the CNT synthesis process composed of 5 main phases - (1) cleaning; (2) heating/reduction; (3) synthesis; (4) delamination; and (5) cooling (see section 2.2.1) - in these experiments, the whole process was stopped immediately after the reduction phase. Table 6.2 show the process parameters used in these experiments: the gas flows that flow during the reduction phase; and the reduction time, measured after the tube is heated to the desired temperature (480 ^{o}C).

SEM analysis

Scanning Electron Microscope (SEM) was performed in order to evaluate the catalyst formation in the carbon fiber samples generated by the described experiments, and results have shown that the formerly enumerated issues were also found. First, when comparing

Table 6.2: Gas flows and reduction time used in the experiments used to access the catalyst reduction phase.

Exp.	Gas flows [sccm]		Reduction Time
	Hydrogen	Argon	[min]
1	50	200	0
2	50	200	5
3	50	200	10
4	100	400	0
5	100	400	5
6	100	400	10
7	200	800	0
8	200	800	5
9	200	800	10

the weave's edge closer to the tube entrance (leading edge) and the one further away (trailing edge), it was found that the former had more generated catalyst particles. This is

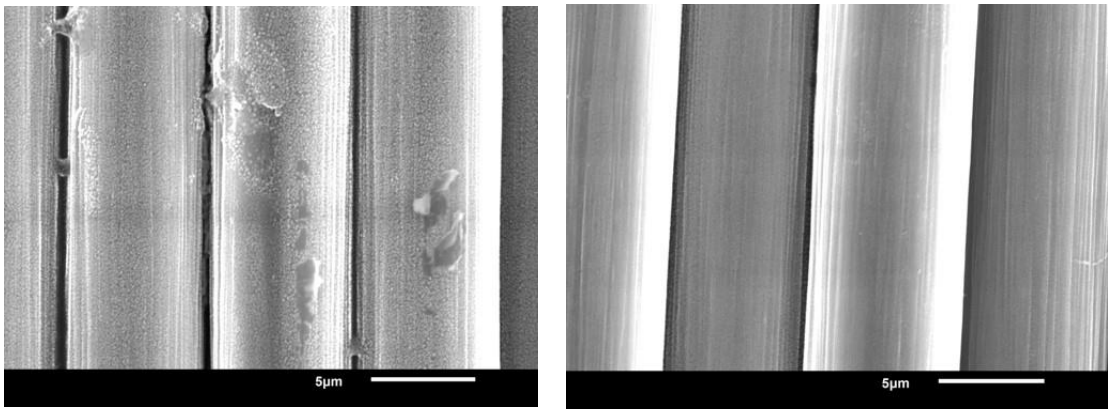

(a) **(b)**

Figure 6.5: Weave's (a) leading and (b) trailing edges after the reduction phase. More particles were formatted in the leading edge than in the trailing one.

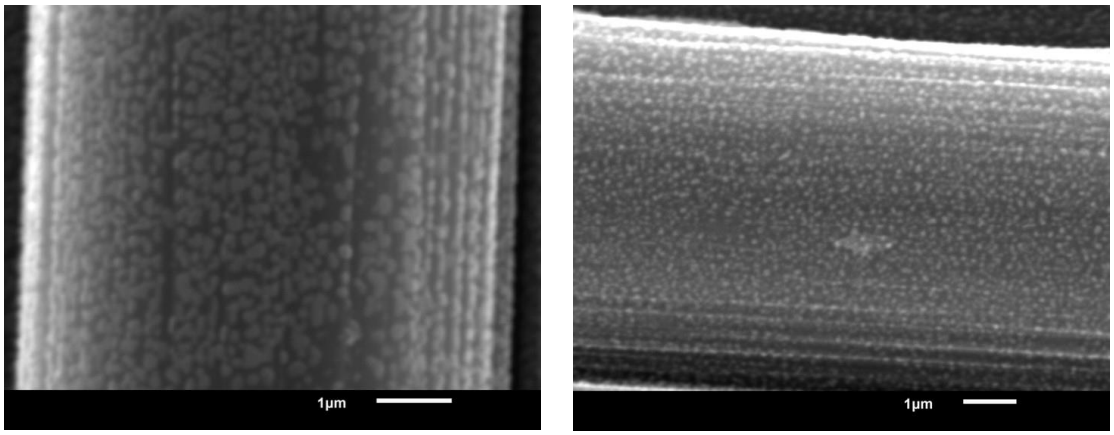

(a) **(b)**

Figure 6.6: Weave's (a) surface and (b) interior. Although catalyst particles were generated in the weave's inside, they are smaller than the ones in its surface, which may lead to a poorer growth inside the weave.

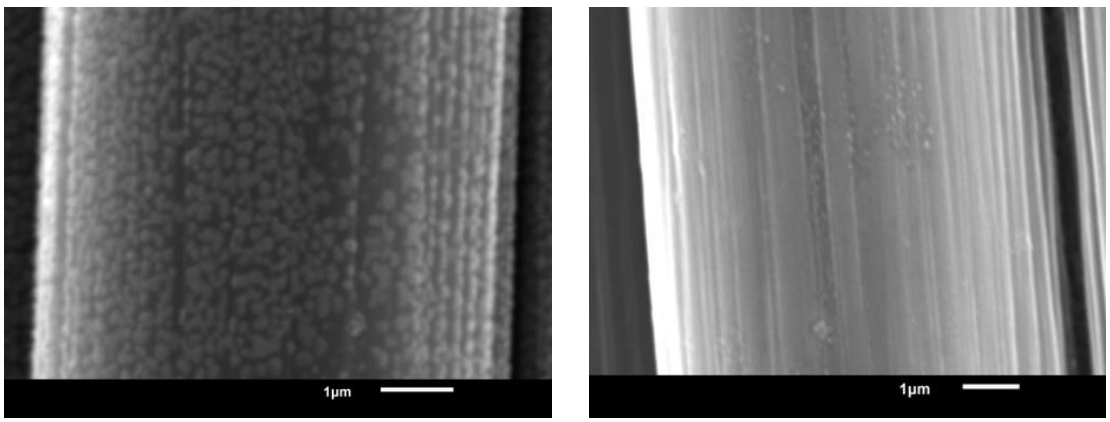

(a) **(b)**

Figure 6.7: (a) 1st and (b) 3rd experiments of the same day. The lack of particles in the latter pertain the previously described growth of the day dependency issue.

noticeable in Figure 6.5, where the carbon fibers at the trailing edge have a smoother surface, i.e. without the little dots, than the ones at the leading edge.

Secondly, it was found that, although particles were created in the weave's interior, these were different than the ones encountered in its surface (see Figure 6.6). The generated particles inside the weave have smaller diameter than the ones at its surface. This difference may, posteriorly, lead to different CNTs growth, pertaining the aforementioned lack of uniformity.

Finally, when comparing samples generated in different experiments of the same day, the particle's generation's dependency on this factor was also noted (see Figure 6.7). The smoother surface of carbon fibers at the 3rd experiment of the day and the spots noticeable on the 1st experiment are indicators that these experiments result in different catalyst particles formation.

All these results validate the proposed hypothesis that the aforementioned issues are due to the reduction phase and not to the growth phase. Thus, in order to properly use CFD modelling with chemical reactions to support the process of tackling these issues, a new model, focused on the reduction phase of the CVD process, was designed.

6.2.3. Reduction Phase Model

With the validation of the proposed hypothesis that the growth uniformity issues were due to a poorly catalyst particles formation, a CFD-based model with chemical reactions, focused on the reduction phase, was designed and simulated using the ANSYS FLUENT solver. As depicted in Figure 6.8, only half of both the quartz tube and the carbon fiber

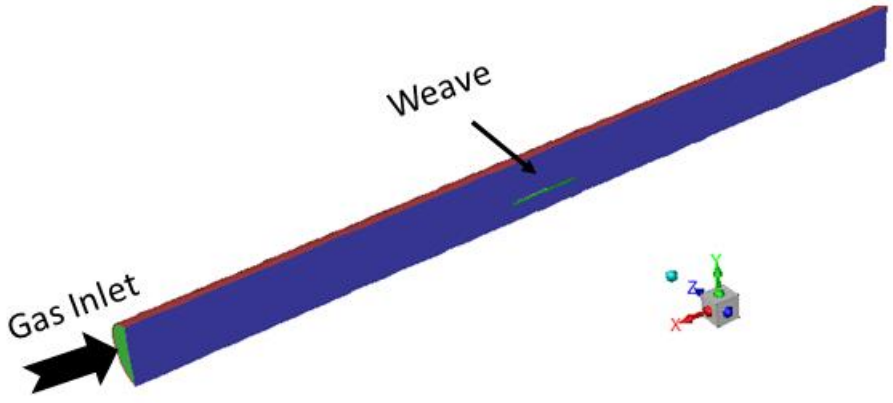

Figure 6.8: Designed model, focused in the reduction phase of the CNT synthesis process (taken from [3]).

Table 6.3: Configuration parameters used in the mesh of the chemical reactions model.

Parameter	Value
Use Advanced Size Function	On: Proximity and Curvature
Relevance Center	Coarse
Mesh Defeaturing	Yes
Transition	Fast
Span Angle Center	Coarse
Num. of Cells Across Gap	3

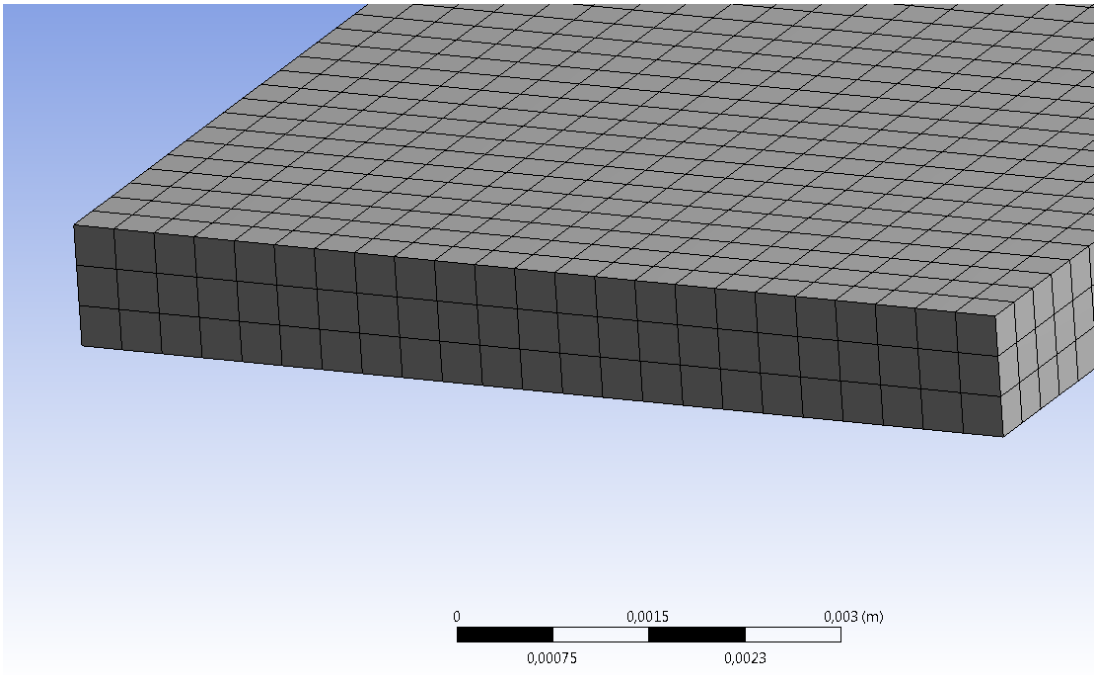

Figure 6.9: Screenshot of the generated mesh for the weave in the CVD setup.

weave was modeled, having a symmetry wall in the center. Since the focus of the performed analysis was the compounds dispersion as well as interaction on the weave's surface and in its interior, only the central section of the quartz tube, which is embraced by the furnace, was modeled. This section has a total length of 350 mm. Moreover, the weave's dimensions, used in this "half model" were 10 mm width, 25 mm length and 1 mm thick.

Table 6.3 shows the configuration parameters for the used mesh, which is depicted in Figure 6.9. Being this a primarily analysis to the effects of the process parameters in the catalyst particles formation inside the CF weave, simulations with a reduced computational time were envisioned. Thus a mesh of 3 cells across gap was defined, which would reduce the simulation time without compromising the results (see section 2.3.2). Each simulation

had a total number of 1000 iterations, which had guaranteed the models' convergence via the software's criteria of achieving a residual less than 1e-6.

Being focused in the reduction phase, the occurring chemical reactions are only dependent on the catalyst, which was sodium hydroxide (NaOH), and the inlet gases that flow during this phase: hydrogen (H_2) and argon (Ar). Since the latter is an inert gas, only the other two are considered in the modeled reactions. The first reaction (Eq. 6.2) is the hydrogen's breakdown into radicals and the second reaction (Eq. 6.3) is the hydrogen radical reaction with sodium hydroxide, forming sodium and water vapor. Table 6.4 depicts the values for the pre-exponential factor and activation energy parameters used by the Arrhenius equation for the kinetics of the simulated chemical reactions. The Arrhenius equation (see Eq. 6.4) relates the reaction's rate constant, k, with its pre-exponential factor, A, and activation energy, E_a, as well as the temperature, T, and the universal gas constant, R. Moreover, Table 6.5 shows the compounds' properties used in these simulations.

$$H_2 \rightarrow 2H \qquad \textbf{Eq. 6.2}$$

$$NaOH + H \rightarrow Na + H_2O \qquad \textbf{Eq. 6.3}$$

Table 6.4: Used parameters for reactions' Arrhenius equations, taken from the National Institute of Standards and Technology[1].

Reaction	Pre-exponential Factor	Activation Energy [j/kg.mol]
$\boldsymbol{H_2 \rightarrow 2H}$	3.68e-9	425,000
$\boldsymbol{NaOH + H \rightarrow Na + H_2O}$	5.97e-12	1,900

$$k = Ae^{\frac{-E_a}{RT}} \qquad \textbf{Eq. 6.4}$$

6.2.4. Chemical Reactions' Sensitivity Analysis

The designed model was used to support the experimental work in overcoming two of the CNT synthesis issues: lack of growth uniformity throughout and inside the weave. Such model was used to analyze which parameters of the reduction phase have more

[1] URL: http://kinetics.nist.gov/kinetics/welcome.jsp

Table 6.5: Gases properties.

Variable	Argon (Ar)	Atomic Hydrogen (H)	Hydrogen (H_2)	Sodium (Na)	Sodium Hydroxide (NaOH)	Water Vapor (H_2O)
Density [kg/m3]	1.6228	0.040948	0.08189	970	2,100	0.5542
Specific Heat [j/kg.K]	520.64	20,621	14,283	1,230	1,491.61	2,014
Thermal Cond. [w/m.K]	0.0158	0.2316	0.1672	0.7517	0.688	0.0261
Viscosity [kg/m.s]	2.125e-5	7.49e-6	8.411e-6	6.8e-4	4e-3	1.34e-5
Mol. Weight [kg/kmol]	39.948	1.00797	2.01594	22.99	39.997	18.01534
Enthalpy [j/kg.mol]	-3,117.711	2.18e8	0	2,410	-197.76	-2.42e8
Entropy [j/kg.mol.K]	154,719.3	114,593.4	130,579.1	57.86	228.47	188,696.4
Ref. Temp. [K]	298.15	298.15	298.15	300	300	298.15

influence in the formation of the catalyst particles. Considering the modeled chemical reactions (Eq. 6.2 and Eq. 6.3), the formation of these particles can be measured by the kinetics of the 2nd reaction. In other words, considering a uniform catalyst deposition in the carbon fiber samples, the greater the kinetic rate of the 2nd reaction is related with more particles being formatted.

In order to evaluate the catalyst particles' formation dependency in the process parameters, two sensitivity analysis were performed. One where the gas flows are expressed as the flows itself, and other where they are expressed as a ratio between them. In the first one, the gas flows are based in the existent mass flow controllers' maximum and minimum flows. As for the second one, they are based in the hydrogen ratio, when compared to the total flow.

In addition to the hydrogen and argon flows (or the ratio between them), the analysis also considered variations to the furnace temperature, which, as demonstrated by previously performed sensitivity analysis (see section 5.4.1), it also has influence on the compounds' behavior inside the tube.

In both analysis, the furnace temperature was simulated for values of 480, 500 and 550 ^{o}C. These values were selected taking into account the experimentally used furnace temperature (480 ^{o}C) and the temperature, above which, the carbon fiber starts disintegrating (550 ^{o}C).

In the first sensitivity analysis - the flow-driven one - each gas (hydrogen and argon) was simulated for 50, 500 and 1000 sccm. As in Chapter 4, these values were selected equidistantly, taking into account the range of possible flows by the mass flow controllers (0 to 1000 sccm), and the minimum flow was substituted for a non-zero value (50 sccm). Through this analysis, it is envisioned to have an overview of the setup's behavior. More specifically, to evaluate which gas flow has more influence in the nanoparticles formation throughout the CF weave.

On the other hand, in the ratio-driven sensitivity analysis, the relation between both gas flows was taking into account when selecting the simulation scenarios to perform. Since hydrogen is the compound affecting the chemical reactions (Eq. 6.2 and Eq. 6.3), its flow was selected first, being the argon's flow computed by the hydrogen-ratio. This ratio is defined as the percentual relation between the hydrogen's flow and the total flow (Eq. 6.5). For instance, if a 200 sccm is used for both the hydrogen and argon flows, the ratio is 50%. In the sensitivity analysis, the hydrogen flow was tested for 200, 400 and 800 sccm, and the ratio was tested for 60% (60% Hydrogen - 40% Argon), 80% and 100%.

$$ratio = \frac{hydrogen\ flow}{hydrogen\ flow + argon\ flow} \qquad \textbf{Eq. 6.5}$$

Table 6.6: Flows and furnace temperature used in the performed flows-driven sensitivity analysis.

Exp.	H_2 flow [sccm]	Ar flow [sccm]	Furnace Temp. [^{o}C]
1	50	50	480
2	50	500	500
3	50	1,000	550
4	500	50	500
5	500	500	550
6	500	1,000	480
7	1,000	50	550
8	1,000	500	480
9	1,000	1,000	500

Table 6.7: Hydrogen ratio, flow and furnace temperature used in the ratio-driven sensitivity analysis.

Exp.	H_2 flow [sccm]	H_2 Ratio [%]	Furnace Temp. [ºC]
1	200	60	480
2	400	60	500
3	800	60	550
4	200	80	500
5	400	80	550
6	800	80	480
7	200	100	550
8	400	100	480
9	800	100	500

The Taguchi Orthogonal Arrays were used to select the sets of simulations to perform, presented in Table 6.6 and Table 6.7 for the first and second sensitivity analysis.

As aforementioned, these sensitivity analysis intend to evaluate which process parameter has more influence in the catalyst nanoparticles formation throughout the CF weave. Such phenomenon was numerically measured by the kinetic rate of the 2nd reaction (Eq. 6.3). Taking into account the synthesis issues, the analysis should address this rate at both the top and inside the CF weave. Thus, in each simulation, a total of five different planes (two across the weave's width and three across the weave's height) were created (see Figure 6.10). The kinetic rate was measured at the intersections of these planes, resulting in a total of six lines, at different heights and widths, throughout the CF weave:

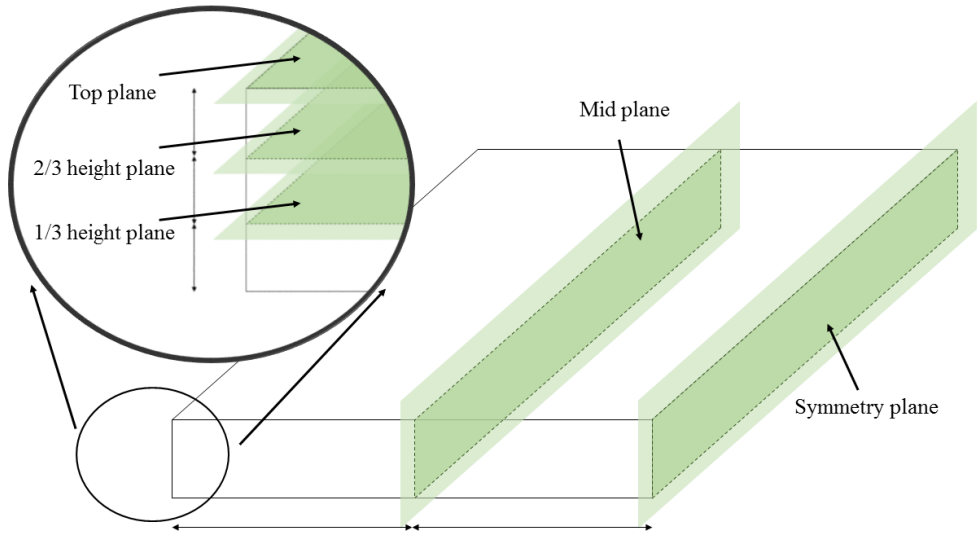

Figure 6.10: Planes in the weave's width and height, whose combinations were used to measure the kinetic rate of the 2nd reaction.

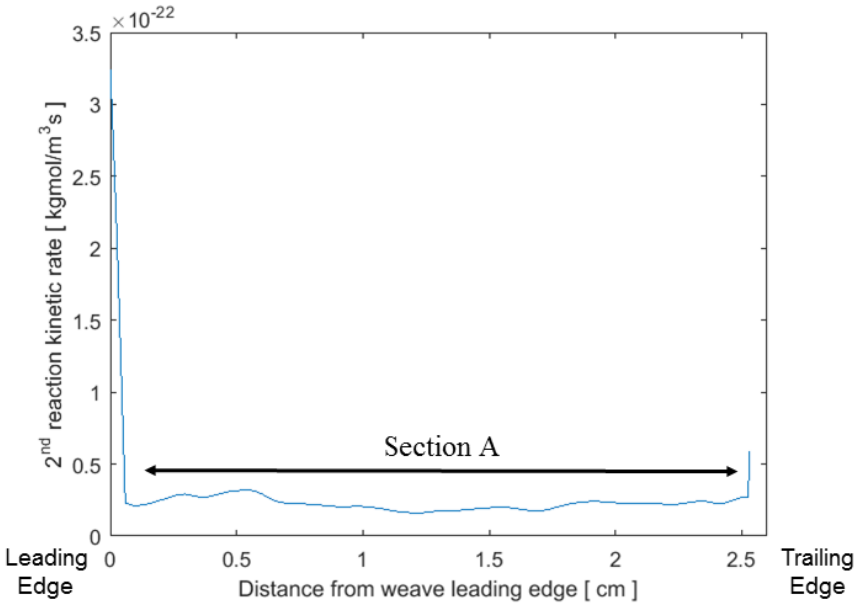

Figure 6.11: Typical evolution of the kinetic rate of 2nd reaction throughout the weave.

top plane with mid plane, top plane with symmetry plane, 2/3 height plane with top plane, etc.

Figure 6.11 depicts a typical evolution of the kinetic rate of the 2nd reaction throughout the CF weave. There is a spike on the reaction kinetics at both edges of the weave, which comes in accordance with results obtained in the previous model [3]. Being the weave a solid placed inside the tube, it affects the gases dispersion nearby, leading to higher concentrations at its edges and, consequently, higher kinetic rate.

An evolution of the reaction's kinetic rate throughout the CF weave can be measured for each one of the six possible lines. However, using the Taguchi orthogonal arrays to perform the sensitivity analysis requires the simulations' output variable to be expressed as a number (see sections 3.3 and 3.4). Thus the kinetic rate throughout these lines should be combined into a single number.

For a given line, i, resulting from the intersection of the previously referred planes (see Figure 6.10), the average value of the kinetic rate across the center section of the weave (Section A in Figure 6.11), $kr_{Section\ A_i}$, was computed in order to obtain the kinetic rate of that given line, kr_i (Eq. 6.6). Then the average of all six individual values of the kinetic rate were used to calculate an overall kinetic rate across the weave for each simulation, KR_s (Eq. 6.7). Finally, following the same methodology as in the previously performed sensitivity analysis (see section 3.3), the dependencies of the addressed variable were

analyzed.

$$kr_i = \overline{kr_{Section\ A_i}} \quad \text{Eq. 6.6}$$

$$KR_s = \frac{\sum kr_i}{6} \quad \text{Eq. 6.7}$$

6.3. Results and Discussion

Both the flow-driven and the ratio-driven sensitivity analysis were performed to address the process parameters' effects in the catalyst nanoparticles formation throughout the weave and the results are shown in this section. Moreover, following the same methodology as before (see section 3.3), a percentual ranking was computed for each case.

Since each gas is tested for a wider range of values, the flow-driven sensitivity analysis gives a broader view of the compounds' effects of the nanoparticles formation. Its results are presented in Figure 6.12. The kinetic rate of the 2nd reaction decreases with the increase of both the gas flows and the temperature. Being the CF weave a porous structure, with very small gaps for the gases to get through, the gas mixture must have a specific conditions to reach the weaves inside. For instance, if the compounds have a higher velocity (flow), their particles cannot get through the weaves porous surface and reach its inside, leading to a lower kinetic rate and thus a lower nanoparticles formation. Moreover, the

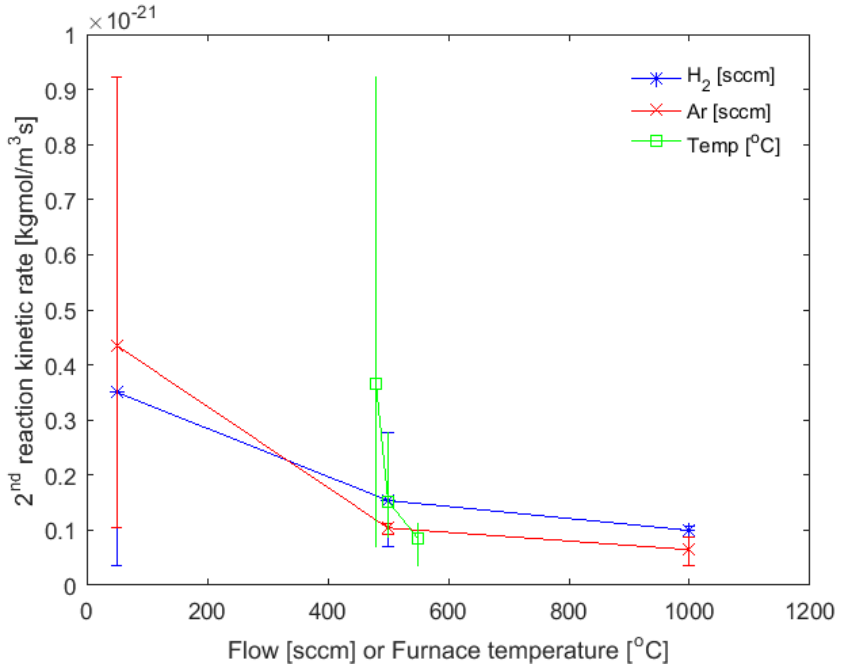

Figure 6.12: Results obtained for the flow-driven sensitivity analysis.

Table 6.8: Percentual dependencies of the kinetic rate of 2nd reaction on the process parameters addressed in the flow-driven sensitivity analysis.

Flow-driven sensitivity analysis		
H_2 flow	**Ar flow**	**Furnace Temp.**
28%	41%	31%

uncertainty, expressed by the error bars, is higher if the flow of one gas is small. Since each gas flow is simulated for all gas flows of the other gas, including the 1000 sccm one, there is more variation on the results. For instance, the minimum value with an argon flow of 50 sccm corresponds to the simulation where the hydrogen flow is 1000 sccm (scenario number 07 in Table 6.6). The temperature effects on the addressed variable are more indirect. As shown in section 4.2.2, the mixture's dynamic viscosity increases with its temperature. Although having a lower velocity, it is harder for this more viscous mixture to get through the CF weave's narrow gaps, leading to less compounds concentration inside it and hence a lower reaction's kinetic rate.

The percentual dependencies of this sensitivity analysis were computed and are presented in Table 6.8. Even though it is the main compound used in the 2nd chemical reaction (Eq. 6.3), hydrogen is the parameter with less percentual dependency. This is explained by comparing the hydrogen and argon curves for both 50 and 1,000 sccm. For the later, having a higher flow of hydrogen is better than having a higher flow of argon, since it is ensured a higher hydrogen concentration throughout the tube, which leads to a higher kinetic rate. On the contrary, having a 50 sccm flow of hydrogen is worse than having the same flow for argon, because it is not ensured a high hydrogen concentration and thus leads to a lower kinetic rate.

Having a higher kinetic rate for 1000 sccm, and a lower kinetic rate for 50 sccm, than the argon trend line, hydrogen has a smaller variation than argon for the same flow variation, which leads to a smaller percentual dependency (see formula in section 3.3). It is this duality when comparing a high and low flow that reduces hydrogen's percentual dependency and, consequently, increases the argon and temperature ones.

Moreover, this duality is confirmed by the ratio-driven sensitivity analysis, whose results are presented in Figure 6.13 and Table 6.9. Because the model is not being tested for scenarios where the argon flow is greater than the hydrogen's, a sufficiently high hydrogen concentration in ensured, reducing the argon's effects on the 2nd reaction kinetic

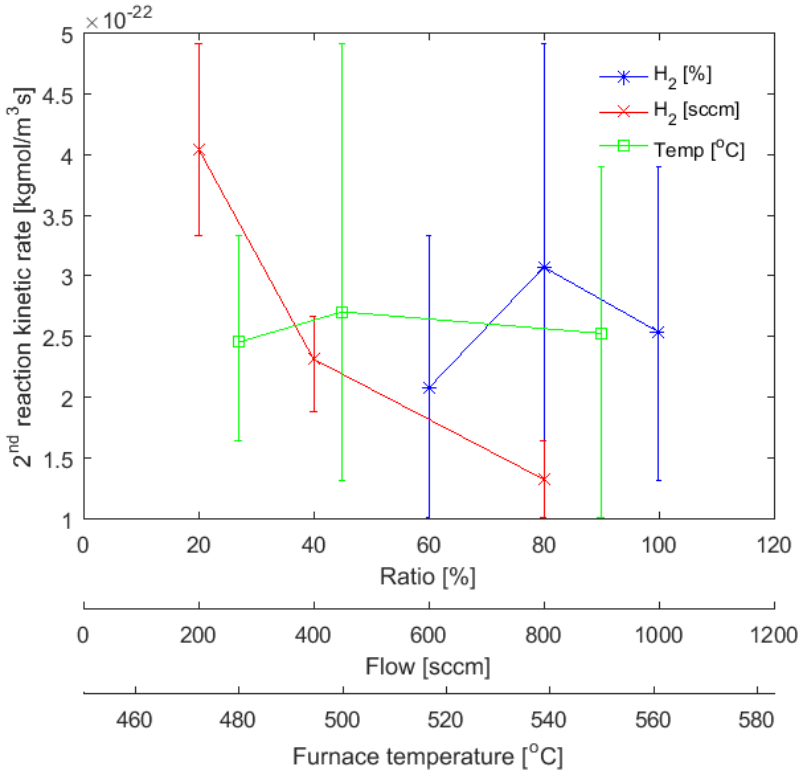

Figure 6.13: Results obtained for the ratio-driven sensitivity analysis.

Table 6.9: Percentual dependencies of the kinetic rate of 2nd reaction on the process parameters addressed in the ratio-driven sensitivity analysis.

Ratio-driven sensitivity analysis		
H_2 flow	**H_2 ratio**	**Furnace Temp.**
69%	25%	6%

rate and increasing the hydrogen ones (see Table 6.9). In fact, both argon and the furnace temperature do not have significant effect on the addressed variable. This makes more sense than the previous results, since hydrogen is the only compound which affects the catalyst particles formation (Eq. 6.3), being the formation higher for smaller hydrogen flows (see Figure 6.13). In fact, the scenarios which lead to the maximum points in the argon and temperature error bars are the ones, where the hydrogen flow was smaller.

These sensitivity analysis present a better understanding of the system, which can be used to plan the experiments to perform in the CVD setup in order to tackle the previously described synthesis issues.

6.4. Final Considerations

In this case study, chemical reactions kinetics were added to computational fluid

dynamics to design a model capable of analyzing aspects of the CVD process, which could not be possible with the previously designed models. These kinetics enable the possibility of evaluating how compounds present in the synthesis process can interact with each other in order to create other substances, not initially present in the model.

For this specific case study, the reactions, which occur in the CVD process reduction phase, were analyzed in order to evaluate how each process parameter affect the catalyst particle formation, which has been proven to have influence in some uniformity issues present in the experimental setup.

In the scope of the main goal of this thesis work - develop a CFD-based tool to support the transition between different setups to synthesize CNTs - it is believed that the same chemical reaction kinetics capabilities can be added to the previously designed transition methodology in order to tackle the transition between setups, whose CNT synthesis is based in different hydrocarbons. Because each hydrocarbon has a distinct set of thermal reactions, the formation of compounds, which have an impact in the CNTs synthesis, is also different. Such differences can only be modeled by a chemical reactions approach where each set of reactions is simulated and the compounds' concentrations are measured. For instance, such transition methodology could be used to support the transition between a setup based in ethylene synthesis and a second setup based in acetylene.

References

[1] ANSYS Inc, Modeling Surface Chemistry, 2009.

[2] E.J. Garcia, B.L. Wardle, A. John Hart, N. Yamamoto, Fabrication and multifunctional properties of a hybrid laminate with aligned carbon nanotubes grown In Situ, Compos. Sci. Technol. 68 (2008) 2034–2041. doi:10.1016/j.compscitech.2008.02.028.

[3] H.K. Cornwell, Tensile and Interfacial Properties of Radially Aligned CNT Grown Carbon Fibers, Massachusetts Institute of Technology, 2017.

[4] S.A. Steiner, Carbon Nanotube Growth on Challenging Substrates: Applications for Carbon-Fiber Composites, Mater. Sci. Eng. Massachusetts Inst. Technol. (2004) 315.

[5] R. Li, P. Florin, B.L. Wardle, B. Engineering, Nanoengineered Hierarchical Carbon Fiber Composites Without Fiber Strength Loss, in: 19th Int. Conf. Compos. Mater., 2013: pp. 1–8.

[6] A. Magrez, J.W. Seo, R. Smajda, B. Korbely, J.C. Andresen, M. Mionić, S. Casimirius, L. Forró, Low-temperature, highly efficient growth of carbon nanotubes on functional materials by an oxidative dehydrogenation reaction, ACS Nano. 4 (2010) 3702–3708. doi:10.1021/nn100279j.

Chapter 7

CONCLUSIONS

The main goal of this thesis was to develop a methodology, based in CFD tools, to support the transition process between different CVD setups to synthesize CNTs. Such objective was thought as a more methodic way to overcome the process' inconsistency issues than a commonly used trial-and-error practice. These inconsistencies not only hinder the knowledge and research findings transfer within the scientific community, but also impose limits when a synthesis scale up is envisioned.

Sensitivity Analysis

In order to design such transition model, a sensitivity analysis was initially performed to four different CVD setups to evaluate which process parameter had more influences in several conditions inside the setup during the growth phase. The setups were computationally designed and modelled in various synthesis scenarios, differed by the gas flows used in the process. Due to the huge number of possible combinations of gas flows, the selection of the set of simulations to be performed was defined by following the Taguchi orthogonal arrays, which reduced the number of combinations to take into account, while still being possible to take conclusions regarding the whole system's behavior. Several synthesis conditions, such as compounds' concentrations, temperature and velocity, were

measured for each simulated scenario. Posteriorly, trend lines depicting the relation between each synthesis condition to each process parameter were constructed, resulting in a graphical representation of which parameter most affects each addressed condition. For proper comparison, these effects were quantitatively computed as percentual dependencies, from which was concluded that the hydrocarbon, in this case ethylene, was the gas whose flow most affects the assessed conditions. This sensitivity analysis not only resulted in a better understanding of the CVD process and the interactions between different conditions which occur inside the setup, but also identified which process parameter should be taken more into account when designing the envisioned transition methodology.

Transition Model

With such understanding of the CVD synthesis process, it was then possible to design the transition methodology. Being based in CFD tools, the transition between different CVD setups was defined as the act of mimicking synthesis conditions inside the setups' tubes during the growth phase. Thus, the proposed methodology was based in a comparison between the conditions measured in both setups, resulting in an optimization problem, whose goal was to seek the set of process parameters in the second setup, which would mimic the most the synthesis conditions previously measured in the first setup. Being the CNTs' synthesis by CVD based in the thermal breakdown of the used hydrocarbon, the conditions to be considered in the transition methodology were its concentration, temperature and velocity. Moreover, due to the effects of the compounds' viscosity on their velocity throughout the tube, which affects their temperature, the defined synthesis conditions were measured taking into account the substrate position inside the tube, which is defined by its distance to the tube entrance and to the tube center. Considering insights from the performed sensitivity analysis, the set of simulations to be used in the transition methodology was defined by only varying the ethylene flow, while maintaining the hydrogen and helium flows constant. For a given simulation scenario in the first setup, after measuring the synthesis conditions, the simulations domain of the second setup was searched for the parameters, i.e. gas flows and substrate position, which would result in synthesis conditions most similar to the previously measured ones. The comparison between these two sets of conditions was computed as the percentual error between them. Following such methodology resulted in percentual errors less than 2% for most of the tested cases and never higher than 7% for the remaining ones. After evaluating the individual percentual errors of each synthesis condition, it was hypothesized that the

achieved results could be improved by considering the furnace temperature effects on the synthesis conditions inside the tube. For instance, increasing the furnace temperature would increase the heat transfer between the tube walls the compounds and thus enabling them to reach temperatures closer to the desired ones. This hypothesis was validated by performing a sensitivity analysis addressing the effects of the furnace temperature on the synthesis conditions. Once validated, the hypothesis was tested by including simulation scenarios, where the furnace temperature was also varied, in the search domain of the second setup and by performing the same previously followed transition methodology. This temperature based methodology was followed for various substrate positioning heights, as well as without fixing the searching height to a pre-defined value. Results showed that the inclusion of the temperature effects would reduce the achieved percentual error, especially for higher ethylene flows where, due to the compounds' higher velocity, increasing the furnace temperature would have more influence in the heat transferred to the mixture. Since increasing the furnace temperature also affects the velocity profile, its improvement was reduced for searching heights nearer the tube center or walls, being them more noticeable for heights between them. As before, performing this methodology without fixing the searching height, would result in a percentual error inferior to 1% for more than half the evaluated scenarios. The designed transition methodology was considered a viable tool to support the transition process between different CVD setups. Such methodology not only can be used to transmit knowledge and research findings within the scientific community, but would also ease scale-up processes of certain results.

CFD with Chemical Reactions

However, such transition tool has its limitations. Since one of the synthesis conditions to mimic between setups is the concentration of the used hydrocarbon, the transition methodology is only applicable if the addressed setups use the same gases. As depicted in section 2.2.2, there are various possible compounds combinations that result in CNT synthesis. Thus, how could the transition tool be adapted in order to tackle transition between setups, which use different compounds? In order to evaluate other capabilities of the CFD modelling of the CVD process, a case study was performed in collaboration with the NECSTLab research group of the AeroAstro Department in the Massachusetts Institute of Technology. The main objective of this case study was to minimize uniformity issues occurring in an acetylene-based synthesis of CNTs in carbon fiber weaves, with sodium-based catalyst: growth uniformity (i) throughout the weave; (ii) inside the weave; and (iii)

throughout the day. To tackle these issues it was defined that both experimental and computational work should be performed. A CFD model of the setup, integrated with chemical reactions kinetics, had been previously designed to analyze the growth phase. However, experiments showed that the same uniformity issues were happening in the reduction phase, since the catalyst particles, upon which CNTs should grow, were not correctly formed. Consequently, in the performed case study, the CFD model of the setup was re-designed to assess the chemical reactions, occurring in the reduction phase. Such reactions were based in the sodium-based catalyst breakdown when in presence with hydrogen. A sensitivity analysis of the model was performed in order to understand the effects of certain process parameters during the reduction phase on the formation of catalyst particles inside the weave. This analysis involved the simulation of various scenarios, where the furnace temperature as well as the flows of both hydrogen and argon. As previously, this set of scenarios was selected based on the Taguchi orthogonal arrays and both the trend lines and the effects of the process parameters in the assessed variable were analyzed. The catalyst particles formation was measured by the reaction's kinetic rate, to whom it is directly proportional. The performed analysis concluded that a higher particles formation could be achieved by fixing the hydrogen flow to smaller values. Thus experimental validation these findings is required.

Final Considerations

For the development of the computational tool to support the transition between different CVD setups, some research questions were previously defined (see section 1.4), whose answers would lead the proper investigation of the proposed research work. These answers were addressed throughout this thesis and are briefly stated as follow.

Which conditions affect the CNTs' synthesis in the CVD process?

Being the CVD process solely based in thermochemical reactions, the main conditions that affect the CNTs' synthesis are the gases temperature, the compounds dispersion rate throughout the tube and the catalyst sample position inside the tube. The synthesis phase of the CVD technique is based in the thermal decomposition of a hydrocarbon gas, such as ethylene and acetylene, into hydrogen and carbon atoms. These later are then deposited in a catalyst sample. Being thermochemical reactions, both the decomposition and deposition occur at a specific temperature range (400-1200 ºC). The compounds dispersion rate affects their concentration throughout the tube,

altering the rate at which these reactions occur and, thus, the CNT synthesis rate. Lastly, the catalyst sample position inside the tube affects the carbon atoms deposition in it. Since the hydrocarbon gas is flowing through the tube, its pyrolysis occurs at a certain distance from the tube entrance, which influences the catalyst sample position where the carbon atoms deposition is optimal (see section 2.2.1).

How can CVD process setups be different?

CVD setups can differ by the used compounds, but also in their physical configuration. As aforementioned, the CNT synthesis by CVD is based in the thermal decomposition of a hydrocarbon gas, such as ethylene or acetylene. The resulting carbon atoms are then adhered to catalyst particles which can be injected into the tube by a carrier gas, such as ferrocene, or by priory placing a metal based compound, such as iron or nickel, inside the tube. The CVD process can also use a reducer gas, usually hydrogen, to reduce the catalyst into smaller particles, where CNTs will then be synthesized. An inert gas, such as argon or helium, can also be used to control the pressure and compounds flow inside the tube (see section 2.2.2).

The CVD process can also differ in its physical configuration. In this thesis four distinct setups were considered and analyzed. These differed by the tube's dimensions - radius and length, the tube's entrance configuration - concentric or lateral - and by the existence or not of a pre-heater. These physical features affect the compounds dispersion throughout the tube and, consequently, the synthesis conditions inside it. All these elements and their different configuration make the entire synthesis process more complex to control and tune (see chapters 3 and 4).

How are these synthesis conditions affected by the process parameters?

The variable with most effect on the synthesis conditions is the heat transfer rate between the furnace and the compounds inside the tube. This depends on the compounds' flow rates and furnace temperature itself. Reducing the first one, or increasing the second one, leads to a higher heat transfer rate, which results in thermochemical reactions earlier in the tube (closer to its entrance) and thus different synthesis conditions (see chapter 4 and section 5.4.1).

How should the transition between setups be defined?

In this thesis, the transition between setups was defined as the ability to achieve the same synthesis conditions in different setups. Such transition was performed by measuring the desired synthesis conditions in the first setup and comparing them with the conditions measured in the second setup by varying the used ethylene gas flow and furnace temperature. Thus, the transition was tackled as a minimization problem, where the variable to minimize was the percentual error between the desired synthesis conditions and the ones measured in the second setup. Through this comparison and measurement of the percentual error, the second setup is searched for the process parameters, i.e. ethylene flow, furnace temperature and substrate position, which result in the set of synthesis conditions which better mimic the desired ones, previously measured in the first setup (see section 5.2).

Which synthesis conditions are considered critical?

Since the synthesis is based in a thermochemical reaction, the synthesis conditions considered critical were the ethylene concentration and the mixture's velocity and temperature. The reaction rate of the hydrocarbon's decomposition is directly affected by its dispersion throughout the tube and by the heat transferred to the hydrocarbon. The ethylene dispersion throughout the tube is reflected by its concentration and by the mixture's velocity. Moreover, the mixture's temperature is a direct measurement of the heat transferred to the compounds (see section 5.2).

How can these synthesis conditions be changed?

Given the results from the performed sensitivity analyses, the process parameters which can most directly change the defined synthesis conditions are the ethylene flow and the furnace temperature. Having a higher molar mass, ethylene has more influence in several conditions occurring inside the tube than the other compounds. Following the proposed transition methodology by only considering simulation scenarios in the second setup, which differ by the ethylene flow, percentual errors less than 2% were achieved for most of the tested cases. Such findings come in accordance with the results of the sensitivity analysis in chapter 4, suggesting the ethylene flow

as the one which most affects several conditions inside the tube (see section 5.2).

Later, it was hypothesized if these percentual errors could be improved by also considering the furnace temperature in the scenarios of the second setup. The same transition methodology was followed for this set of scenarios and results have shown improvements to the percentual error, especially if a specific positioning height was considered. As aforementioned the CNT synthesis via CVD is based in a thermochemical reaction. Thus, varying the furnace temperature has a direct effect in the heat transfer between the tube walls and the mixture, increasing its temperature, considered a synthesis condition which defines the transition between setups (see section 5.4).

Are there any other parameters relevant to the setups' transition?

The CNT synthesis via CVD can also be analyzed in terms of the reactions' kinetics, i.e. which reactions occur and at what rate. Since CVD setups can also differ from the used compounds (hence the occurring reactions), considering chemical reactions capabilities in the transition method enables the transition between setups with different compounds. For instance, between ethylene and acetylene based CVD setups (see chapter 6).

Future Work

The future work within the scope of this research project consists of both experimental and computational work. Regarding the latter, it was thought that the inclusion of chemical reactions kinetics could potentiate the adaptation of the previously developed transition methodology in order for it to tackle the transition between CVD setups, whose synthesis is based in different hydrocarbons. The inclusion of the reactions kinetics capabilities in the model enable the analysis of other synthesis conditions, resulted from the interaction between the different compounds.

On the other hand, within the envisioned experimental work, it is thought the validation of the designed transition methodology as well as of its future adaptation with chemical reactions. In either case, experimental validation of the achieved results should be achieved. Such validation should be first be assessed within the same research group (for instance, between the 30 mm and the 80 mm setups) and, if successful, it should be tackled with the transition between CVD setups existent in distinct research groups (for

example, between the University of Minho and the MIT CNTs synthesis setups).

In order to lead proper development of this future work, several research questions were thought, and are present as follow. As before, further research should address their answers.

- How to properly validate the proposed transition methodology?
- What chemical reactions are presented in synthesis with different hydrocarbons?
- When addressing a transition methodology between these setups, what are the synthesis conditions that should be mimicked between them?